DEVELOPMENT AND APPLICATION OF METABOLOMIC TECHNIQUES FOR IDENTIFICATION AND QUANTIFICATION OF INTERCELLULAR METABOLITES RELEVANT TO GLUCOSE STIMULATED INSULIN SECRETION IN β-CELLS

by

Matthew A. Lorenz

A dissertation submitted in partial fulfillment
of the requirements for the degree of
Doctor of Philosophy
(Chemistry)
in The University of Michigan
2011

Doctoral Committee:

Professor Robert T. Kennedy, Chair
Professor Philip C. Andrews
Professor Charles F. Burant
Professor Kristina I. Håkansson

2011

DEDICATION

To Katherine whose unwavering love and support made this endeavor possible.

ACKNOWLEDGEMENTS

I first and foremost thank my advisor Robert Kennedy for his support and mentorship throughout my graduate career. I extend a special thanks to our collaborator Charles Burant for his generosity with resources, ideas, and especially his time. I also thank Kristina Håkansson and Philip Andrews for their participation in my graduate committee and their great ideas for the project.

I am truly grateful for the collaboration, support, and friendship of all the members of the Kennedy and Burant Labs. They have made this graduate school experience remarkably enjoyable. I am especially appreciative of Jinghua Xu and Mary Treutelaar for training me in the nuances of cell culture and Charles Evans for his friendship and insightful discussions of all-things metabolomics.

TABLE OF CONTENTS

LIST OF TABLES

LIST OF FIGURES

LIST OF ABBREVIATIONS

General Abbreviations

AEX	anion exchange
APCI	atmospheric pressure chemical ionization
APPI	atmospheric pressure photo ionization
CE	capillary electrophoresis
CE-MS	capillary electrophoresis - mass spectrometry
DART	direct analysis in real time
DESI	desorption electrospray ionization
DI	direct injection
EI	electron ionization
ESI	electrospray ionization
GC	gas chromatography
GC-MS	gas chromatography - mass spectrometry
GSIS	glucose stimulated insulin secretion
HEPES	4-(2-hydroxyethyl)-1-piperazineethanesulfonic acid
HILIC	hydrophilic interaction liquid chromatography
HPLC	high pressure liquid chromatography
KRHB	Krebs-Ringer-HEPES buffer
LC	liquid chromatography
LC-MS	liquid chromatography - mass spectrometry
LIT	linear ion trap
MALDI	matrix assisted laser desorption ionization
MS	mass spectrometry
NMR	nuclear magnetic resonance
PPP	pentose phosphate pathway
TCA	tricarboxylic acid cycle

TOF	time of flight
UHPLC	ultra high pressure liquid chromatography
QQQ	triple quadrupole
Q-TOF	quadrupole-time of flight

Metabolite Abbreviations

2PG	2-phosphoglycerate
3PG	3-phosphoglycerate
6PG	6-phosphogluconic acid
aCoA	acetyl-Coenzyme A
ADP	adenosine diphosphate
AKG	alpha-ketoglutarate
AMP	adenosine monophosphate
Asn	asparagine
Asp	aspartic acid
ATP	adenosine triphosphate
CDP	cytidine diphosphate
CIT	citrate
CMP	cytidine monophosphate
CTP	cytidine triphosphate
F6P	fructose-6-phosphate
FAD	flavin adenine dinucleotide
FBP	fructose 1,6-bisphosphate
FUM	fumarate
G3P	glycerol-3-phosphate
G6P	glucose-6-phosphate
GAR	glycineamideribotide
GDP	guanosine diphosphate
Gln	glutamine
Glu	glutamic acid
GMP	guanosine monophosphate
GTP	guanosine triphosphate

HMG-CoA	3-hydroxy-3-methylglutaryl-Coenzyme A
ICIT	isocitrate
LAC	lactate
Lys	lysine
MAL	malate
mCoA	malonyl-Coenzyme A
NAD^+	nicotinamide adenine dinucleotide
NADH	nicotinamide adenine dinucleotide, reduced
$NADP^+$	nicotinamide adenine dinucleotide phosphate
NADPH	nicotinamide adenine dinucleotide phosphate, reduced
Orn	ornithine
PEP	phosphoenolpyruvate
PRPP	phosphoribosyl pyrophosphate
R5P	ribose phosphate
S7P	sedoheptulose-7-phosphate
sCoA	succinyl-CoA
Ser	serine
SUC	succinate
UDP	uridine diphosphate
UMP	uridine monophosphate
UTP	uridine triphosphate
ZMP	aminoimidazole carboxamide ribonucleotide

CHAPTER 1
Introduction

Metabolomics Background

The study of metabolism is vital to understand biological systems and their potential dysregualtion in disease states. Metabolites supply not only the building blocks for all classes of biological molecules including DNA, RNA, and proteins but also regulate their expression and activities. It is of little surprise that the field of metabolomics, the global measurement of metabolites[1], has seen explosive growth in the post-genomic era coincident with advances in analytical instrumentation, data processing, and chemometric tools designed to facilitate efficient and accurate large-scale metabolite quantification. Since the Nicholson Group at The Imperial College of London and the Fiehn group at The Max-Planck Institute of Molecular Plant Physiology in Germany coined the terms “metabonomics”[2] and "metabolomics"[1] in 1999 and 2002, respectively, the number of publications indexed by these terms (now generally considered interchangeable)[3, 4] has grown exponentially to ~900 PubMed indexed citations in 2010 (Figure 1-1). Accordingly, metabolomics has become a vital tool in biomedical research as practiced independently to study metabolite interaction or in combination with genomic, transcriptomic, and/or proteomic data to study biological systems in a holistic manner (e.g. systems biology).

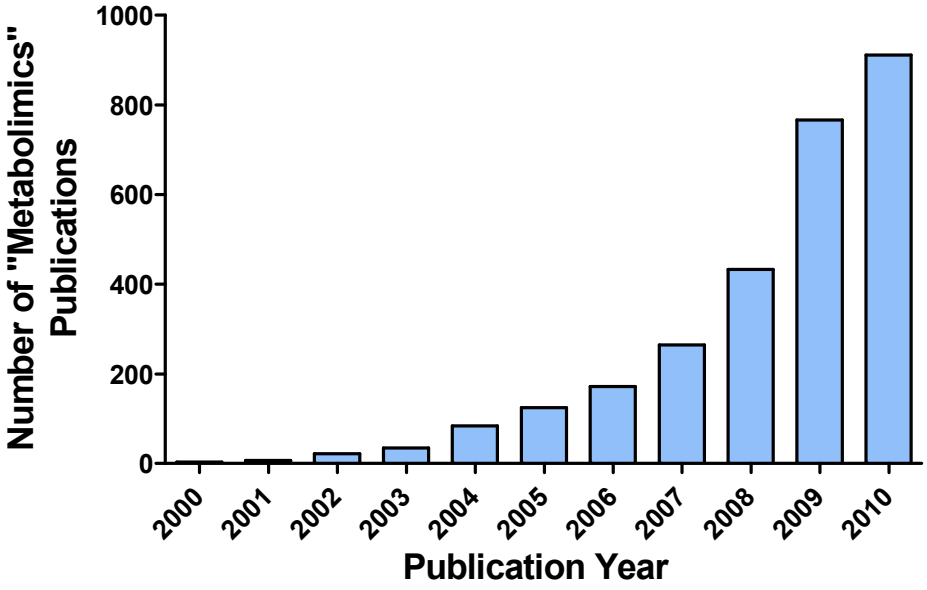

Figure 1-1. Number of Publications Returned with “Metabolomics” Keyword Search of NCBI- PubMed.

Metabolomics Approaches and Platforms. Analytical approaches for metabolomic analysis of biological systems can be classified broadly as directed (targeted) or undirected (untargeted). This distinction is dependent upon whether the methodology implemented is designed to quantify a number of specific metabolites (directed) or to measure a generally larger set of metabolites restricted only by the sensitivity and applicability of the analytical platform(s) and data processing employed (undirected). These approaches have found widespread use in biological investigations of biomarkers of disease[5], pharmacological toxicity[3], functional genomics[6], and nutrigenomics[7]. Metabolomic platforms can be categorized based on the detection method used (generally MS or NMR) as detailed below. Sample types commonly investigated include plant tissue, plasma, urine, cerebral spinal fluid, mammalian tissue, and cultured eukaryotic and prokaryotic cells. Accordingly, efficient extraction of metabolites from these various samples through customized sample preparation procedures is a critical parameter in accurate metabolomic analysis as discussed in Chapter 3. Moreover, the human metabolome, for example, is estimated to be comprised of ~2400 compounds[8] with diversity in structure ranging from polar sugars to

lipophilic triacylglycerols, therefore complementary preparation techniques and analysis platforms are necessary to approach true global metabolite measurement.

Directed Metabolomics. Quantification of small numbers of metabolites (< 10) in biological samples has been commonplace for decades. Initial studies used chemical or enzymatic assays to convert a metabolite of interest into a detectable product or cofactor. These approaches do not require advanced analytical equipment and are therefore still used in many research laboratories today. ^{1}H-NMR has seen limited use for absolute quantification of metabolites due to inherent sensitivity and specificity limitations, although studies have reported quantification of 11 metabolites in urine[9] 48 in whole blood[10] ~100 in urine[11]. Separation based techniques such as HPLC-UV and GC-FID have been used for metabolite quantification but suffer from limited sensitivity and selectivity critical for successful analysis in complex biological matrices. Larger sets of specified metabolites (as many as 205) have been quantified recently in biofluids and cellular extracts using separations based approaches coupled with mass spectrometry detection (CE-MS[12], GC-MS[13], and LC-MS[14, 15]) as discussed below.

Undirected Metabolomics. Undirected metabolomic studies strive to measure all the metabolites in a given sample. While the chemical identity of each unique "feature" or signal measured in an analysis may ultimately be important for a given study, undirected experiments generally begin with a simple hypothesis that differences in metabolite concentrations can be measured between groups of samples. Accordingly, the initial goal of an undirected analysis is to discover these differences. Advanced data processing techniques are used in the undirected approach as discussed below. Studies that terminate at "feature" identification fall under the category of "metabolite profiling" and can be useful in areas such as biomarker identification. Alternately, these features can be further interrogated and structurally identified leading to new ideas regarding the alteration in biochemical processes responsible for the observed differences. Hence, this class of experiment is often referred to as "hypothesis generating".

NMR. Nuclear magnetic resonance spectroscopy is a powerful analytical tool for chemical structural characterization and has been used extensively for metabolite profiling. ^{1}H-NMR experiments are commonly employed and involve measuring energy

absorbed and re-emitted from hydrogen nuclei in a magnetic field. This approach is nearly universal due to the ubiquity of protons in metabolite species. ^{1}H-NMR offers full scan compatibility, fast analysis times (~5 min/sample), is non-destructive, and quantitative. However, NMR suffers from inherent low sensitivity and is generally employed as a profiling tool to find biomarker signals as opposed to quantifying specific metabolites. Although, hardware improvements such as cryogenically cooled probes and advances in spectral deconvolution software[16] have improved the utility of NMR as a quantitative tool for metabolite measurement in biological samples.[11] For example, as many as 100 metabolites have been quantified in plasma using these advanced approaches.[10]

Mass Spectrometry. Mass spectrometry detection has become synonymous with absolute metabolite quantification in recent years based primarily on the technique's high sensitivity relative to NMR. The sensitivity and selectivity of MS are improved considerably when coupled to separation techniques such as GC, CE, and HPLC. Accordingly, dozens of practical combinations of separation technique, ionization source, and mass analyzer have been employed for metabolomic analysis based on analytical considerations such as sample size, metabolite class of interest, required sensitivity, desired mass accuracy, dynamic range, and need for full scan capability. Accordingly, no single analytical platform is ideal for all types of metabolomic analysis.

Mass Analyzer. Mass analyzers commonly used in metabolomic analysis include quadrupole, quadrupole ion trap (QIT), linear ion trap (LIT), time-of-flight (TOF), Fourier transform ion cyclotron resonance (FT-ICR), and Orbitrap. Hybrid systems containing multiple mass analyzers such as triple-quadrupole (QQQ) and quadrupole-time of flight (Q-TOF) are used routinely to further increase the sensitivity and specificity of mass spectrometry based detection. The use of high resolution advanced hybrid instruments such as TOF-TOF[17] and LIT-Orbitrap[18] has been reported recently to improve selectivity for non-separation based or “shotgun” metabolomic analysis. The operating principals and advantages of each instrument type for metabolomics are beyond the scope of this dissertation, but reviewed recently.[19]

Ionization Source. The selection of ionization source is a critical parameter in mass spectrometry as analytes must be ionized for separation based on mass to charge ratio to occur. Electron ionization (EI) is omnipresent in gas chromatography and offers the unique advantages of near universal gas-phase volatile analyte ionization and reproducible analyte fragmentation. Electrospray ionization (ESI) dominates liquid based direct injection (DI) and separation approaches.[20] ESI provides adequate sensitivity for a wide variety of metabolites but is susceptible to poor reproducibility caused by ionization suppression. Ionization suppression involves the reduction (or enhancement) in analyte ionization and signal intensity due to coelution with interfering analytes through a mechanism involving gas-phase or liquid-phase interactions still under investigation.[21] This issue is compounded in metabolomic analysis due to the ubiquity of suppressive species such as salts and organic buffers common in biological matrices such urine, plasma, and cellular extracts. The impact of ionization suppression on quantification can be corrected through careful sample matrix control and/or the use of isotopically labeled internal standards as discussed below. Atmospheric pressure chemical ionization (APCI) is used less frequently due to lower sensitivity for most metabolites but has been demonstrated to complement ESI by improving metabolome coverage through detection of neutral/lipophilic species such as cholesterol.[20] Atmospheric pressure photo ionization (APPI) has not been commonly applied to metabolomic analysis but was recently demonstrated to provide complementary ionization of non-polar analytes relative to ESI and APCI.[22] Analysis of solid samples such as blood spots and whole islets has been reported using non-separation based ionization techniques such as matrix assisted laser desorption/ionization (MALDI)[23-25], desorption electrospray ionization (DESI)[26], and direct analysis in real time (DART)[27]. These approaches have the advantage of speed although this benefit generally comes with a severe loss of sensitivity and specificity. To overcome these issues, such methods have been coupled with high resolution TOF-TOF[17] and LIT-Orbitrap[18] mass spectrometers to improve mass spectral resolution and specificity.

Stable Isotopes in Quantification. In addition to the plethora of routine factors that plague reproducibility in preparation and analysis of biological samples (e.g. degradation, heterogeneity, and biological variability) accurate quantification using mass spectrometry suffers from signal variability due to ionization suppression (discussed above). Traditional approaches to correct for matrix interferences such as standard

addition may be used, but are cumbersome, time-consuming, and impractical for multi-analyte analysis with large sample sets. Recently, stable isotope-labeled standards incorporating ^{13}C, ^{2}H, and ^{15}N have become available for many common metabolites to correct for such variability and are used extensively to improve the accuracy of metabolite quantification. Isotopically labeled standards have highly similar if not identical chemical properties to their endogenous analogs and therefore experience identical measurement variability caused by instrument response drift and ionization suppression. Identical chromatographic behavior is generally observed for ^{13}C and ^{15}N labeled analytes[28] while separation can occur for ^{2}H labeled analytes[29] leading to less accurate quantification and variable ionization suppression. Variability introduced during sample preparation (e.g. metabolite degradation and incomplete derivatization) are corrected by this approach also since both labeled and non-labeled species are impacted identically. However, many stable labeled standards have limited availability and/or are prohibitively expensive to synthesize.

As a solution to these issues, novel approaches to large-scale metabolite quantification in microbes have been reported recently involving the use of stable labeled internal references for all endogenously synthesized metabolites. These standards are generated through the use of metabolite extracts of microbes grown on stable labeled substrate (e.g. [U-^{13}C]-glucose).[30] Alternately, an approach has been demonstrated that involves growth of both microbial and mammalian cells used in biological experimentation with labeled substrate allowing for use of non-isotopically labeled authentic standards as internal standards.[31] Complications in quantification with these approaches may arise due to incomplete isotopic labeling which can generate a wide distribution of metabolite isotopes thereby decreasing the sensitivity and specificity of mass spectrometry detection.

Derivatization approaches with stable isotopically labeled reagents such as dansyl chloride have also been reported as an alternative approach to multi-analyte internal standard correction. This technique labels primary amine, secondary amine, and phenolic hydroxyl groups with labeled or unlabeled substrate for absolute quantification and differential profiling of metabolites.[32] The use of labeled silation reagents has also been reported for GC x GC analysis of metabolites in plasma.[33]

Separation Methods

GC-MS. Gas chromatography based separations are commonly used in metabolomic analysis. GC provides excellent chromatographic resolution and can be coupled with EI ionization sources which are less susceptible to ionization suppression and allow for rapid and unambiguous library based identification of unknowns. A major drawback of metabolite analysis by GC is that analytes must be volatile. Therefore GC is most commonly employed in conjunction with sample preparation procedures that use derivatization (e.g. trimethyl silane) to increase the volatility of metabolite classes such as sugars, sugar phosphates, amino acids, and fatty acids. These sample handling steps often decrease reproducibility and therefore require internal standardization to provide acceptable precision. Derivatization procedures also increase sample complexity and decrease sensitivity as multiple derivatives often form for a given metabolite dividing analyte signal between several chromatographic peaks. The inability to analyze important metabolite classes such as nucleotides and acyl-CoAs due to their high molecular weight and/or thermal lability is a further drawback.

LC-MS. LC techniques provide adequate separation for a broad range of metabolites but offer generally lower chromatographic resolution than GC. Several modes of HPLC separation including reverse-phase, ion pairing, and HILIC have been reported for metabolite analysis as detailed extensively in Chapter 2.

CE-MS. CE is an excellent separation technique for highly polar and ionic analytes making it a natural choice for metabolite analysis. CE also generates fast and highly efficient separations (several hundred thousand theoretical plates)[34] primarily due to the flat flow profile (non-laminar) and absence of slow mass transfer considerations in the separation process. Due to extremely low flow rates, interface with ESI nebulizers to achieve stable spray has been challenging; however, methods for detection of 198 metabolites in *E coli* have been reported.[35] Several approaches to coupling CE and ESI-MS have been developed and recently reviewed.[12] Unfortunately, the performance of CE-MS for routine metabolomic analysis has drawbacks such as the inability to separate neutral analytes. Micellar electrokinetic chromatography can overcome this issue although the surfactants required for this mode of separation are not MS friendly. Further limitations of commercial CE-MS instrumentation include poor reproducibility and

have led some researches to conclude LC-MS and GC-MS platforms are better suited to routine metabolomic analysis.[36]

Multi-Platform Techniques. Due to the inherent limitations of the various separation and ionization techniques, several groups have proposed using parallel approaches (e.g. GC-MS and LC-MS) to increase coverage of the metabolome.[36, 37] GC-MS and LC-MS are commonly used in parallel as GC-MS generally offers superior analysis of metabolite classes such as fatty acids whereas LC is superior in the assay of higher molecular weight and multiply charged metabolite classes such as nucleotides and acyl-CoAs. Dual HPLC methods have been proposed including HILIC for amines and ion-pairing for carboxylic acids and sugar phosphates.[38] Combined HILIC and reverse phase approaches have also been reported.[39]

Multidimensional separations have also been applied to metabolomic analysis to improve sensitivity and peak capacity. The application of GC x GC has been reported for the metabolomic analysis of microbes and plasma.[33, 37, 40] Although, the focus of much of the GC x GC research effort has been on methodology to improve chemometrics since the 3D data sets generated by the technique are particularly difficult to process.[41] LC x LC has been applied in a limited number of studies of microbes[42, 43] and found to substantially increase the number of detectable metabolites.

Data processing. Directed metabolomic analysis does not require specialized software as this approach can leverage conventional packages for chemical and biochemical analysis. Processing of undirected data offers unique challenges, primarily due to the > 1000 features (chromatographic peaks with mass/charge and retention time values) commonly detected in a chromatogram. Hence, data analysis remains a major bottleneck in an undirected metabolomic workflow and a great deal of effort has been placed on software development over the past several years. The ideal software application must accurately "pick" features (e.g. chromatographic peaks) from total ion chromatograms, accurately integrate often non-Gaussian or poorly resolved peaks, and identify the molecular ion based on concurrent detection of common adducts and/or fragments. Subsequent steps include feature "alignment" (binning of features across injections based on specified mass/charge and retention time windows) for group comparison and statistical analysis. Many applications have been developed by research groups to perform such analysis including XCMS[44], MZ Mine[45], and Maven[46].

The software company ACD/Labs has also developed the IntelliXtrac package for metabolomics. In addition, major instrument manufactures have developed proprietary software suites such as Mass Hunter / Mass Profiler Professional from Agilent Technologies, MarkerLynx from Waters, SIEVE from Thermo Scientific, and MarkerView from AB Sciex in an effort to provide "total solutions" for metabolomics analyses when combined with their hardware.

Metabolite Identification. Metabolite identification is a major challenge in LC-MS based metabolomics and can be costly and time consuming.[47] Databases have been developed to aid in metabolite ID such as METabolite LINk (METLIN)[48], the Human Metabolome Database (HMDB)[49], Kyoto Encyclopedia of Genes and Genomes (KEGG)[50], Madison Metabolomics Consortium Database (MMCD)[51], and ChemSpider, all reviewed recently.[47] These databases are searchable by measured m/z and provide a starting point for feature identification. Proposed metabolite identifications can then be evaluated based on match between theoretical and observed molecular weights and isotopic distribution patterns. MS/MS spectra are now available through many of these databases to improve the quality of proposed identifications.[47] The gold standard for unknown metabolite identification is retention time comparison to an authentic standard through a spiking study in addition to matching MS/MS spectra obtained on identical equipment.

Diabetes Background

β-cells found in the islets of Langerhans secrete insulin in response to elevated blood glucose through glucose stimulated insulin secretion (GSIS). The hormone insulin signals to liver, muscle, and fat cells to take up glucose from the blood and store it as the polymer glycogen for later use. Failure to adequately regulate insulin levels and consequently blood glucose causes diabetes resulting in serious long-term complications such as cardiovascular disease, chronic renal failure, and retinal damage.

GSIS is triggered by closure of K_{ATP} channels due to an increase in the ATP/ADP ratio concurrent with metabolism of glucose, primarily though glycolysis (Figure 1-3), the TCA cycle (Figure 1-4) and Pentose Phosphate Pathway (Figure 1-5). Closure of K_{ATP} channels cause membrane depolarization, opening of voltage sensitive Ca^{2+} channels, and subsequent exocytosis of insulin vesicles (Figure 1-2a). Besides this well established K_{ATP} dependent mechanism, considerable evidence supports the concept

that other metabolic processes also facilitate GSIS in K_{ATP} independent or amplifying pathways.[52] A variety of metabolic coupling factors including NADPH and long-chain acyl-CoAs have been implicated in both amplifying and triggering pathways. These coupling factors are generated through established pathways of energy metabolism in addition to cross-mitochondrial membrane cycling pathways (Figure 1-2b) as recently reviewed.[53-55] The pyruvate/malate shuttle involves conversion of oxaloacetate to malate then pyruvate before returning to oxaloacete generating NADPH at the expense of ATP and NADH. The pyruvate/citrate shuttle converts oxaloacetate and acetyl-CoA to citrate which is exported to the cytosol where it is converted back to oxaloacetate and acetyl-CoA. Oxaloacetate can then form pyruvate as in the pyruvate/malate shuttle generating NADPH. Acetyl-CoA can form malonyl-CoA to generate long-chain acyl-CoAs in fatty acid synthesis. The pyruvate/isocitrate shuttle involves oxaloacetate condensation with acetyl-CoA to form citrate, which is converted to isocitrate, then α-ketoglutarate and back to oxaloacetate generating NADPH. Fatty acid signaling has also been proposed which involves the synthesis of long-chain acyl-CoAs and phospholipids from malonyl-CoA generated by glycolysis and TCA cycle which inhibits fatty acid oxidation and increases the synthesis of long-chain acyl-CoAs and complex lipids which may participate in signaling.

Despite years of extensive β-cell research the precise metabolic pathways that facilitate GSIS and the mechanistic impact of metabolic coupling factors in β-cells are not fully understood.[56] Accordingly, there is a clear opportunity to develop and apply emerging analytical techniques such as LC-MS metabolomics platforms to gain further insight into the metabolic pathways involved in GSIS.

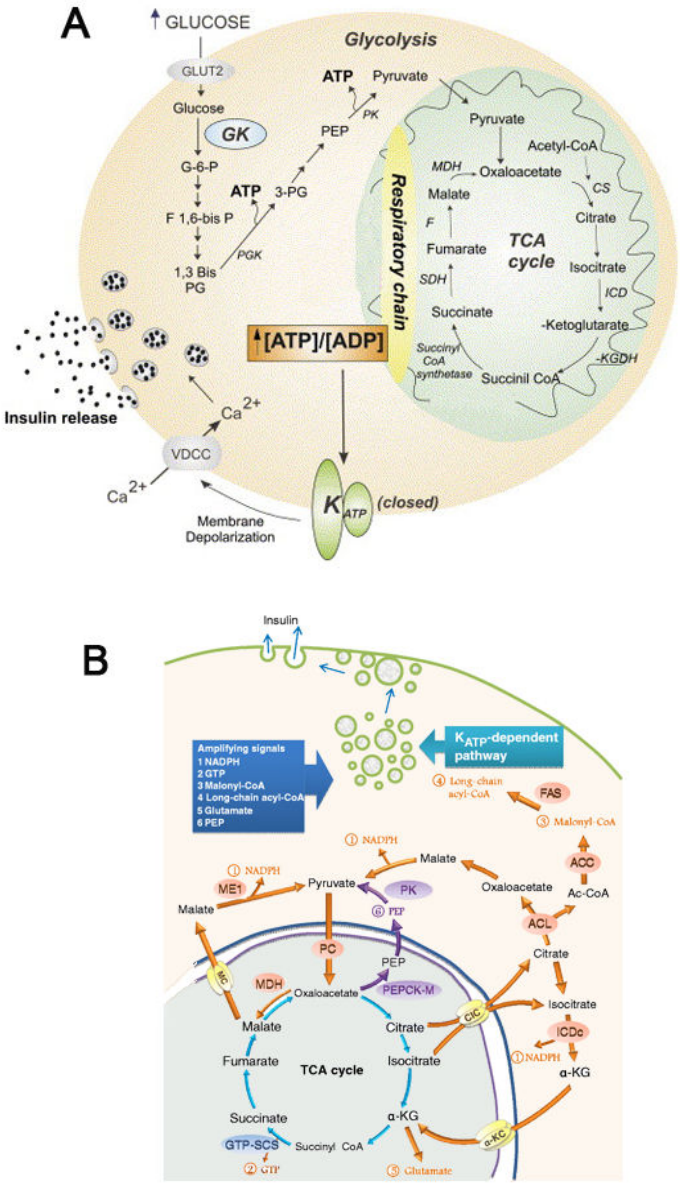

Figure 1-2. K_{ATP} Dependent and Independent Pathways of GSIS.

(A) Glucose-stimulated insulin release from pancreatic β-cells (adapted from[57]). Abbreviations are: glucose-6-phosphate (G-6-P), fructose 1,6-bisphosphate (F 1,6-bis P), 1,3-bisphosphoglycerate (1,3 Bis PG), 3-phosphoglycerate (3-PG), phosphoenolpyruvate (PEP), voltage dependent calcium channel (VDCC), citrate synthase (CS), isocitrate dehydrogenase (ICD), ketoglutarate dehydrogenase (KGDH), succinate dehydrogenase (SDH), fumarase (F), and malate dehydrogenase (MDH).

(B) Mitochondrial biochemical pathways that are involved in K_{ATP}-independent GSIS (adapted from[53]). Abbreviations are: acetyl-CoA (Ac-CoA), α-ketoglutarate (α-KG), isocitrate dehydrogenase (ICDc), acetyl-CoA citrate lyase (ACL), acetyl-CoA carboxylase (ACC), fatty acid synthase (FAS), pyruvate carboxylase (PC), malate dehydrogenase (MDH), malate carrier (MC), malic enzyme (ME), pyruvate kinase (PK), phosphoenolpyruvate carboxykinase (PEPCK), and citrate/isocitrate carrier (CIC).

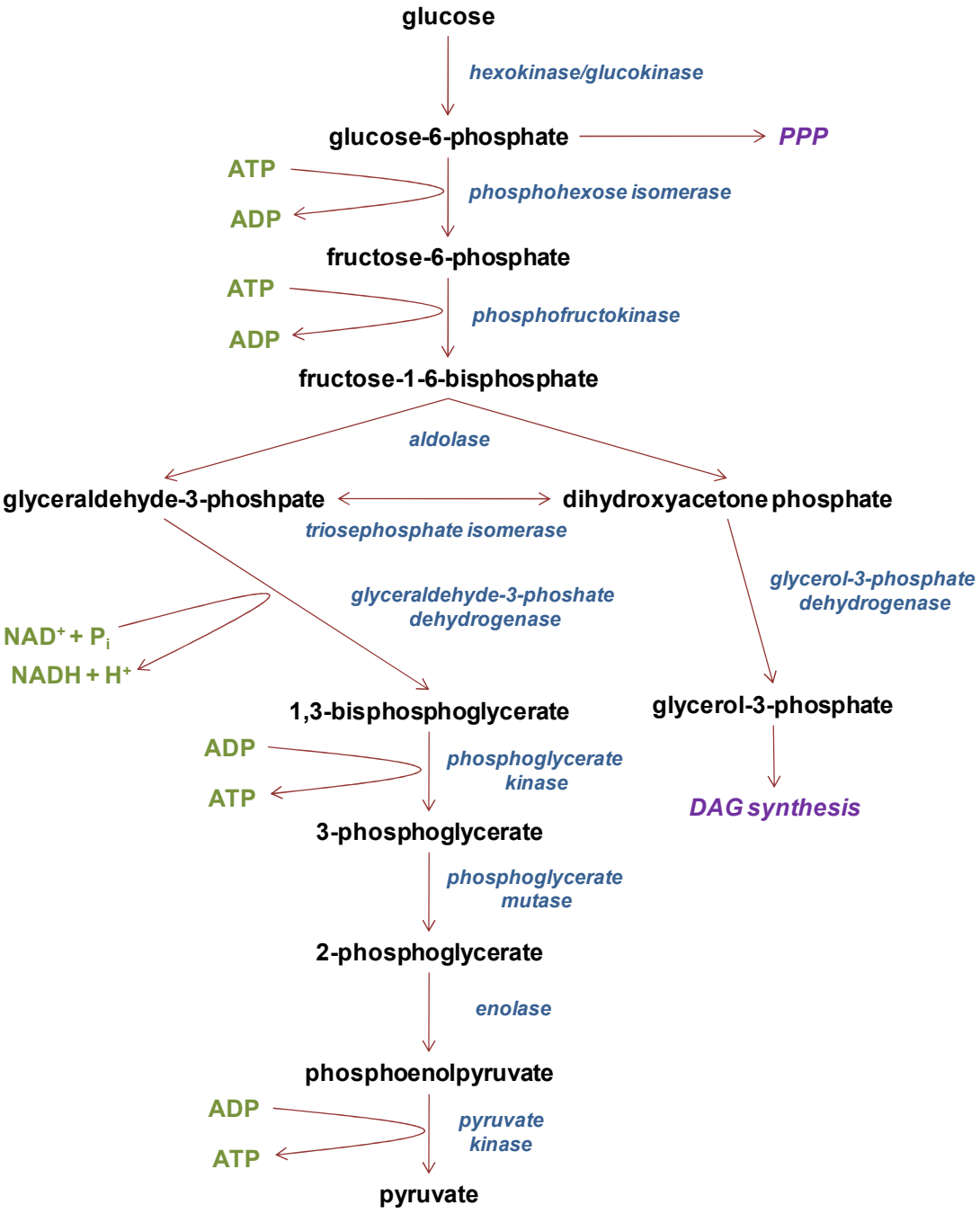

Figure 1-3. Glycolysis Pathway Map

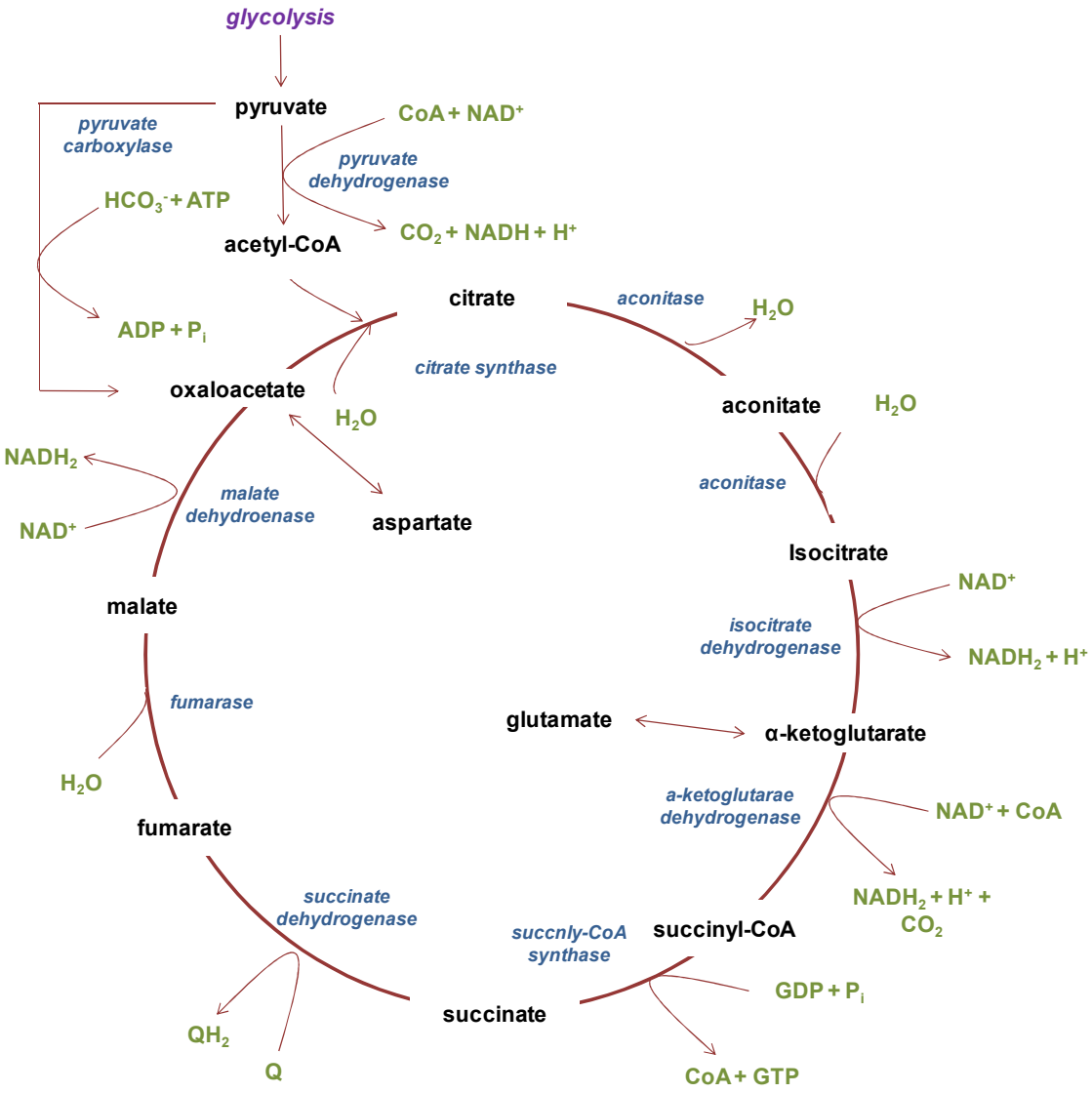

Figure 1-4. Pathway Map of the Tricarboxylic Acid (TCA) Cycle.

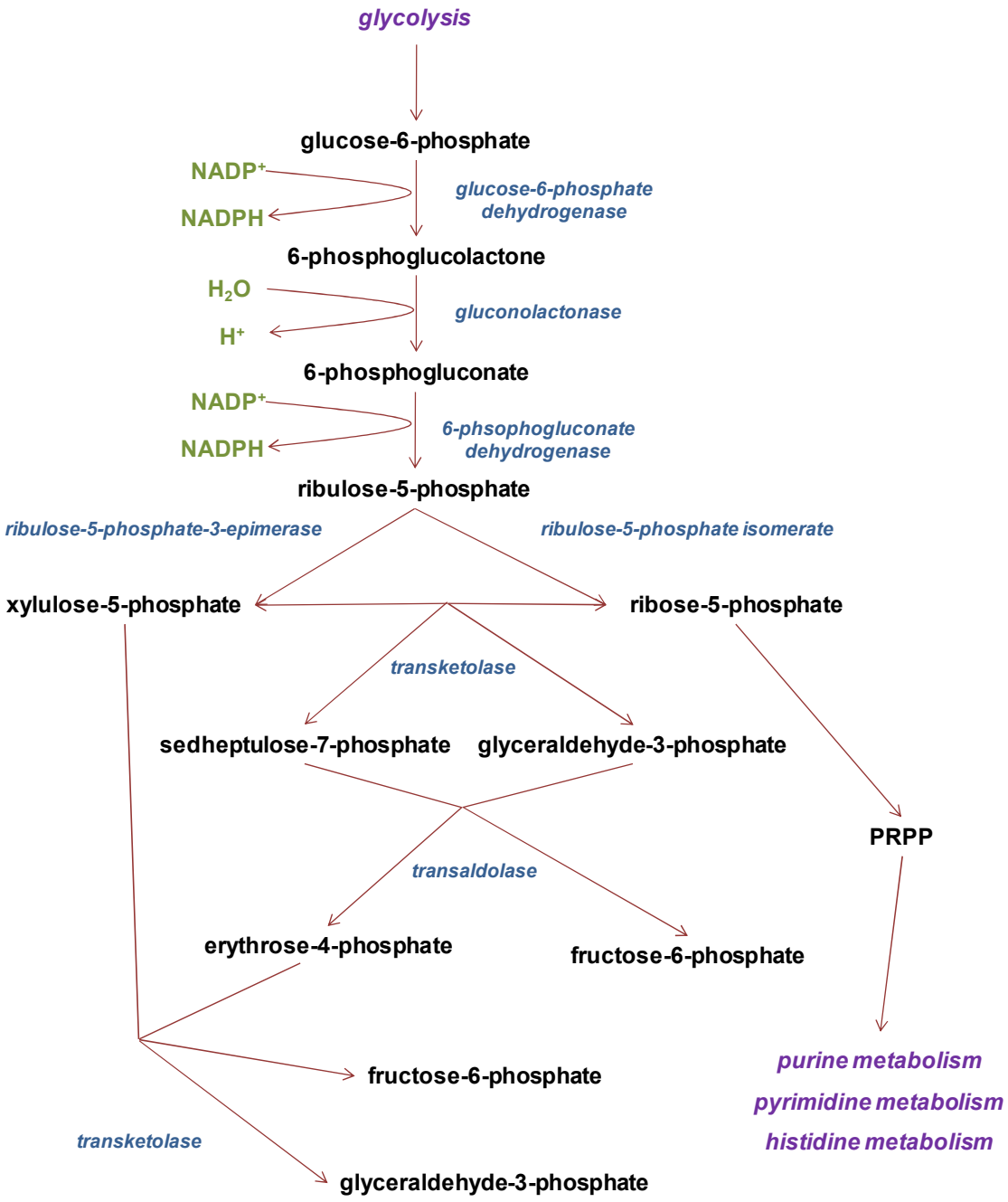

Figure 1-5. Pathway Map of the Pentose Phosphate Pathway (PPP).

Analytical Methods for Metabolite Measurement in β-Cells

Extensive investigations into mammalian β-cell metabolism have been conducted over the past 50 years to study biochemical responses to glucose and reviewed thoroughly.[52-54, 58-61] A fundamental breakthrough in mammalian β-cell research occurred in 1965 with the development of biological techniques to isolate islets from rat pancreas[62] enabling *ex vivo* experimentation. Primary islets were used nearly exclusively for experimentation through 1981 before clonal insulinoma lines were developed starting with MIN6 derived from hamster islets.[63] This discovery substantially accelerated β-cell research since islet tissue is difficult to isolate in analytically relevant quantities. The use of as many as 800 islets (total combined isolation of 5 rats) has been reported to generate enough material for a single replicate biological measurement.[64] Dozens of immortal lines have followed MIN6 and their properties recently reviewed.[65] These lines include INS-1 832/13 which has been used extensively since its introduction in 2000 to study fuel induced insulin secretion.[66] INS-1 832/13 shares many properties with primary β-cells including biphasic physiological response to glucose and normal response to non-glucose secretagogues.[61, 66] The analytical approaches used historically and at present to measure metabolites in β-cells are highlighted below.

Initial studies of isolated islets in the 1960s included research introducing fundamental concepts such as the dose-response relationship between glucose concentration and oxidation rate in β-cells and the preferential flux through oxidative pathways by measuring the specific activity of $^{14}CO_2$ generated during metabolism of [1-^{14}C]- and [6-^{14}C]-glucose.[67] Another study measured elevated levels of citrate using an enzymatic assay with fluorometric detection in islets of hyperglycemic mice.[68] An enzymatic cycling procedure was applied to measure glucose-6-phosphate and 6-phosphogluconate which were shown to increase in relation to extracellular glucose concentration.[69] A more comprehensive *in vivo* study used enzymatic fluorimetric procedures combined with an oil well method and enzymatic cycling of pyridine nucleotides to improve sensitivity in the 1970s. This study rivaled those carried out through the 2000s in scope by simultaneously measuring increases in 6 metabolites (glucose, glucose-6-phosphate, fructose-1,6-bisphoshpate, 6-phosphogluconate, ATP, and phosphocreatine) in rat islets at ~2, 5, and 60 min following glucose infusion concurrent with insulin release.[64] The scope and analytical techniques for metabolite

measurement evolved in the 1980s with measurement of 11 nucleotides in isolated rat islets by an anion exchange HPLC-UV method.[70] HPLC-UV was also reported for measurement of short chain acyl-CoAs in islets while total long chain acyl-CoAs were determined by an enzymatic-fluorimetric method.[71, 72]

In the 2000s, ^{1}H-NMR was used to measure incorporation of ^{13}C into glutamate from metabolism of [U-^{13}C]-glucose demonstrating pyruvate cycling (substrate cycle converting pyruvate to malate and back to pyruvate as a shuttle of reducing equivalents) in INS-1 cells.[73, 74] The use of ^{31}P-NMR was also reported for measuring mitochondrial ATP production in combination with tandem LC-MS (QQQ) to measure ADP, ATP, malate, citrate and aspartate.[75] QQQ was also used to study acetyl, succinyl, malonyl, and HMG-CoA in INS-1 832/13 cells.[76] Surprisingly, in the same study enzymatic assay remained the method of choice to measure malate, citrate, isocitrate, glutamate, aspartate, aconitate, and α-ketoglutarate yielding 11 metabolites total.[76] GC-FID was employed to measure lipids in INS-1 832/13 cells and 112 lipid species were reported.[77] GC-MS methodology was also used to measure pyruvate, lactate, citrate, α-ketoglutarate, succinate, fumarate, malate in INS1-832/13 cells[78] and a larger set of 16 metabolites (amino acids, carboxylic acids, and sugar phosphates) in a subsequent study.[79] In a novel application, MALDI was applied to the analysis of metabolites in islet tissue.[23] The utility of LC x LC in increasing detectable features was also demonstrated for metabolite profiling in islets. In the 2010s, GC-MS was used to quantify a more comprehensive set of amino acids, carboxylic acids, and sugar phosphates in INS-1 in a study of sample preparation (33 total)[80] and a study of GSIS (38 total) combined with a substantial set of unidentified features (164 total) through undirected analysis.[81]

β-Cell Metabolomics

The vast majority of studies into β-cell metabolism involve comparative measurement of a small number of metabolites in different experimental groups under culture conditions or with glucose stimulation at single time points. While such studies are useful, they provide limited insight into temporal and dose-dependent changes in β-cell metabolism important to a comprehensive investigation of insulin secretion.

Limited studies have investigated changes in metabolites with extracellular secretagogue concentration including measurement of glucose-6-phosphate and 6-phosphogluconate in islets with glucose.[69] The dose-response behavior of 10 nucleotides was measured in islets from 5 to 30 mM glucose[70] and 5 nucleotides from 0

to 20 mM glucose.[82] In another study, citrate and malate levels were measured in INS-1 with glucose concentrations from 4 to 20 mM.[83]

Additional studies have investigated temporal changes of select metabolites following stimulation. ATP was measured in INS-1 from 1 to 30 min post glucose stimulation comparing INS-1 exposed to leptin and control.[84] Another study measured malate, citrate, and aspartate in INS-1 cells from 5 to 120 min following glucose stimulation[75] and demonstrated increases in malate and citrate after as little as 5 min. Adenosine and guanine nucleotides were measured 15 s to 30 min post glucose stimulation in islets[85] and ADP, ATP, GDP, GTP, and UTP were measured from 5 to 60 min post glucose stimulation in islets.[82] ATP/ADP ratio and glucose-6-phosphate were measured from 1 to 8 min following glucose stimulation of mouse islets.[86] A time-course study from 0 to 8 min following glucose stimulation of islets was also used to demonstrate oscillations in ATP and citrate (up to 2-fold)[87] although the study lacked replicate measurements and confirmatory findings have not been published.

Clearly, measurement of the dose-response and temporal behavior of a more comprehensive portion of the β-cell metabolome concurrent with GSIS would prove beneficial in advancing our understanding of GSIS in β-cells and is a primary focus of this dissertation.

Dissertation Overview

The initial objectives of this research were to advance the field of metabolomics by developing an improved analytical method for LC-MS metabolite profiling and a sample preparation procedure amenable to rapid analysis of adherent mammalian cells such as INS-1. In the second phase of this project, these improved techniques were applied to study GSIS in INS-1 832/13 cells and investigate both dose-response and temporal changes in metabolite concentrations concurrent with GSIS to provide new insights into metabolic mechanisms and test prevailing hypothesis of GSIS.

Chapter 2 describes the development and performance of a hybrid AEX/HILIC-MS method for metabolite profiling well suited to the directed and undirected analysis of metabolites and cofactors implicated in β-cell metabolism. Chapter 3 describes the comprehensive development of a rapid sampling method for adherent mammalian cells. These improved methods were employed in Chapter 4 to study metabolic pathways and evaluate prevailing hypothesis of GSIS through dose-response and time-resolved

experiments. Alterations in metabolic pathways concurrent with decreased GSIS due to exposure to lipotoxic and glucotoxic culture conditions are demonstrated in Chapter 5.

References

1. Fiehn, O. 2002. Metabolomics – the link between genotypes and phenotypes. *Plant Molecular Biology* 48:155-171.
2. Nicholson, J.K., Lindon, J.C., and Holmes, E. 1999. 'Metabonomics': understanding the metabolic responses of living systems to pathophysiological stimuli via multivariate statistical analysis of biological NMR spectroscopic data. *Xenobiotica* 29:1181-1189.
3. Robertson, D.G. 2005. Metabonomics in Toxicology: A Review. *Toxicological Sciences* 85:809-822.
4. John C. Lindon, J.K.N., and Elaine Holmes. 2007. The Handbook of Metabonomics and Metabolomics. J.K.N. John C. Lindon, and Elaine Holmes, editor. Netherlands: Elsevier 1-33.
5. Mamas, M., Dunn, W., Neyses, L., and Goodacre, R. 2011. The role of metabolites and metabolomics in clinically applicable biomarkers of disease. *Archives of Toxicology* 85:5-17.
6. Saghatelian, A., Trauger, S.A., Want, E.J., Hawkins, E.G., Siuzdak, G., and Cravatt, B.F. 2004. Assignment of Endogenous Substrates to Enzymes by Global Metabolite Profiling†. *Biochemistry* 43:14332-14339.
7. Gibney, M.J., Walsh, M., Brennan, L., Roche, H.M., German, B., and van Ommen, B. 2005. Metabolomics in human nutrition: opportunities and challenges. *The American Journal of Clinical Nutrition* 82:497-503.
8. Fiehn, O. 2007. The Handbook of Metabonomics and Metabolomics. In *The Handbook of Metabonomics and Metabolomics*. J.K.N. John C. Lindon, and Elaine Holmes, editor. Netherlands: Elsevier 35-54.
9. Weljie, A.M., Newton, J., Mercier, P., Carlson, E., and Slupsky, C.M. 2006. Targeted Profiling: Quantitative Analysis of 1H NMR Metabolomics Data. *Analytical Chemistry* 78:4430-4442.
10. Serkova, N.J., Zhang, Y., Coatney, J.L., Hunter, L., Wachs, M.E., Niemann, C.U., and Mandell, M.S. 2007. Early detection of graft failure using the blood metabolic profile of a liver recipient. *Transplantation* 83:517-521.
11. Wishart, D.S., Querengesser, L.M.M., Lefebvre, B.A., Epstein, N.A., Greiner, R., and Newton, J.B. 2001. Magnetic Resonance Diagnostics: A New Technology for High-Throughput Clinical Diagnostics. *Clin Chem* 47:1918-1921.
12. Monton, M.R.N., and Soga, T. 2007. Metabolome analysis by capillary electrophoresis-mass spectrometry. *Journal of Chromatography A* 1168:237-246.
13. Begley, P., Francis-McIntyre, S., Dunn, W.B., Broadhurst, D.I., Halsall, A., Tseng, A., Knowles, J., Goodacre, R., and Kell, D.B. 2009. Development and Performance of a Gas Chromatography−Time-of-Flight Mass Spectrometry Analysis for Large-Scale Nontargeted Metabolomic Studies of Human Serum. *Analytical Chemistry* 81:7038-7046.
14. Wei, R., Li, G., and Seymour, A.B. 2010. High-Throughput and Multiplexed LC/MS/MRM Method for Targeted Metabolomics. *Analytical Chemistry* 82:5527-5533.
15. Lu, W., Clasquin, M.F., Melamud, E., Amador-Noguez, D., Caudy, A.A., and Rabinowitz, J.D. 2010. Metabolomic Analysis via Reversed-Phase Ion-Pairing Liquid Chromatography Coupled to a Stand Alone Orbitrap Mass Spectrometer. *Analytical Chemistry* 82:3212-3221.

16. Zheng, C., Zhang, S., Ragg, S., Raftery, D., and Vitek, O. 2011. Identification and quantification of metabolites in 1H NMR spectra by Bayesian model selection. *Bioinformatics* 27:1637-1644.
17. Sun, G., Yang, K., Zhao, Z., Guan, S., Han, X., and Gross, R.W. 2007. Shotgun Metabolomics Approach for the Analysis of Negatively Charged Water-Soluble Cellular Metabolites from Mouse Heart Tissue. *Analytical Chemistry* 79:6629-6640.
18. Weber, R.J.M., Southam, A.D., Sommer, U., and Viant, M.R. 2011. Characterization of Isotopic Abundance Measurements in High Resolution FT-ICR and Orbitrap Mass Spectra for Improved Confidence of Metabolite Identification. *Analytical Chemistry* 83:3737-3743.
19. Lei, Z., Huhman, D., and Sumner, L.W. 2011. Mass Spectrometry Strategies in Metabolomics. *Journal of Biological Chemistry*.
20. Nordstrom, A., Want, E., Northen, T., Lehtio, J., and Siuzdak, G. 2007. Multiple Ionization Mass Spectrometry Strategy Used To Reveal the Complexity of Metabolomics. *Analytical Chemistry* 80:421-429.
21. Côté, C., Bergeron, A., Mess, J.-N., Furtado, M., and Garofolo, F. 2009. Matrix effect elimination during LC–MS/MS bioanalytical method development. *Bioanalysis* 1:1243-1257.
22. An, Z., Chen, Y., Zhang, R., Song, Y., Sun, J., He, J., Bai, J., Dong, L., Zhan, Q., and Abliz, Z. 2010. Integrated Ionization Approach for RRLC−MS/MS-based Metabonomics: Finding Potential Biomarkers for Lung Cancer. *Journal of Proteome Research* 9:4071-4081.
23. Edwards, J.L., and Kennedy, R.T. 2005. Metabolomic Analysis of Eukaryotic Tissue and Prokaryotes Using Negative Mode MALDI Time-of-Flight Mass Spectrometry. *Analytical Chemistry* 77:2201-2209.
24. Wang, H.-Y., Chu, X., Zhao, Z.-X., He, X.-S., and Guo, Y.-L. 2011. Analysis of low molecular weight compounds by MALDI-FTICR-MS. *Journal of Chromatography B* 879:1166-1179.
25. Koulman, A., Petras, D., Narayana, V.K., Wang, L., and Volmer, D.A. 2009. Comparative High-Speed Profiling of Carboxylic Acid Metabolite Levels by Differential Isotope-Coded MALDI Mass Spectrometry. *Analytical Chemistry* 81:7544-7551.
26. Jackson, A.U., Werner, S.R., Talaty, N., Song, Y., Campbell, K., Cooks, R.G., and Morgan, J.A. 2008. Targeted metabolomic analysis of Escherichia coli by desorption electrospray ionization and extractive electrospray ionization mass spectrometry. *Analytical Biochemistry* 375:272-281.
27. Zhou, M., McDonald, J., and Fernández, F. 2010. Optimization of a direct analysis in real time/time-of-flight mass spectrometry method for rapid serum metabolomic fingerprinting. *Journal of the American Society for Mass Spectrometry* 21:68-75.
28. Di Palma, S., Raijmakers, R., Heck, A.J.R., and Mohammed, S. 2011. Evaluation of the deuterium isotope effect in ZIC-cHILIC separations for implementation in a quantitative proteomic approach. *Analytical Chemistry*:null-null.
29. Zhang, R., Sioma, C.S., Wang, S., and Regnier, F.E. 2001. Fractionation of Isotopically Labeled Peptides in Quantitative Proteomics. *Analytical Chemistry* 73:5142-5149.
30. Uehara, T., Yokoi, A., Aoshima, K., Tanaka, S., Kadowaki, T., Tanaka, M., and Oda, Y. 2009. Quantitative Phosphorus Metabolomics Using Nanoflow Liquid Chromatography-Tandem Mass Spectrometry and Culture-Derived Comprehensive Global Internal Standards. *Analytical Chemistry* 81:3836-3842.
31. Bennett, B.D., Yuan, J., Kimball, E.H., and Rabinowitz, J.D. 2008. Absolute quantitation of intracellular metabolite concentrations by an isotope ratio-based approach. *Nat. Protocols* 3:1299-1311.
32. Guo, K., and Li, L. 2009. Differential 12C-/13C-Isotope Dansylation Labeling and Fast Liquid Chromatography/Mass Spectrometry for Absolute and Relative Quantification of the Metabolome. *Analytical Chemistry* 81:3919-3932.
33. Huang, X., and Regnier, F.E. 2007. Differential Metabolomics Using Stable Isotope Labeling and Two-Dimensional Gas Chromatography with Time-of-Flight Mass Spectrometry. *Analytical Chemistry* 80:107-114.

34. Skoog, D.A.H., F.J.; Nieman, T.A. 1998. *Principles of Instrumental Analysis*. Philadelphia: Saunders college Publishing.
35. Ohashi, Y., Hirayama, A., Ishikawa, T., Nakamura, S., Shimizu, K., Ueno, Y., Tomita, M., and Soga, T. 2008. Depiction of metabolome changes in histidine-starved Escherichia coli by CE-TOFMS. *Molecular BioSystems* 4:135-147.
36. Bu□scher, J.r.M., Czernik, D., Ewald, J.C., Sauer, U., and Zamboni, N. 2009. Cross-Platform Comparison of Methods for Quantitative Metabolomics of Primary Metabolism. *Analytical Chemistry* 81:2135-2143.
37. Yang, S., Sadilek, M., Synovec, R.E., and Lidstrom, M.E. 2009. Liquid chromatography-tandem quadrupole mass spectrometry and comprehensive two-dimensional gas chromatography-time-of-flight mass spectrometry measurement of targeted metabolites of Methylobacterium extorquens AM1 grown on two different carbon sources. *Journal of Chromatography A* 1216:3280-3289.
38. Reaves, M.L., and Rabinowitz, J.D. 2011. Metabolomics in systems microbiology. *Current Opinion in Biotechnology* 22:17-25.
39. Yang, Q., Shi, X., Wang, Y., Wang, W., He, H., Lu, X., and Xu, G. 2010. Urinary metabonomic study of lung cancer by a fully automatic hyphenated hydrophilic interaction/RPLC-MS system. *Journal of Separation Science* 33:1495-1503.
40. Dunn, W.B., Knowles, J.D., Broadhurst, D., Williams, R., Ashworth, J.J., Cameron, M., and Kell, D.B. 2006. Closed-Loop, Multiobjective Optimization of Two-Dimensional Gas Chromatography/Mass Spectrometry for Serum Metabolomics. *Analytical Chemistry* 79:464-476.
41. Pierce, K.M., Hoggard, J.C., Mohler, R.E., and Synovec, R.E. 2008. Recent advancements in comprehensive two-dimensional separations with chemometrics. *Journal of Chromatography A* 1184:341-352.
42. Edwards, J.L., Edwards, R.L., Reid, K.R., and Kennedy, R.T. 2007. Effect of decreasing column inner diameter and use of off-line two-dimensional chromatography on metabolite detection in complex mixtures. *Journal of Chromatography A* 1172:127-134.
43. Fairchild, J.N., Horvath, K., Gooding, J.R., Campagna, S.R., and Guiochon, G. 2010. Two-dimensional liquid chromatography/mass spectrometry/mass spectrometry separation of water-soluble metabolites. *Journal of Chromatography A* 1217:8161-8166.
44. Smith, C.A., Want, E.J., O'Maille, G., Abagyan, R., and Siuzdak, G. 2006. XCMS:□ Processing Mass Spectrometry Data for Metabolite Profiling Using Nonlinear Peak Alignment, Matching, and Identification. *Analytical Chemistry* 78:779-787.
45. Katajamaa, M., Miettinen, J., and Orešič, M. 2006. MZmine: toolbox for processing and visualization of mass spectrometry based molecular profile data. *Bioinformatics* 22:634-636.
46. Melamud, E., Vastag, L., and Rabinowitz, J.D. 2010. Metabolomic Analysis and Visualization Engine for LC−MS Data. *Analytical Chemistry* 82:9818-9826.
47. Kertesz, T.M., Hill, D.W., Albaugh, D.R., Hall, L.H., Hall, L.M., and Grant, D.F. 2009. Database searching for structural identification of metabolites in complex biofluids for mass spectrometry-based metabonomics. *Bioanalysis* 1:1627-1643.
48. Smith, C.A., O'Maille, G., Want, E.J., Qin, C., Trauger, S.A., Brandon, T.R., Custodio, D.E., Abagyan, R., and Siuzdak, G. 2005. METLIN: a metabolite mass spectral database. *Ther Drug Monit* 27:747-751.
49. Wishart, D.S., Knox, C., Guo, A.C., Eisner, R., Young, N., Gautam, B., Hau, D.D., Psychogios, N., Dong, E., Bouatra, S., et al. 2009. HMDB: a knowledgebase for the human metabolome. *Nucleic Acids Research* 37:D603-D610.
50. Okuda, S., Yamada, T., Hamajima, M., Itoh, M., Katayama, T., Bork, P., Goto, S., and Kanehisa, M. 2008. KEGG Atlas mapping for global analysis of metabolic pathways. *Nucleic Acids Research* 36:W423-W426.
51. Markley, J.L., Anderson, M.E., Cui, Q., Eghbalnia, H.R., Lewis, I.A., Hegeman, A.D., Li, J., Schulte, C.F., Sussman, M.R., Westler, W.M., et al. 2007. New bioinformatics resources for metabolomics. *Pac Symp Biocomput*:157-168.

52. Jensen, M.V., Joseph, J.W., Ronnebaum, S.M., Burgess, S.C., Sherry, A.D., and Newgard, C.B. 2008. Metabolic cycling in control of glucose-stimulated insulin secretion. *Am J Physiol Endocrinol Metab* 295:E1287-1297.
53. Jitrapakdee, S., Wutthisathapornchai, A., Wallace, J.C., and MacDonald, M.J. 2010. Regulation of insulin secretion: role of mitochondrial signalling. *Diabetologia* 53:1019-1032.
54. Henquin, J.C., Nenquin, M., Ravier, M.A., and Szollosi, A. 2009. Shortcomings of current models of glucose-induced insulin secretion. *Diabetes Obes Metab* 11 Suppl 4:168-179.
55. Muoio, D.M., and Newgard, C.B. 2008. Molecular and metabolic mechanisms of insulin resistance and [beta]-cell failure in type 2 diabetes. *Nature Reviews Molecular Cell Biology* 9:193-205.
56. Jensen, M.V., Joseph, J.W., Ronnebaum, S.M., Burgess, S.C., Sherry, A.D., and Newgard, C.B. 2008. Metabolic cycling in control of glucose-stimulated insulin secretion. *Am. J. Physiol. Endocrinol. Metab.* 295:E1287-1297.
57. Remedi, M.S., Nichols, C.G., and Koster, J.C. 2006. The mitochondria and insulin release: Nnt just a passing relationship. *Cell Metabolism* 3:5-7.
58. Sener, A., and Malaisse, W.J. 1984. Nutrient metabolism in islet cells. *Experientia* 40:1026-1035.
59. Nolan, C.J., and Prentki, M. 2008. The islet [beta]-cell: fuel responsive and vulnerable. *Trends in Endocrinology and Metabolism* 19:285-291.
60. Tarasov, A., Dusonchet, J., and Ashcroft, F. 2004. Metabolic Regulation of the Pancreatic Beta-Cell ATP-Sensitive K+ Channel. *Diabetes* 53:S113-S122.
61. Straub, S.G., and Sharp, G.W.G. 2002. Glucose-stimulated signaling pathways in biphasic insulin secretion. *Diabetes/Metabolism Research and Reviews* 18:451-463.
62. Keen, H., Sells, R., and Jarrett, R. 1965. A method for the study of the metabolism of isolated mammalian islets of Langerhans and some preliminary results. *Diabetologia* 1:28-32.
63. Santerre, R.F., Cook, R.A., Crisel, R.M., Sharp, J.D., Schmidt, R.J., Williams, D.C., and Wilson, C.P. 1981. Insulin synthesis in a clonal cell line of simian virus 40-transformed hamster pancreatic beta cells. *Proc Natl Acad Sci U S A* 78:4339-4343.
64. Matschinsky, F.M., Ellerman, J.E., Krzanowski, J., Kotler-Brajtburg, J., Landgraf, R., and Fertel, R. 1971. The Dual Function of Glucose in Islets of Langerhans. *Journal of Biological Chemistry* 246:1007-1011.
65. Skelin, M., Rupnik, M., and Cencic, A. 2010. Pancreatic beta cell lines and their applications in diabetes mellitus research. *Altex* 27:105-113.
66. Hohmeier, H.E., Mulder, H., Chen, G., Henkel-Rieger, R., Prentki, M., and Newgard, C.B. 2000. Isolation of INS-1-derived cell lines with robust ATP-sensitive K+ channel-dependent and -independent glucose-stimulated insulin secretion. *Diabetes* 49:424-430.
67. Jarrett, R.J., and Keen, H. 1966. GLUCOSE METABOLISM OF ISOLATED MAMMALIAN ISLETS OF LANGERHANS. *The Lancet* 287:633-635.
68. Matschinsky, F.M., Rutherford, C.R., and Ellerman, J.E. 1968. Accumulation of citrate in pancreatic islets of obese hyperglycemic mice. *Biochemical and Biophysical Research Communications* 33:855-862.
69. Montague, W., and Taylor, K.W. 1969. Islet-cell metabolism during insulin release. Effects of glucose, citrate, octanoate, tolbutamide, glucagon and theophylline. *Biochem J* 115:257-262.
70. Hoenig, M., and Matschinsky, F.M. 1987. HPLC analysis of nucleotide profiles in glucose-stimulated perifused rat islets. *Metabolism* 36:295-301.
71. Liang, Y., and Matschinsky, F.M. 1991. Content of CoA-esters in perifused rat islets stimulated by glucose and other fuels. *Diabetes* 40:327-333.
72. Prentki, M., Vischer, S., Glennon, M.C., Regazzi, R., Deeney, J.T., and Corkey, B.E. 1992. Malonyl-CoA and long chain acyl-CoA esters as metabolic coupling factors in nutrient-induced insulin secretion. *Journal of Biological Chemistry* 267:5802-5810.
73. Lu, D., Mulder, H., Zhao, P., Burgess, S.C., Jensen, M.V., Kamzolova, S., Newgard, C.B., and Sherry, A.D. 2002. 13C NMR isotopomer analysis reveals a connection

between pyruvate cycling and glucose-stimulated insulin secretion (GSIS). *Proceedings of the National Academy of Sciences of the United States of America* 99:2708-2713.
74. Boucher, A., Lu, D., Burgess, S.C., Telemaque-Potts, S., Jensen, M.V., Mulder, H., Wang, M.-Y., Unger, R.H., Sherry, A.D., and Newgard, C.B. 2004. Biochemical Mechanism of Lipid-induced Impairment of Glucose-stimulated Insulin Secretion and Reversal with a Malate Analogue. *Journal of Biological Chemistry* 279:27263-27271.
75. Pongratz, R.L., Kibbey, R.G., Kirkpatrick, C.L., Zhao, X., Pontoglio, M., Yaniv, M., Wollheim, C.B., Shulman, G.I., and Cline, G.W. 2009. Mitochondrial Dysfunction Contributes to Impaired Insulin Secretion in INS-1 Cells with Dominant-negative Mutations of HNF-1α and in HNF-1α-deficient Islets. *Journal of Biological Chemistry* 284:16808-16821.
76. MacDonald, M.J., Smith, A.D., 3rd, Hasan, N.M., Sabat, G., and Fahien, L.A. 2007. Feasibility of pathways for transfer of acyl groups from mitochondria to the cytosol to form short chain acyl-CoAs in the pancreatic beta cell. *Journal of Biological Chemistry* 282:30596-30606.
77. MacDonald, M.J., Dobrzyn, A., Ntambi, J., and Stoker, S.W. 2008. The role of rapid lipogenesis in insulin secretion: Insulin secretagogues acutely alter lipid composition of INS-1 832/13 cells. *Archives of Biochemistry and Biophysics* 470:153-162.
78. Jensen, M.V., Joseph, J.W., Ilkayeva, O., Burgess, S., Lu, D., Ronnebaum, S.M., Odegaard, M., Becker, T.C., Sherry, A.D., and Newgard, C.B. 2006. Compensatory responses to pyruvate carboxylase suppression in islet beta-cells. Preservation of glucose-stimulated insulin secretion. *Journal of Biological Chemistry* 281:22342-22351.
79. Fernandez, C., Fransson, U., Hallgard, E., Spégel, P., Holm, C., Krogh, M., Wårell, K., James, P., and Mulder, H. 2007. Metabolomic and Proteomic Analysis of a Clonal Insulin-Producing β-Cell Line (INS-1 832/13). *Journal of Proteome Research* 7:400-411.
80. Danielsson, A.P.H., Moritz, T., Mulder, H., and Spégel, P. 2010. Development and optimization of a metabolomic method for analysis of adherent cell cultures. *Analytical Biochemistry* 404:30-39.
81. Spegel, P., Malmgren, S., Sharoyko, V.V., Newsholme, P., Koeck, T., and Mulder, H. 2011. Metabolomic analyses reveal profound differences in glycolytic and tricarboxylic acid cycle metabolism in glucose-responsive and -unresponsive clonal beta-cell lines. *Biochemical Journal* 435:277-284.
82. Detimary, P., Van den Berghe, G., and Henquin, J.-C. 1996. Concentration Dependence and Time Course of the Effects of Glucose on Adenine and Guanine Nucleotides in Mouse Pancreatic Islets. *Journal of Biological Chemistry* 271:20559-20565.
83. Schuit, F., De Vos, A., Farfari, S., Moens, K., Pipeleers, D., Brun, T., and Prentki, M. 1997. Metabolic fate of glucose in purified islet cells. Glucose-regulated anaplerosis in beta cells. *Journal of Biological Chemistry* 272:18572-18579.
84. Lam, N., Cheung, A., Riedel, M., Light, P., Cheeseman, C., and Kieffer, T. 2004. Leptin reduces glucose transport and cellular ATP levels in INS-1 beta-cells. *Journal of Molecular Endocrinology* 32:415-424.
85. Meglasson, M.D., Nelson, J., Nelson, D., and Erecinska, M. 1989. Bioenergetic response of pancreatic islets to stimulation by fuel molecules. *Metabolism* 38:1188-1195.
86. Nilsson, T., Schultz, V., Berggren, P.O., Corkey, B.E., and Tornheim, K. 1996. Temporal patterns of changes in ATP/ADP ratio, glucose 6-phosphate and cytoplasmic free Ca2+ in glucose-stimulated pancreatic beta-cells. *Biochemical Journal* 314 (Pt 1):91-94.
87. MacDonald, M.J., Fahien, L.A., Buss, J.D., Hasan, N.M., Fallon, M.J., and Kendrick, M.A. 2003. Citrate oscillates in liver and pancreatic beta cell mitochondria and in INS-1 insulinoma cells. *Journal of Biological Chemistry* 278:51894-51900.

CHAPTER 2
Development of a Hybrid Anion Exchange/Hydrophilic Interaction Liquid Chromatographic Method for Metabolomic Analysis

Introduction

HPLC-MS dominates metabolomic measurements due to its high sensitivity, specificity, and ease of multi-analyte quantification.[1] HPLC-MS also offers advantages over GC-MS such as the ability to assay a wider range of analytes including high molecular weight and thermally labile species.

Separation of metabolites from salts, buffers, and other metabolites present in a sample is necessary to achieve reproducible and sensitive quantification in HPLC-MS, primarily due to ionization suppression[2-4] as discussed in Chapter 1. Chromatographic separation is also important for metabolite identification by mass spectrometry since many metabolites have similar or identical molecular weights. Moreover, structural similarities may also lead to identical collision induced dissociation fragments thereby diminishing the potential for MS-MS based separation.[5] Selectivity is further diminished with common isotopic labeling experiments that substantially increase the mass range impacted by a given analyte though extended isotopic distribution patterns. Hence, good chromatographic performance is vital to maximize the sensitivity and selectivity possible with mass spectrometry based analysis.

Adequate retention and separation of small polar metabolites is especially challenging. Many metabolites of interest in central metabolism are hydrophilic sugars, sugar phosphates, carboxylic acids, and nucleotides that are poorly retained by conventional reversed phase approaches. Separation of polar metabolites from suppressive salts and buffers common in biofluids and cell culture media is challenging since these species have similar chromatographic properties to metabolites and can be present at concentrations several orders of magnitude higher than analytes of interest. Furthermore, common metabolites have tricarboxylic acid and tri-phosphate

functionalities that participate in strong secondary interactions with metal impurities in silica stationary phases causing poor peak shape.

A variety of chromatographic approaches have been developed for metabolomic analysis. Several reverse phase methods have been proposed using C_{18} columns that incorporate polar embedded groups to protect against stationary phase collapse. These methods are compatible with 100% aqueous mobile phases to provide enhanced retention of polar analytes.[6-8] However, performance of this approach remains poor with inadequate retention and resolution of many metabolite classes such as sugars, sugar phosphates, and nucleotides.[9] Also, peak broadening is problematic due to high levels of organic solvents commonly present in cellular extracts (e.g. band spreading at the column head with injection of strong solvent). To improve retention, methods using volatile ion pairing agents such as tributyl amine have been developed.[10-12] These methods have proven effective for the analysis of charged metabolites, although the pairing agent contaminates the HPLC system (tubing and degasser); therefore, HPLC equipment must be dedicated for use with these methods.[13, 14]

Hydrophilic Interaction Liquid Chromatography (HILIC) has been increasingly used in the past decade for polar metabolite analysis.[7-9, 12, 15-17] The HILIC mode of separation is based on analyte interaction with an adsorbed water layer on the surface of a polar stationary phase and offers excellent retention of polar molecules. However, chromatographic efficiencies for these polar stationary phases are generally lower than conventional C_{18} phases.[14] A novel hybrid HILIC/anion exchange method (HILIC/AEX) employing a cationic polar stationary phase was reported recently[9] using a Luna propyl amine column and basic mobile phase (20 mM ammonium acetate, pH 9.45) allowing for weak anion exchange interaction in addition to the HILIC mechanism of retention.

In this study, we evaluated a polar embedded reverse phase column (Atlantis C_{18}), and several HILIC columns (Halo HILIC, Luna HILIC, Diamond Hydride, and Luna NH_2) for the analysis of metabolites important in the study of central energy metabolism such as those from glycolysis, the TCA cycle, amino acids, and related nucleotide cofactors. The Luna NH_2 column (HILIC/AEX method) was found to provide superior performance. The impact of operating conditions such as temperature and ionic strength were evaluated for this column and conditions chosen to maximize sensitivity, reproducibility, and column lifetime. We report a HILIC/AEX method using the Luna NH_2 column well-suited to the global metabolite profiling of cellular extracts.

Experimental

Materials. All reagents were purchased from Sigma-Aldrich (St. Louis, MO) unless otherwise noted. HPLC grade acetonitrile was purchased from Burdick & Jackson (Muskegon, MI). Mass spectrometry grade formic acid, ammonium acetate, and ammonium hydroxide was used for all mobile phase preparation. pH adjustment was performed without contact between the pH meter electrode and the bulk mobile phase to reduce contamination.

Equipment. Chromatographic separations were performed with an Agilent Technologies (Santa Clara, CA) 1200 HPLC system and Agilent LC/MSD-TOF. HPLC columns studied in these experiments are listed in Table 2-1.

Column Screen. A set of key metabolites (Table 2-2) was assayed using five different silica based HPLC columns to assess chromatographic performance (R_s and k') of each method. Reverse phase, HILIC, and HILIC/AEX methods were tested using columns and conditions detailed in Table 2-3. The operating parameters used for all experiments are detailed in Table 2-4. A pH of 9.9 was chosen for the HILIC/AEX method based on the k' for GTP, the most strongly retained metabolite investigated. Mobile phase pH was increased from pH 9.5 (reported previously) to 9.9 to afford a k' of ~2 for GTP with 100% aqueous mobile phase (i.e., the strongest mobile phase).

Method Optimization. The effect of column temperature on the chromatographic performance (R_s and k') of key metabolites was assessed at 15, 25, 30, 35, and 40 °C. The HPLC column was equilibrated for 30 min at each temperature prior to each injection. The impact of ionic strength was also evaluated (concentration of pH 9.9 NH_4OAc in mobile phase B) on chromatographic performance of key metabolites at 5, 10, 20, and 40 mM. The HPLC column was equilibrated for 20 column volumes in each mobile phase prior to injection.

Table 2-1. Columns and Mobile Phase for HPLC Metabolite Screen

Manufacturer	Support Line	Phase	Dimensions	Mobile Phase
Waters	Atlantis	C_{18}	2.1 x 150 mm, 2.7 µm	0.1% formic acid pH 2.3
Advance Material Technology	Halo HILIC	SiO_2	2.1 x 150 mm, 3.5 µm	10 mM NH_4OAc pH 6.8
Phenomenex	Luna HILIC	diol	2.1 x 150 mm, 3 µm	10 mM NH_4OAc pH 6.8
Cogent	Diamond Hydride	SiH	2.1 x 150 mm, 4 µm	10 mM NH_4OAc pH 6.8
Phenomenex	Luna NH_2	propyl amine	2.1 x 150 mm, 3 µm	10 mM NH_4OAc pH 9.9

Table 2-2. Metabolites Evaluated in Standard Mix

Glycolysis	TCA	Nucleotides + Cofactors	Amino Acids
glucose-6-phosphate	citrate	cAMP	alanine
fructose-6-phosphate	isocitrate	AMP	arginine
fructose-1,6-bisphosphate	succinate	ADP	aspartic acid
2-phosphoglycerate	fumarate	ATP	cystine
3-phosphoglycerate	acetyl-CoA	cGMP	glutamic acid
phosphoenolpyruvate	succinyl-CoA	GMP	glycine
lactate		GDP	histidine
		GTP	isoleucine
		NAD^+	lysine
		NADH	methionine
		FAD	phenylalananine
			proline
			serine
			threonine
			tyrosine
			valine

Table 2-3. Chromatographic Conditions for Column Screen

Parameter	Value
HPLC	Agilent 1200SL
column	as listed in Table 2-1
column temperature	30 °C
flow rate	210 µL/min
injection volume	3 µL
sample	20 µM standards as listed in Table 2-2
mobile phase A	acetonitrile
mobile phase B	as listed in Table 2-1
gradient program	10%B to 90%B over 30 min, hold 5 min.

Table 2-4. Chromatographic Conditions for Temperature and Ionic Strength Studies

Parameter	Value
HPLC	Agilent 1200SL
column	Luna NH_2, 2.1 x 150 mm, 3 µm
column temperature	25 °C (unless otherwise specified)
flow rate	250 µL/min
injection volume	2 µL
sample	20 µM standards as listed in Table 2-2
mobile phase A	acetonitrile
mobile phase B	20 mM NH_4OAc pH 9.9 (unless otherwise specified)
gradient program	45%B (hold 2 min) to 65%B over 0 min (hold 0 min) to 75%B over 15 min (hold 0 min) to 100%B over 0 min (hold 5 min)

Table 2-5. Mass Spectrometer Conditions

Parameter	Value
mass spectrometer	Agilent LC/MSD-TOF
ion source	dual ESI (negative mode)
gas temperature	350 °C
drying gas flow	10 L/min
nebulizer	20 psig
vcap	3500 V
fragmentor	150 V
skimmer	65 V
acquisition rate	1 spectra/s
mass range	50-1200 m/z
data storage	centroid
reference mass correction	on

Results and Discussion

Column Screen. Metabolites from glycolysis, the TCA cycle, nucleotide cofactors, and amino acids (Table 2-2) were screened using columns and mobile phases that encompassed reversed phase, HILIC, and AEX/HILIC approaches (Table 2-1). Representative chromatograms for amino acids (leucine/isoleucine), sugar phosphates (glucose-6-phosphate), organic acids (citrate + isocitrate), and nucleotides (cAMP, AMP, ADP) are shown in Figure 2-1. The reverse phase method was not effective in resolving or retaining the analytes of interest. k' values ranged from 0.44 to 0.56 and no resolution was observed between leucine and isoleucine or AMP and ADP. Improved retention of polar analytes using this stationary phase (Waters Atlantis) and other similar columns has been observed using 100% aqueous mobile phase[6, 9] as opposed to the 90% aqueous starting condition used here, although the issue of poor retention of many polar analytes such as glucose-6-phosphate and ATP cannot be overcome.[9] Hence, reverse phase was set aside in favor of more promising methods.

The HILIC columns investigated demonstrated improved retention with a minimum k' of 1.0 for cAMP by the Diamond Hydride column. Halo HILIC, Luna HILIC, and Diamond Hydride columns provided adequate retention but poor peak shape and resolution for many metabolites. The Halo HILIC column inadequately resolved leucine and isoleucine (R_s = 0.48) and only broad baseline disturbances were observed at the m/z corresponding to citrate and isocitrate. A small broad peak for AMP was observed and ADP was not detected. Luna HILIC performed similarly with leucine and isoleucine resolved slightly (R_s = 0.71) and no defined peak detected for citrate or isocitrate. AMP peak shape was improved relative to Halo HILIC, although it was not baseline resolved from cAMP (R_s = 0.85). Surprisingly, a peak was not detected for glucose-6-phosphate with this diol phase, presumably due to a broad elution caused by strong secondary stationary phase interaction. The Diamond Hydride column retained leucine and isoleucine with a k' of 4.2 although no resolution was achieved. Like other HILIC columns, no peaks for citrate or isocitrate were detected. cAMP and AMP were retained and resolved, however ADP eluted as a broad peak with low intensity. The Luna NH_2 performed remarkably compared to the other columns investigated. Leucine and isoleucine were well retained (k' = 4.0) and resolved (R_s = 1.5). Citrate and isocitrate were retained well with R_s 1.0. cAMP, AMP, and ADP showed excellent retention and resolution. All peaks for these representative compounds were narrow and symmetrical.

These findings are in agreement with a study that reported better chromatography for a similar method compared to Waters HILIC (SiO_2), Luna CN (cyanopropyl), and TSK Gel Amide 80 (carbamoyl).[9] Since the Luna NH_2 exhibited superior performance to all other methods investigated, this column was chosen for further optimization and method development.

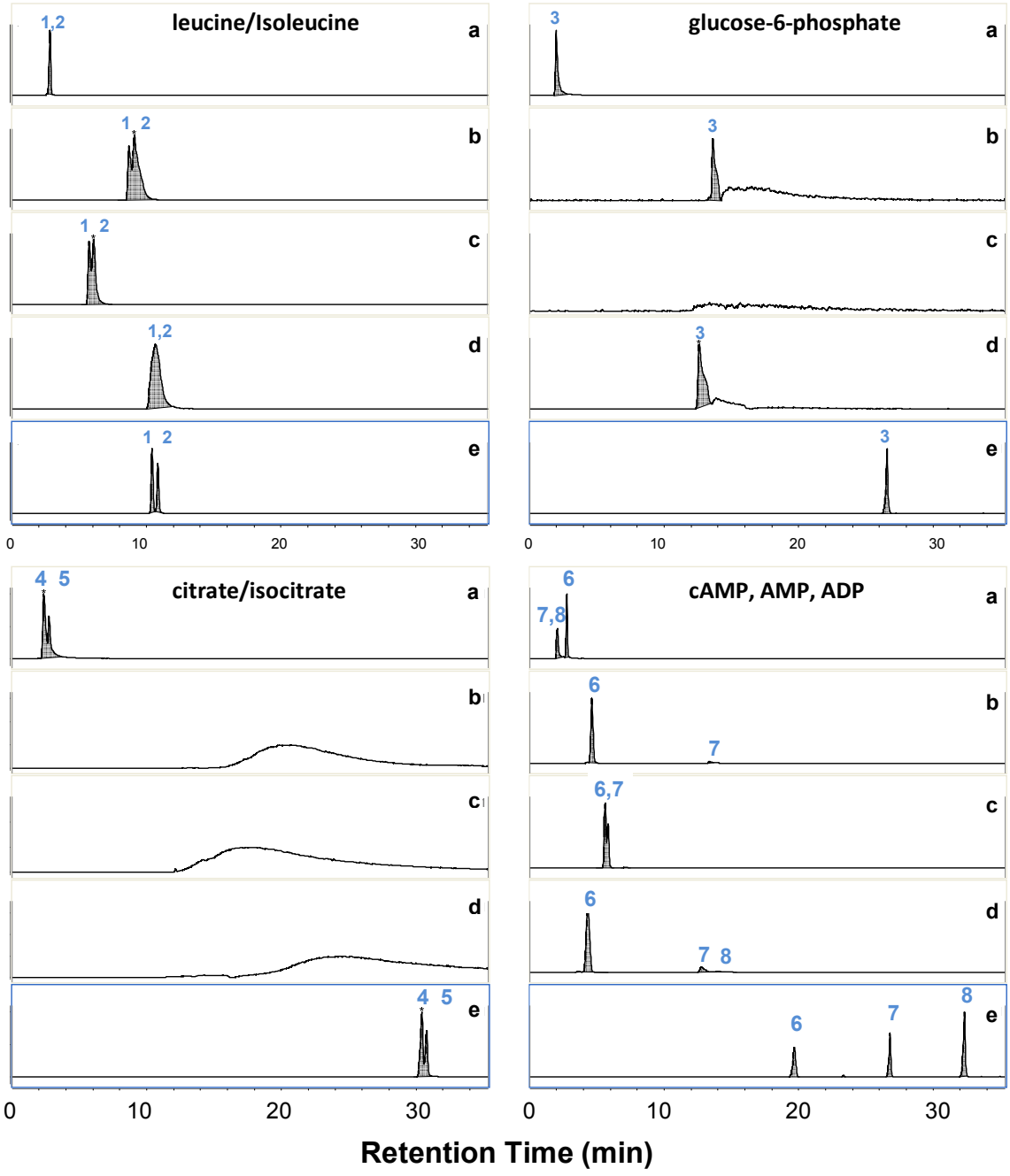

Figure 2-1. LC-MS Chromatograms of Select Metabolites by Reverse Phase, HILIC, and HILIC/AEX Methods.

Columns studied were Atlantis C_{18} with acidic pH (a), Halo SiO_2 with neutral pH (b), Luna Diol with neutral pH (c), Microsolv Diamond Hydride with neutral pH (e), and Luna NH_2 with basic pH (e). Peak labels are leucine (1), isoleucine (2), glucose-6-phosphate (3), citrate (4), isocitrate (5), cAMP (6), AMP (7), and ADP (8). Traces are theoretical $[M\text{-}H]^-$ ± 70 ppm. HPLC conditions are listed in Table 2-3.

Column Temperature. The impact of temperature on retention and selectivity was assessed from 15 to 40 °C for the standard set of metabolites (Figure 2-2). The retention time for all metabolites increased with temperature which is unexpected since elevated temperatures are associated with generally faster elution.[18] The increase in retention observed here is possibly due to a change in pKa of the propyl amine stationary phase with temperature. Temperature impacted selectivity as the k' for metabolites such as fructose-bisphosphate changed from 7.3 to 11.2 over the temperature interval studied whereas the k' for GTP changed only from 12.7 to 13.6. This variability demonstrates that temperature can be valuable parameter in adjusting selectivity with the HILIC/AEX method. Peak shape did not change significantly with temperature. Although these variations were observed, we ultimately chose a moderate temperature of 25 °C to minimize potential degradation of the silica based stationary phase which may be accelerated at elevated temperatures, an important consideration when also operating at elevated pH.[18]

Ionic Strength. Ionic strength strongly influences retention in ion exchange chromatography through competition with analytes for charged groups on the stationary phase. We measured the influence of mobile phase ionic strength on k' from 5 to 20 mM NH_4OAc at pH 9.9 (Figure 2-3). As predicted, we observed decreased retention for all metabolites with increasing ionic strength. However, a trend of decreasing sensitivity with ionic strength was also observed (Figure 2-4), presumably due to ionization suppression. Selectivity and peak shape were minimally impacted. Therefore 5 mM NH_4OAc was chosen as the buffer concentration for the final method.

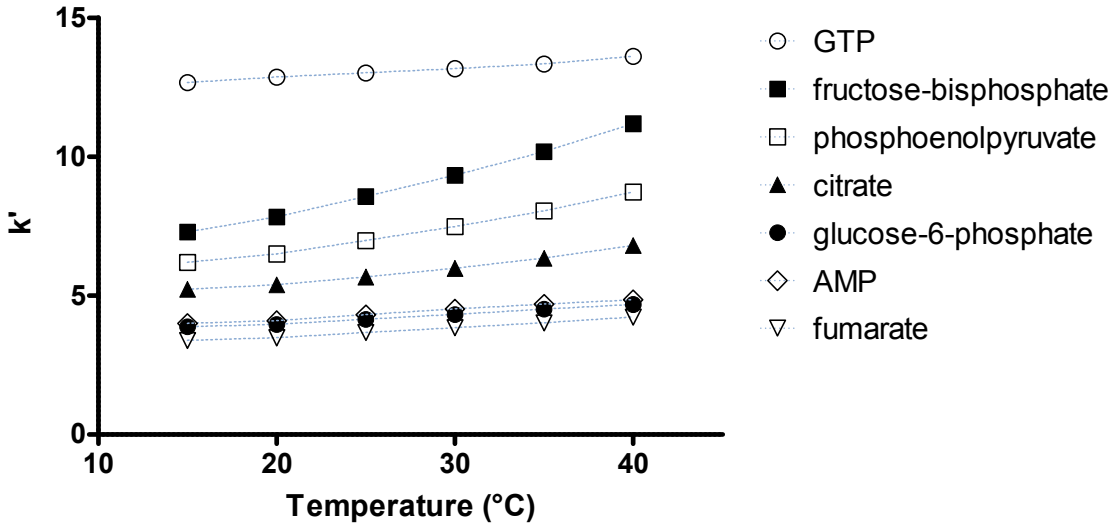

Figure 2-2. k' versus Temperature for Select Metabolites.

HPLC conditions as listed in Table 2-4, Mass spectrometer settings as listed in Table 2-5.

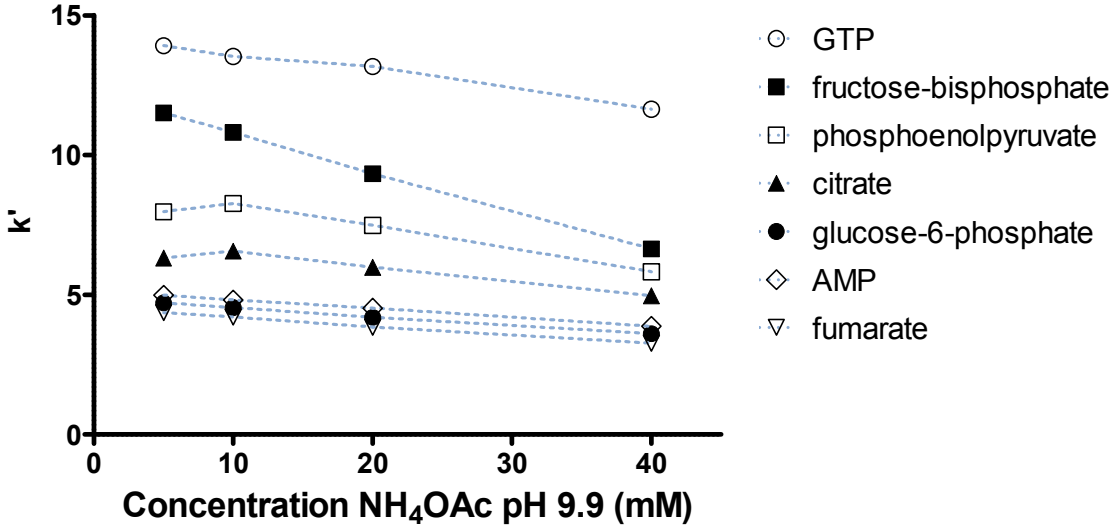

Figure 2-3. Impact of Ionic Strength on Retention Factor (k').

Retention factor versus concentration pH 9.9 NH_4OAc in mobile phase B. HPLC conditions as listed in Table 2-4, Mass spectrometer settings as listed in Table 2-5.

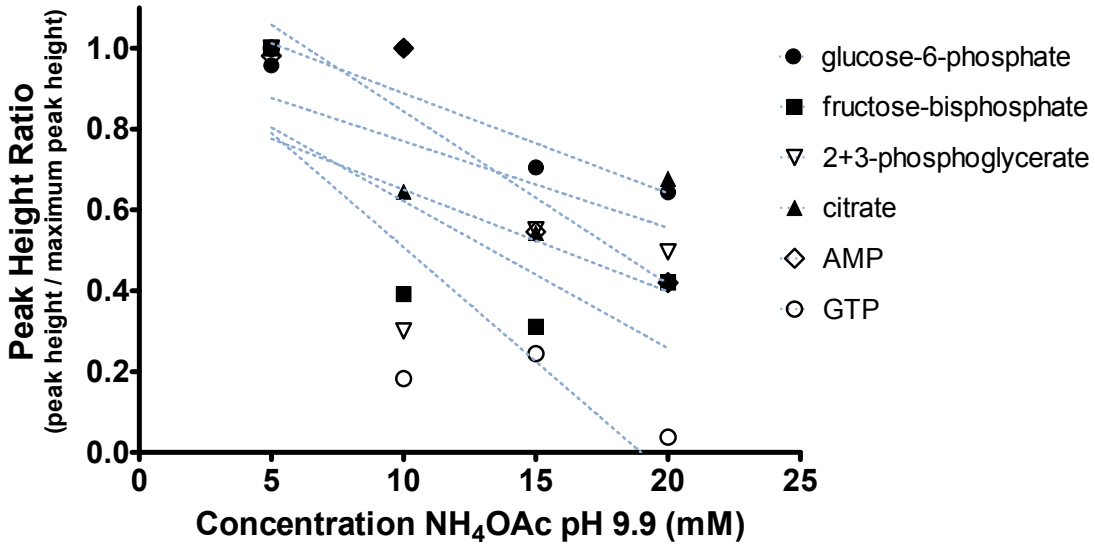

Figure 2-4. Impact of Ionic Strength on Sensitivity.

Concentration NH_4OAc in mobile phase B versus peak height. HPLC conditions are listed in Table 2-3.

Final Method. We adopted a linear gradient (20 to 100% B over 20 min) using a 5 mM NH_4OAc buffer at pH 9.9 and column temperature of 25 °C for routine analysis. An example chromatogram of an INS-1 cellular extract is show in Figure 2-5 and demonstrates adequate sensitivity of many key metabolites of glycolysis, the TCA cycle and related cofactors in a biological sample. Peak shape for all metabolites quantified is adequate despite the high sample loading.

We evaluated a 3-step gradient method employing a shallow segment in which %B (strong solvent) changed at a rate of 0.67 %/min as opposed to 2.7 %/min to attempt improvement of resolution. Resolution for many metabolites is improved (Figure 2-6). Resolution of 1.1 was achieved for 2-phosphoglycerate and 3-phosphoglycerate and resolution of citrate and isocitrate was 1.0. Little selectivity for the TCA cycle dicarboxylic acids succinate, fumarate, and malate was observed, although these structurally similar compounds are resolved by mass. While providing enhanced resolution, retention time reproducibility was poor with this approach owing presumably to instrument variability in delivering the gradient and changes in column characteristics with use. Diminished performance was also observed when analyzing cellular extracts as opposed to idealized standards. For example, resolution between the critical pairs

citrate / isocitrate and 2-phosphoglycerate / 3-phosphoglycerate diminished with injection of complex sample matrix (e.g. lipids, proteins, salts, buffers) and higher sample loads necessary to achieve detection of lower level metabolites such as NADPH. We therefore adopted the linear gradient (above) for routine analysis.

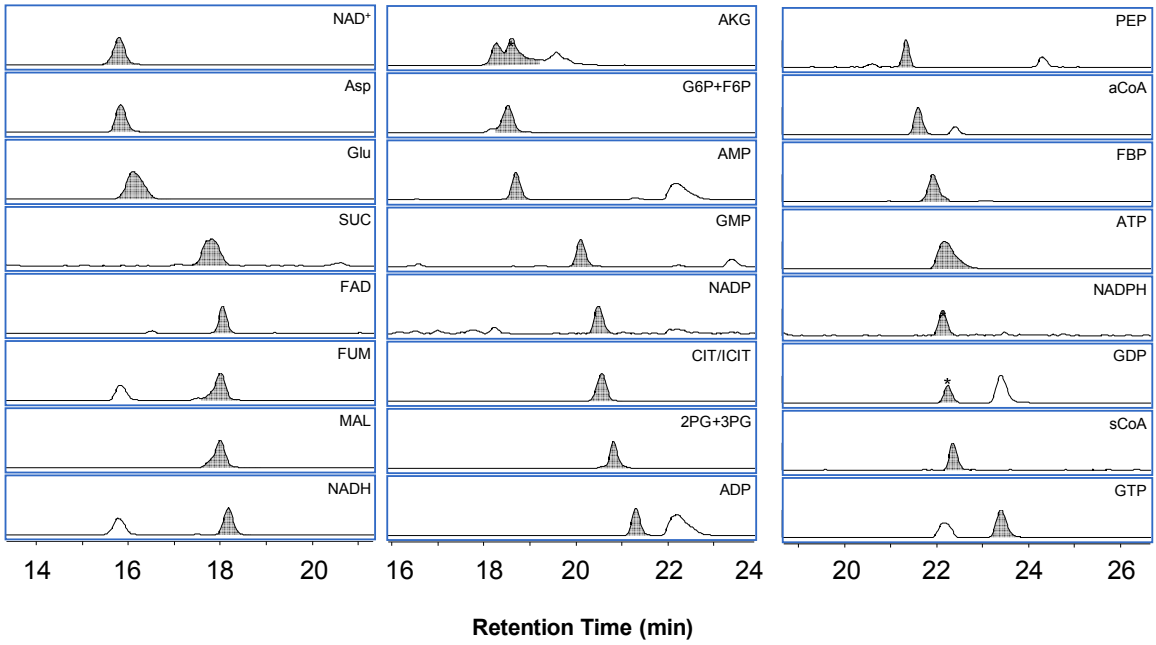

Figure 2-5. HILIC-AEX Chromatograms of an INS-1 Extract.

HPLC Conditions are: Column: Luna NH_2, 2.1 x 150 mm, 3 µm; flow: 200 µL/min; temperature: 25 °C; mobile phase A: acetonitrile, mobile phase B: 5 mM NH_4OAc pH 9.9. Gradient: 20% B to 100% B over 20 min, hold 5 min at 300 µL/min. Injection volume: 80 µL.

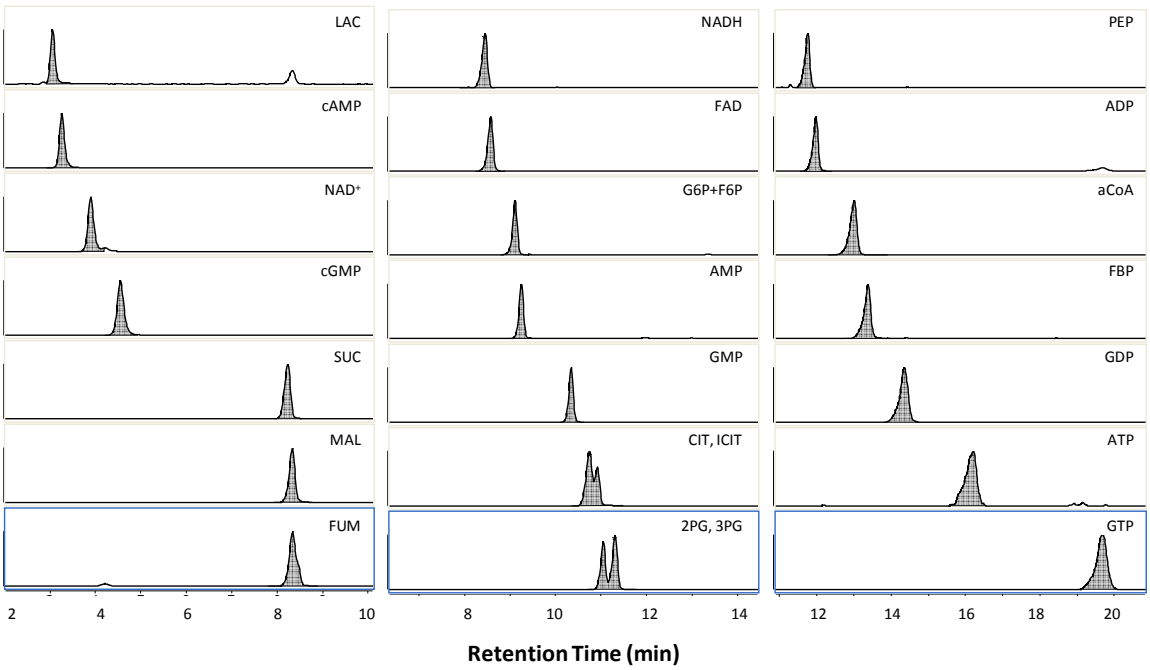

Figure 2-6. HILIC-AEX Chromatograms of Standard Mixture.

HPLC Conditions are: Column: Luna NH_2, 2.1 x 150 mm, 3 µm; flow: 250 µL/min; temperature: 25 °C; mobile phase A: acetonitrile, mobile phase B: 5 mM NH_4OAc pH 9.9. Gradient: 45% B, hold 2 min, to 70% B over 0.1 min, 0 hold, to 80% B over 14.9 min, to 100% B over 0.1 min, hold 5 min.

Long Term Assessment. This method has been used extensively for screening cellular extracts and has performed adequately. The most significant issues with this method include poor run-to-run retention time reproducibility and decreased column lifetime (e.g. degradation in peak shape and decreased retention) relative to reverse phase columns, presumably due to the high pH used. The inability of this method to chromatograph the key energy metabolites oxaloacetate and pyruvate (presumably due to strong stationary phase interaction with alpha-keto acid groups) is also an issue. Regardless, we have found the overall performance of this approach useful to generate unique insights into cellular metabolism. We have used this method to quantify ~90 metabolites in INS-1 cells on a directed basis and hundreds of features on an undirected basis as demonstrated in Chapters 3 and 4.

Conclusions

We developed a HILIC/AEX method that provides excellent chromatographic performance for the metabolomic analysis of polar metabolites relevant to energy metabolism. This method uses a Luna propyl amine stationary phase at elevated pH that affords better chromatographic performance (e.g. retention and peak shape) than other reverse phase and HILIC columns often used in metabolite analysis. The impact of column temperature and mobile phase ionic strength on chromatographic performance was evaluated and conditions selected to provide enhanced sensitivity and column lifetime. The performance of the method was demonstrated through adequate detection of many metabolites from glycolysis, the TCA cycle, and related cofactors in INS-1 cellular extracts. Potential improvements to this method could be realized through application of recent advances in stationary phase chemistry. Ideally, the commercialization of a propyl amine stationary phase on an advanced hybrid silica (e.g. Waters ethylene bridged hybrid) with better high pH stability and sub 2 µm particles could provide improved reproducibility and speed though an increase in column stability and lowered plate height.

References

1. Lu, W., Clasquin, M.F., Melamud, E., Amador-Noguez, D., Caudy, A.A., and Rabinowitz, J.D. 2010. Metabolomic Analysis via Reversed-Phase Ion-Pairing Liquid Chromatography Coupled to a Stand Alone Orbitrap Mass Spectrometer. *Analytical Chemistry* 82:3212-3221.
2. Liu, G., Ji, Q.C., and Arnold, M.E. 2010. Identifying, Evaluating, and Controlling Bioanalytical Risks Resulting from Nonuniform Matrix Ion Suppression/Enhancement and Nonlinear Liquid Chromatography−Mass Spectrometry Assay Response. *Analytical Chemistry* 82:9671-9677.
3. Nordstrom, A., Want, E., Northen, T., Lehtio, J., and Siuzdak, G. 2007. Multiple Ionization Mass Spectrometry Strategy Used To Reveal the Complexity of Metabolomics. *Analytical Chemistry* 80:421-429.
4. King, R., Bonfiglio, R., Fernandez-Metzler, C., Miller-Stein, C., and Olah, T. 2000. Mechanistic investigation of ionization suppression in electrospray ionization. *Journal of the American Society for Mass Spectrometry* 11:942-950.
5. Lu, W., Kimball, E., and Rabinowitz, J.D. 2006. A High-Performance Liquid Chromatography-Tandem Mass Spectrometry Method for Quantitation of Nitrogen-Containing Intracellular Metabolites. *Journal of the American Society for Mass Spectrometry* 17:37-50.
6. Edwards, J.L., Edwards, R.L., Reid, K.R., and Kennedy, R.T. 2007. Effect of decreasing column inner diameter and use of off-line two-dimensional chromatography on metabolite detection in complex mixtures. *Journal of Chromatography A* 1172:127-134.

7. Ding, J., Sorensen, C.M., Zhang, Q., Jiang, H., Jaitly, N., Livesay, E.A., Shen, Y., Smith, R.D., and Metz, T.O. 2007. Capillary LC Coupled with High-Mass Measurement Accuracy Mass Spectrometry for Metabolic Profiling. *Analytical Chemistry* 79:6081-6093.
8. Bu□scher, J.r.M., Czernik, D., Ewald, J.C., Sauer, U., and Zamboni, N. 2009. Cross-Platform Comparison of Methods for Quantitative Metabolomics of Primary Metabolism. *Analytical Chemistry* 81:2135-2143.
9. Bajad, S.U., Lu, W., Kimball, E.H., Yuan, J., Peterson, C., and Rabinowitz, J.D. 2006. Separation and quantitation of water soluble cellular metabolites by hydrophilic interaction chromatography-tandem mass spectrometry. *Journal of Chromatography A* 1125:76-88.
10. Luo, B., Groenke, K., Takors, R., Wandrey, C., and Oldiges, M. 2007. Simultaneous determination of multiple intracellular metabolites in glycolysis, pentose phosphate pathway and tricarboxylic acid cycle by liquid chromatography-mass spectrometry. *Journal of Chromatography A* 1147:153-164.
11. Bennette, N.B., Eng, J.F., and Dismukes, G.C. 2011. An LC–MS-Based Chemical and Analytical Method for Targeted Metabolite Quantification in the Model Cyanobacterium Synechococcus sp. PCC 7002. *Analytical Chemistry* 83:3808-3816.
12. Werf, M.J.v.d., Overkamp, K.M., Muilwijk, B., Coulier, L., and Hankemeier, T. 2007. Microbial metabolomics: Toward a platform with full metabolome coverage. *Analytical Biochemistry* 370:17-25.
13. Reaves, M.L., and Rabinowitz, J.D. 2011. Metabolomics in systems microbiology. *Current Opinion in Biotechnology* 22:17-25.
14. Yanes, O., Tautenhahn, R., Patti, G.J., and Siuzdak, G. 2011. Expanding Coverage of the Metabolome for Global Metabolite Profiling. *Analytical Chemistry* 83:2152-2161.
15. Tolstikov, V.V., and Fiehn, O. 2002. Analysis of Highly Polar Compounds of Plant Origin: Combination of Hydrophilic Interaction Chromatography and Electrospray Ion Trap Mass Spectrometry. *Analytical Biochemistry* 301:298-307.
16. Cubbon, S., Bradbury, T., Wilson, J., and Thomas-Oates, J. 2007. Hydrophilic Interaction Chromatography for Mass Spectrometric Metabonomic Studies of Urine. *Analytical Chemistry* 79:8911-8918.
17. Spagou, K., Tsoukali, H., Raikos, N., Gika, H., Wilson, I.D., and Theodoridis, G. 2010. Hydrophilic interaction chromatography coupled to MS for metabonomic/metabolomic studies. *Journal of Separation Science* 33:716-727.
18. Lloyd Snyder, j.k., joseph glajch. 1997. *Practial HPLC Method Development*. New York: John Wiley and Sons.

CHAPTER 3
Sample Preparation for Adherent Mammalian Cell Metabolomics: Reducing Time and Increasing Sensitivity

Introduction

Metabolomic analysis of cells and tissues has emerged as an important technique for studying cellular biochemistry. With the advent of powerful high performance liquid chromatography - mass spectrometry (HPLC-MS) and gas chromatography - mass spectrometry (GC-MS) methods, large numbers of metabolites can be quantified to provide detailed insight into the metabolic status of cells. Despite the power of these methods, sample preparation is critical to achieving meaningful results. In these studies, we sought to develop a novel sample preparation procedure for adherent mammalian cells that would be simpler and faster than conventional methods. We chose INS-1 832/13 cells[1,2] as a model cell line. This clone has proven to be a useful model for the study of insulin secretion with many properties in common with mammalian β-cells including physiological response to glucose. Accurate measurement of metabolites and their changes during glucose-stimulated insulin secretion is expected to add to our understanding of insulin secretion in normal and pathological states.

Many studies on sample preparation for metabolomic analysis of yeast and bacteria have been reported (see recent review[3]). Because of substantial differences in eukaryotic and prokaryotic cells, the findings from these investigations may not be fully applicable to adherent mammalian cells. While minimal media used to culture prokaryotic cells and mammalian culture media both contain interfering anions such as Cl^-, SO_4^-, and PO_4^-, mammalian culture media also contains up to millimolar concentrations of amino acids, Good's buffers, organic acids, and complex biological mixtures such as fetal bovine serum. Unless these components are removed, they can cause substantial electrospray ionization suppression and contaminate the intracellular metabolite pool. These issues are compounded with adherent mammalian cells since

they cannot be concentrated by centrifugation or filtration prior to quenching without trypsination or physical removal, which has been demonstrated to significantly alter the metabolome.[4]

Limited work has focused on development of sample preparation techniques for metabolomic analysis of adherent mammalian cells. One study employed rigorous experimental design to maximize nucleotide recovery, energy charge, fructose 1,6 bisphosphate (FBP) content, and minimize residual protein/DNA.[5] While valuable, the method may not be applicable to global metabolomic studies as it employs a biphasic extraction solvent that may remove non-polar metabolites from the assayed extract and employs elevated temperatures, which may degrade thermally labile metabolites such as nicotinamide adenine dinucleotide (NADH), nicotinamide adenine dinucleotide phosphate (NADPH)[6], and succinyl-CoA (sCoA).[7]

Although rigorous studies of sample preparation for adherent mammalian cells are rare, many metabolomic studies of such cells have been described (see Table 3-1). Extraction approaches vary widely in volume of solvent (e.g., 1 to 26 mL/10 cm plate of cells), number of repeated extractions (1 to 3), and duration of incubation per cycle of extraction (as long as 60 min). A variety of rinsing, quenching, heating, and sample concentration procedures are also used. Without comparative studies, it is difficult to know how performance, e.g., sample stability and metabolite recovery, is impacted by different procedures or if a method could be improved, e.g., by simplification or better removal of interferences.

To better understand how different sample preparation techniques affect the metabolome we measured the quantitative effect of novel and commonly used sample preparation procedures on recovery and stability of 27 known metabolites associated with glycolysis and the tricarboxylic acid (TCA) cycle as well as ~700 unidentified features using an undirected approach. Our initial method incorporated a water rinse to improve sensitivity and remove contaminants, a single rapid extraction with cold organic solvent to minimize sample preparation time, and a novel liquid nitrogen (LN_2) quench step to rapidly halt metabolism and allow for storage of unextracted samples. We then evaluated the impact of additional and/or alternate sample preparation steps on metabolite recovery and stability.

Based on this study, we developed a procedure that removes interfering media components from the cell surface, quenches metabolism, extracts a wide range of metabolites, and generates stable extracts with sufficient concentration to detect many

metabolites by anion exchange / hydrophilic interaction liquid chromatography - electrospray ionization- mass spectrometry (AEX/HILIC-ESI-MS). This method requires as little as 5 min, is convenient, and provides good sensitivity for a variety of metabolites.

Table 3-1. Summary of sample preparation procedures reported for metabolomic analysis of cultured adherent mammalian cells.

Cell Type	Analytical Technique	Rinse	Quench	Extraction	Dry	Ref
Human rhabdo-myosarcoma	NMR	trypsination/ 3X 0 °C PBS	LN_2 (pelleted cells)	10% ice cold TCA in H_2O	yes	[8]
Human breast cancer	NMR	2X ice cold PBS	MeOH	MeOH/ $CHCl_3$/ H_2O biphase	yes	[4]
Human fibroblasts	LC/MS	No	-75 °C 80% MeOH	-75 °C 80% MeOH	yes	[9]
Generic	LC/MS	No	-75 °C 80% MeOH	4 °C 80% MeOH	optional	[10]
Hepatic	GC/MS and LC/MS	No	150 °C Air	boiling H_2O	yes	[11]
INS-1	GC/MS	1x MES, 1x H_2O	-75 °C MeOH	70 °C heating followed by $CHCl_3$/ H_2O biphase	yes	[12]
INS-1	GC/MS	2X ice cold PBS	-80 °C 80% MeOH	82% MeOH	yes	[13]
Canine kidney	LC/UV and conductivity	1x PBS	4 °C MeOH / $CHCl_3$	2x buffered MeOH / $CHCl_3$/ H_2O biphase and 90 °C heating	yes	[5]
CHO	enzyme and GC/MS	60% MeOH	-40 °C 60% MeOH	100% MeOH	yes	[14]
HeLa	LC/MS	2x NH_4OAc	80% MeOH	80% MeOH	no	[15]

Materials and Methods

Materials. All chemicals were purchased form Sigma-Aldrich (St. Louis, MO) unless otherwise noted. HPLC grade acetonitrile was purchased from Burdick & Jackson (Muskegon, MI). RPMI media, fetal bovine serum, 4-(2-hydroxyethyl)-1-piperazineethanesulfonic acid (HEPES), and penicillin-streptomycin were purchased from Invitrogen Corp. (Carlsbad, CA). Cells lifters and 10 cm polystyrene non-pyrogenic culture dishes were purchased from Corning (Lowell, MA).

Cell Culture. Culture media was prepared with RPMI-1640 (+L-glutamine) supplemented with 10% fetal bovine serum (FBS), 1 mM pyruvate, 10 mM HEPES, 50 µM 2-beta mercaptoethanol, and 1 unit penicillin-streptomycin. KRHB (Krebs-Ringer-

HEPES buffer) was prepared containing 20 mM HEPES, 118 mM NaCl, 5.4 mM KCl, 2.4 mM CaCl, 1.2 mM $MgSO_4$, and 1.2 mM KH_2PO_4 and adjusted to pH 7.4 with HCl. INS-1 cells were grown to confluence (~4 x 10^7 cells) in 10 cm polystyrene dishes at 37 °C and 5% CO_2. RPMI media was replaced with KRHB containing 10 mM glucose 30 min prior to quench to generate metabolite changes comparable to those expected from stimulation experiments. (Stimulus-secretion coupling studies of β-cells are generally carried out in KRHB instead of culture media to measure the effect of specific stimulants without other potential fuels and unknown compounds from the media impacting results).

HPLC-MS. Chromatographic separations were performed with an Agilent Technologies (Santa Clara, CA) 1200 HPLC system equipped with a Phenomenex (Torrance, CA) Luna NH_2 2.0 x 150 mm, 3 µm HPLC column equipped with a 2.0 x 4 mm guard column using the following conditions: mobile phase A was 100% acetonitrile (ACN); mobile phase B was 100% 5 mM ammonium acetate pH 9.9 with ammonium hydroxide; gradient program was (time, %B, flow rate) 0 min, 20%, 200 µL/min, 20 min, 100%, 200 µL/min, 20.1 min, 100%, 300 µL/min; column temperature was 25 °C; injection volume was 80 µL, and auto sampler temperature was 4 °C. These chromatographic conditions are similar to those reported previously[16, 17] and provide for a weak AEX/HILIC separation afforded by the polar and partially deprotonated propyl-amine stationary phase. A representative INS-1 extract chromatogram with additional method details is provided in Figure 2-5. Detection was performed on an Agilent Technologies LC/MSD TOF using a dual ESI source in negative-ion mode. Instrument parameters were as follows: gas temp: 350 °C, drying gas: 10 L/min, nebulizer: 20 psig, VCap 3500 V, fragmentor: 150 V, skimmer: 65 V, acquisition rate: 1 spectra/s, mass range: 50-1200 m/z, data storage: centroid with 20 count threshold, reference spray: on.

Nominal Preparation, Quenching, Extraction, and Assay Procedure. Unless otherwise stated, metabolism was quenched and metabolites extracted from INS-1 cells using the following procedure (see also illustration in Figure 3-1). Cells were rapidly rinsed by gently dispensing ~10 mL of 37 °C deionized water to the cell surface. The plate was rocked briefly (~2 s), aspirated, and quenched by directly adding ~15 mL of LN_2 to the dish. Approximately 5 s passed between addition of water and quenching by addition of LN_2. The plates were briefly stored on dry ice, transferred to a -80 °C freezer, and extracted and assayed within 7 d.

For extraction, plates were immediately transferred to a 4 °C cold room and 1.5 mL of ice cold 90% 9:1 MeOH: $CHCl_3$ (MC) was immediately added to each plate and cells scraped/suspended with a cell lifter. The extraction solvent also contained $^{13}C_6$-fructose-6-phosphate (F6P) (10 μM), $^{13}C_1$-phosphoenolpyruvate (PEP) (10 μM), $^{13}C_6$-citrate (CIT) (10 μM), $^{13}C_4$-succinate (SUC) (10 μM), $^{13}C_{10}{}^{15}N_5$-adenosine monophosphate (AMP) (2 μM), $^{13}C_{10}$-adenosine triphosphate (ATP) (20 μM), and $^{13}C_{10}$-guanosine triphosphate (GTP) (10 μM) as internal standards. Extracts were transferred to 1.5 mL microcentrifuge tubes and pelleted at 4 °C for 3 min at 16,100 g. Supernatants were transferred to auto sampler vials and assayed. Using this rapid procedure, a single sample can be quenched, extracted, pelleted, and ready for injection in ~5 min. All experiments were performed in triplicate.

Solvent Screen. INS-1 cells were extracted with 0.7 mL of 100% ethanol (EtOH), ACN, MeOH, and 9:1 MC yielding extracts containing ~70% organic (based on an estimated 300 μL residual water/plate). Samples were assayed within 10 min of extraction solvent and reinjected after 8 h of storage at 4°C.

Optimization of 9:1 MC to Water Ratio for Extraction. INS-1 cells were extracted using the nominal procedure using 1.7 mL of 100:0, 94:6, 88:12, and 82:18 9:1 MC:water yielding extracts containing approximately 85%, 80%, 75%, and 70% 9:1 MC based on 300 μL residual water per confluent 10 cm plate.

Determination of Soluble Protein Content. An aqueous cellular suspension was generated by thawing eight quenched 10 cm plates of INS-1 cells, scraping the cells from the plate surface (without solvent addition) and combining all material into a microcentrifuge tube. The pooled material was sonicated for 10 min in an ice bath and 10 μL of the cellular suspension was spiked per 90 μL of extraction solvent in microcentrifuge tubes. Extraction solvent contained a combination of water with either 9:1 MC or methanol in ratios yielding the designated % organic upon addition of the cellular suspension. Samples were centrifuged for 10 min at 16,100 g after which a 100 to 500 μL aliquot of the supernatant (dependent on anticipated protein content) was transferred to a new microcentrifgue tube and evaporated to dryness. Samples were reconstituted in 110-1000 μL of pH 8.0 50 mM tris and sonicated for 10 min in an ice bath. 100 μL aliquots of each solution were then added to 1 mL of Bradford Reagent

(Coomassie Plus, Thermo Scientific) and UV absorption measured at 595 nm in a 1 cm path length disposable cuvette. Sample were quantified against standards from 1 to 25 µg/mL bovine serum albumin (BSA) fit to a second order polynomial.

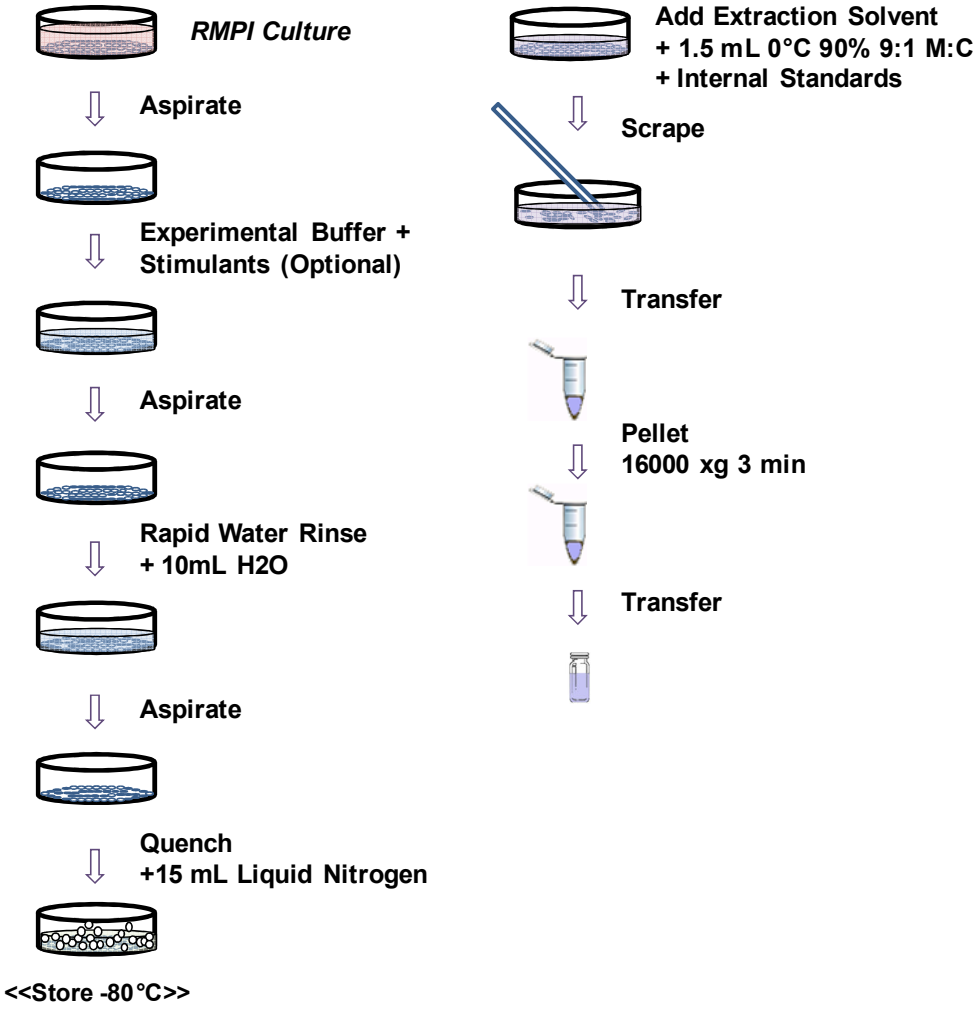

Figure 3-1. Diagram of Metabolite Extraction Procedure.

Note that the final extraction solvent composition is ~75:25 9:1 MC: water after combining 1.5 mL of 90% 9:1 MC with residual ~300 µL water adhered to the dish and cells. Experimental buffer was KRHB with 0.5 mM and/or 10 mM glucose.

Evaluation of Extraction Conditions. To evaluate extraction incubation time, plates of INS-1 cells were quenched using the nominal procedure to the point of extraction solvent addition. Prior to pelleting, three 400 µL aliquots of suspension were transferred to individual microcentrifuge tubes and stored on ice. The suspensions were pelleted after 1, 20, or 40 min of incubation and supernatants assayed.

To evaluate the use of multiple extraction cycles, INS-1 cells were extracted with 1.3 mL of 93:7 9:1 MC: water yielding a 75:25 9:1 MC: water extract. For each replicate, three 650 µL aliquots of suspension were transferred to three individual microcentrifuge tubes and pelleted. The supernatants were transferred to auto sampler vials and the pellets subjected to 0, 1, or 2 additional rounds of extraction with 50 µL of 75:25 9:1 MC:water. A pipette tip was used to break up and resuspended the pellet following each round of extraction. The extracts from subsequent extraction cycles were combined with the previous. To compensate for additional volume introduced by multiple extraction cycles, 100 µL or 50 µL of extraction solvent was added to the supernatant of 1x or 2x extracted samples, respectively.

Short Term Sample Stability. INS-1 samples were prepared using the nominal procedure and each extract split into 3 aliquots and stored at 4 °C for 0 h, 4 h, and 8 h. Following the specified hold period, samples were transferred to LN_2 for storage. Samples were thawed and injected in a single analytical run to minimize the impact of system drift. Additional INS-1 cells were prepared with 1.7 mL of 59:41 methanol:water to yield 50 % methanol solvent extracts. 50 % methanol extracts were injected within 7 min of solvent addition, and reinjected following 2 h of 4 °C storage.

Long Term Sample Stability. One set of INS-1 plates was extracted immediately after quenching. Each replicate was split into 2 aliquots and stored at either -80 °C or in LN_2 (T0 control). A second set of plates was stored without extraction at -80 °C. Stored plates were extracted after 7 d and injected in a single run. For extracts stored in LN_2 or at -80 °C prior to analysis, the extracts were sonicated 3 min in an ice bath, centrifuged 3 min at 16,100 g to pellet any precipitate, and transferred to auto sampler vials.

Impact of Water Rinsing. To assess suppression, cells were rinsed with either 10 mL 37 °C Milli-Q water or 10 mL 37 °C KRHB prior to quenching. To assess rinsing impact on the metabolic profile, control cells were rinsed twice with 10 mL KRHB and

experimental cells were rinsed once with 10 mL 37 °C Milli-Q water (either rapidly or with 30 s incubation) and re-rinsed with an additional 10 mL KRHB to achieve an identical final residue matrix.

Evaluation of Quenching Methods. Following aspiration of the water rinse solution, metabolism was quenched with ~15 mL LN_2, 1.5 mL of -75 °C 90% 9:1 MC, or 1.5 mL ice cold 90% 9:1 MC. Scraping and pelleting was conducted immediately following quench per the nominal method.

Comparison of Metabolite Changes with Glucose Stimulation Using Different Quenching and Preparation Methods. INS-1 cells were grown in 6 cm plates and preincubated in 3 mL KRHB containing 0.5 mM glucose for 30 min. Cells were then quenched (control) or stimulated with 95 µL of 1 M glucose (final concentration 10 mM), incubated 20 min, then quenched. Quenching and extraction were performed using our rapid method and two established methods for adherent mammalian cells. The first, 80% MeOH, involves no rinse, -80 °C 8:2 MeOH:H_2O quench, 3 extraction cycles, and drying/reconstitution of the sample.[18] The second, B-MTC, involves PBS rinse, 4 °C 2:1 MeOH:$CHCl_3$ quench, 2 biphasic extraction cycles with 1:1 MeOH:2.8 mM tricine and $CHCl_3$, heating at 90 °C for 4 minutes, and drying/reconstitution of the sample.[5] All volumes were scaled accordingly to 6 cm plate size. Dried samples were reconstituted in 1:1 MeOH:H_2O for compatibility with the HILIC method.

Residual Water in INS-1 Cell Plates. Plates of INS-1 cells quenched and stored at -80 °C were thawed, scraped, and the resulting suspension transferred to individual microcentrifuge tubes containing a granule of trichloroacetic acid. The samples were sonicated in an ice bath for 10 min, centrifuged to pellet debris, and aqueous volume measured. The average volume was 290 µL plus an estimated 10 µL of residual water remaining in the plate yielding ~300 µL residual water per plate.

Data Processing and Statistics. Compounds were identified based on retention time and m/z match to injections of authentic standards. Quantification was performed using Agilent Technologies MassHunter Quantitative software. Peak areas were measured from extracted ion chromatograms of $[M-H]^-$ metabolite ions with ± 70 ppm detection windows centered on the theoretical mass. $[M-2H]^{2-}$ ions were used for

acetyl-CoA (aCoA) and sCoA to improve sensitivity. Peak areas from internal standards were measured using an identical procedure; however, values were only used to verify instrument stability and not used in endogenous metabolite quantification. Undirected data processing was performed using Agilent Technologies MassHunter Qualitative software for peak picking and MassProfiler Professional for data alignment, statistical analysis, and visualization.

Data are expressed as the mean ± standard error of the mean (SEM). Statistical significance was determined using a non-corrected two-tailed Student's t test, unpaired assuming equal variance. A p-value of < 0.05 was considered significant.

Results and Discussion

Solvent Screen. Initial experiments evaluated EtOH, ACN, MeOH, and 9:1 MC (all 70:30 organic:H_2O) for their ability to extract and stabilize metabolites. All samples were injected within 10 min of extraction solvent addition to minimize metabolite peak area variability due to potential extract instability. The following compounds were measured in the extracts: Glucose-6-phosphate + fructose-6-phospate (G6P+F6P), FBP, 2-phosphoglycerate + 3-phosphoglycerate (2PG+3PG), PEP, aCoA, citrate + isocitrate (CIT+ICIT), α-ketoglutarate (AKG), sCoA, SUC, fumarate (FUM), malate (MAL), AMP, adenosine diphosphate (ADP), ATP, guanosine mono and diphosphate (GMP and GDP), GTP, flavin adenine dinucleotide (FAD), NAD^+, NADH, $NADP^+$, NADPH, Asp, and Glu. The peak area for each metabolite relative to 9:1 MC is shown in Figure 3-2a. Metabolite recoveries with MeOH and 9:1 MC were similar and the highest for nearly all analytes. In contrast to most metabolites, $NADP^+$ showed substantially higher recovery with ACN. These results are consistent with most metabolite extraction studies which find methanolic solutions to be suitable extraction solvents.

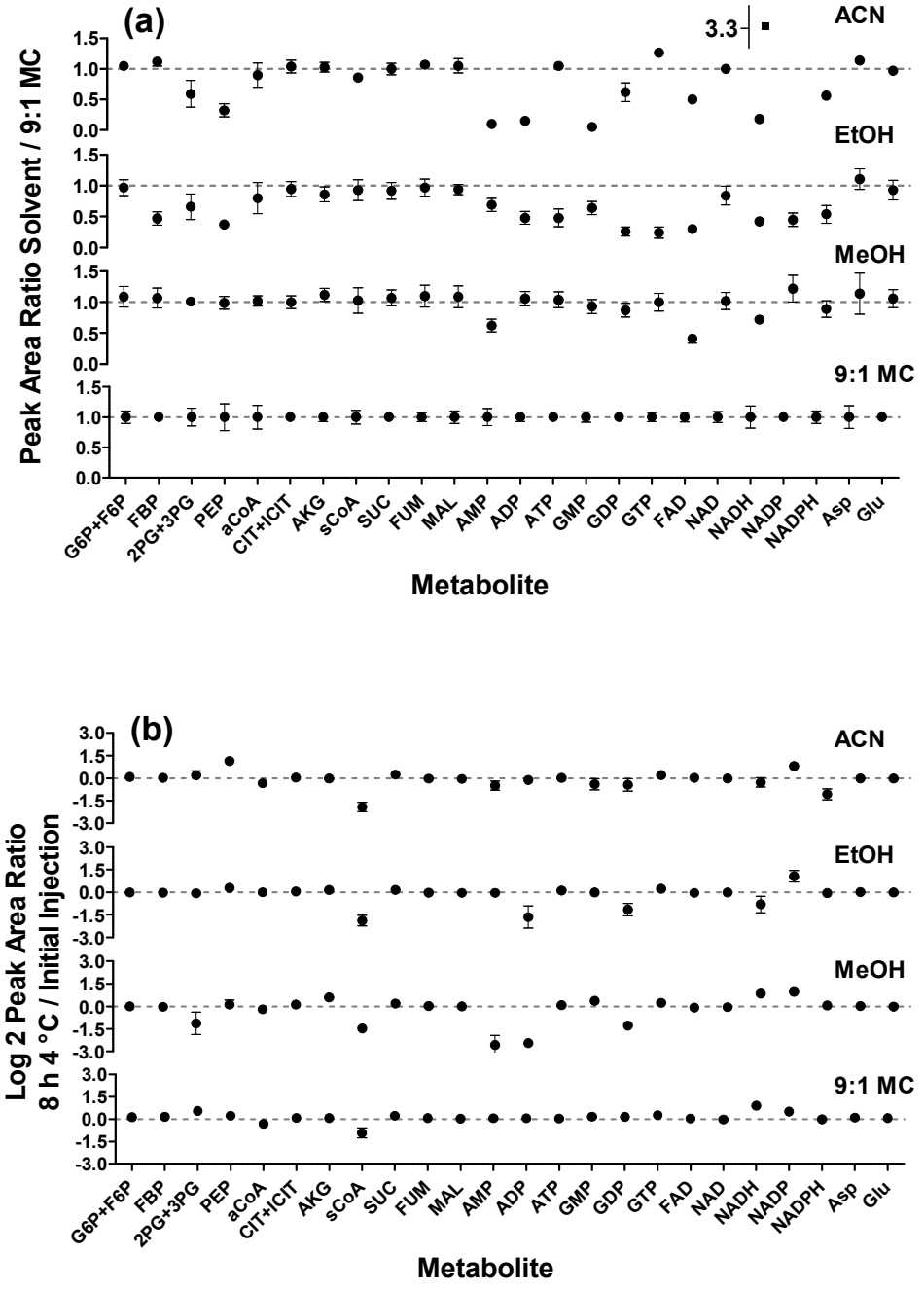

Figure 3-2. Recovery and Stability (4 °C, 8 h) for Metabolites Extracted from INS-1 Cells Using Various Solvents at 70:30 Solvent: Water Ratio in The Final Extract.

Samples injected within 10 min of extraction solvent addition. (a) Metabolite peak area ratio in specified solvent versus 9:1 MC. (b) Log 2 of metabolite peak area ratio after 8 h of 4 °C storage versus initial injection. ACN (acetonitrile), EtOH (ethanol), MeOH (methanol), 9:1 MC (9:1 MeOH: $CHCl_3$). Error bars represent 1 SEM, n = 3.

Extract Stability. Metabolomic studies often require the analysis of many samples prepared simultaneously to reduce variability and improve work flow efficiency. Preparing multiple samples at once can lead to storage times of several hours prior to injection because LC-MS analysis may require 10-60 min per sample; therefore, metabolite stability is a critical parameter. Metabolite instability can be caused by inherent chemical liability, enzymatic action[3, 16], and degradation of macromolecules to release "metabolites".[19] In this regard, metabolite concentrations may either increase or decrease depending on the dominant effects.

To evaluate the impact of organic solvent on stability, samples were reanalyzed after 8 h at 4 °C (mimicking typical auto sampler storage) and metabolite peak areas were compared to initial values obtained following immediate injection (Figure 3-2b). Stability of peak areas for metabolites such as G6P+F6P, FBP, CIT+ICIT, SUC, FUM, MAL, ATP, GTP, NAD, Asp, and Glu were impacted minimally by organic solvent (areas between 96 to 120% of initial values), whereas 2PG+3PG, PEP, AKG, AMP, ADP, GMP, GDP, FAD, NADH, $NADP^+$, and NADPH showed substantial variability in peak area (20 to 220% of initial).

Further study of the nucleotides revealed that much of the instability was due to enzymatic activity (data not shown), in agreement with other reports.[20-22] This finding highlights a disadvantage of cold aqueous-organic mixtures as extraction solvents; they fail to achieve complete enzyme deactivation. Reports have shown that brief heating ameliorates this effect.[3, 5] An advantage of the 75% 9:1 MC mix and cold sample storage used here is low enzymatic activity without risking loss of labile metabolites by heating.

Overall, 9:1 MC produced the most stable extracts of the solvents studied; therefore, further work was performed with this solvent. The ratio of 9:1 MC to water was investigated and 75% 9:1 MC was found to provide the best balance between polar metabolite recovery and soluble protein removal. We also found that additional extraction cycles and longer extraction incubation time did not improve recovery of a broad range analytes compared to a single cycle ~1 min extraction with 9:1 MC (see Figure 3-4). Stability of INS-1 extracts containing 75% 9:1 MC in the final extract (% water adjusted for residual water content of the plate) was comparable to that shown in Figure 3-2 b (see Figure 3-8). Metabolite extracts are stable when stored at -80 °C for 7 d with less than 25% decrease in peak area over that period (see Figure 3-9).

Optimization of Ratio of 9:1 MC to Water. To evaluate the impact of organic-aqueous solvent ratio on metabolite recovery, INS-1 cells were extracted with 70%, 75%, 80%, and 85% 9:1 MC and metabolite peak areas measured (Figure 3-3a). The recovery of most components was unaffected by the ratio of 9:1 MC to water in the extract with the exception of sugar phosphates, di-nucleotides, and tri-nucleotides. Recovery for FBP, 2PG+3PG, PEP, ADP, and $NADP^+$ increased 1.2- 1.9 fold when decreasing 9:1 MC from 85% to 75% but substantially less (1.02- 1.08 fold) from 75% to 70% 9:1 MC. ATP, GDP, and GTP increased 2.0 fold, 2.7 fold, and 3.8 fold, respectively, when decreasing 9:1 MC from 85% to 75% with additional increases at 70% 9:1 MC of 1.2-fold, 1.2-fold, and 1.4-fold. This increased recovery of nucleotides and FBP with increasing polarity of the extraction solvent is consistent with reports from the study of MDCK cells[22] and *E. coli* for CTP and UTP in samples extracted with 80 or 100% methanol although, lower recoveries were observed in 50% methanol and attributed to degradation.[20]

While decreasing the percentage of 9:1 MC in the extraction solvent increases recovery of many polar metabolites, dissolved protein content increases (Figure 3-3b). Such increases in protein content may have deleterious effects on chromatographic performance as well as extract stability (because of residual enzymatic activity). Because the increase in recovery of ATP, GDP, and GTP with 70% as opposed to 75% 9:1 MC is relatively small compared to the 1.9-fold increase in dissolved protein (Figure 3-3), 75% 9:1 MC was chosen as the final extraction solvent. A representative chromatogram of an INS-1 extract using the finalized extraction solvent is shown in Figure 2-5).

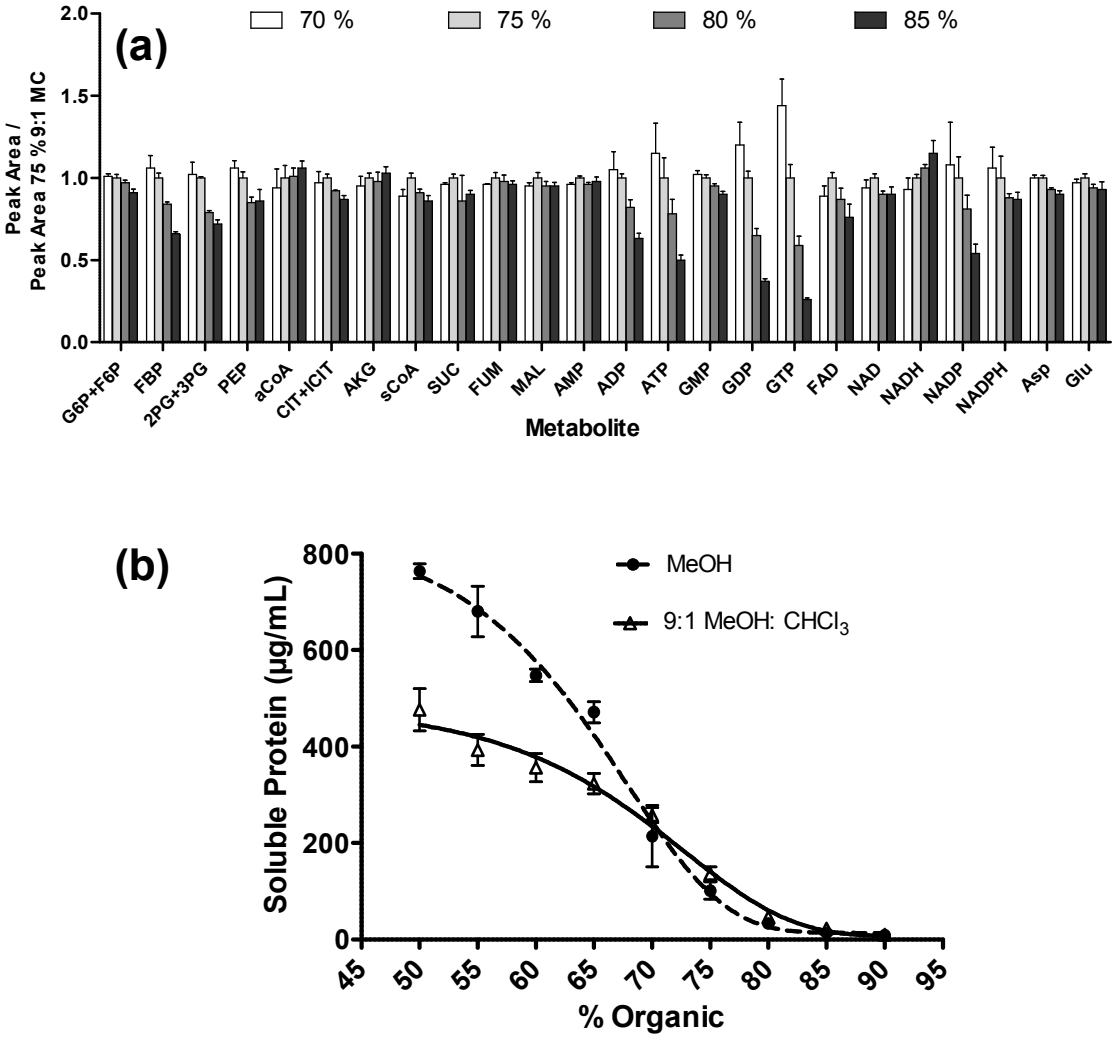

Figure 3-3. Metabolite Peak Areas and Soluble Protein Content for INS-1 Extracts with Varying Ratio of 9:1 MC to Water.

(a) Peak area ratio for metabolites in INS-1 cells extracted with 70% to 85% 9:1 MC versus 75% 9:1 MC. (b) Soluble protein content in methanol (MeOH) and 9:1 methanol: chloroform (9:1 MC) spiked with INS-1 cellular suspensions at various solvent: water ratios. Error bars represent 1 SEM, n = 3.

Extraction. A single rapid extraction cycle is desirable for minimizing systematic error, improving labile metabolite recovery, and increasing throughput; however, longer extraction times (20-60 min) and multiple rounds of extraction (1-3) are often proposed, presumably to improve metabolite recovery. To evaluate the impact of extraction incubation time, peak areas for metabolites of glycolysis, TCA cycle, and related

cofactors in INS-1 extracts were measured in samples extracted for 1, 20, and 60 min prior to pelleting. Peak areas for 20 and 40 min extracted samples relative to 1 min extracted samples were similar (Figure 3-4a) and ranged from 99% - 127% (mean = 108 ± 7%) and 95 - 122% (mean = 105 ± 5%), respectively. Significantly different peak areas were observed for GMP and $^{13}C_1$-PEP for 20 min extracted samples and for SUC in 40 min extracted samples relative to 1 min extracted samples. Metabolite peak areas for samples extracted 2x and 3x relative to 1x (Figure 3-4 b) ranged from 98% to 117% (mean 107 ± 4 %) and 94% to 117% (mean = 104 ± 5%), respectively. No differences in metabolite peak area relative to 1x extraction were significant at $p < 0.05$. Undirected data analysis comparing all features detected for 20 min extraction compared to 1 min extraction (Figure 3-4 c) and 2x extraction cycles versus 1x (Figure 3-4 d) demonstrates little variability in the global metabolite profile with only 16 of 981 and 8 of 746 features detected with fold change > 1.2 and $p < 0.05$, respectively. No features were significant in either experiment with p value correction for multiple testing. In addition, no trend is observed between early and late eluting species (see retention time color key in Figures Figure 3-4b and Figure 3-4c) indicating that a single extraction cycle is sufficient for analytes of a wide polarity range. We conclude that a single extraction cycle with ~1 min incubation time is sufficient to recover the broad range of metabolites detectable by this method.

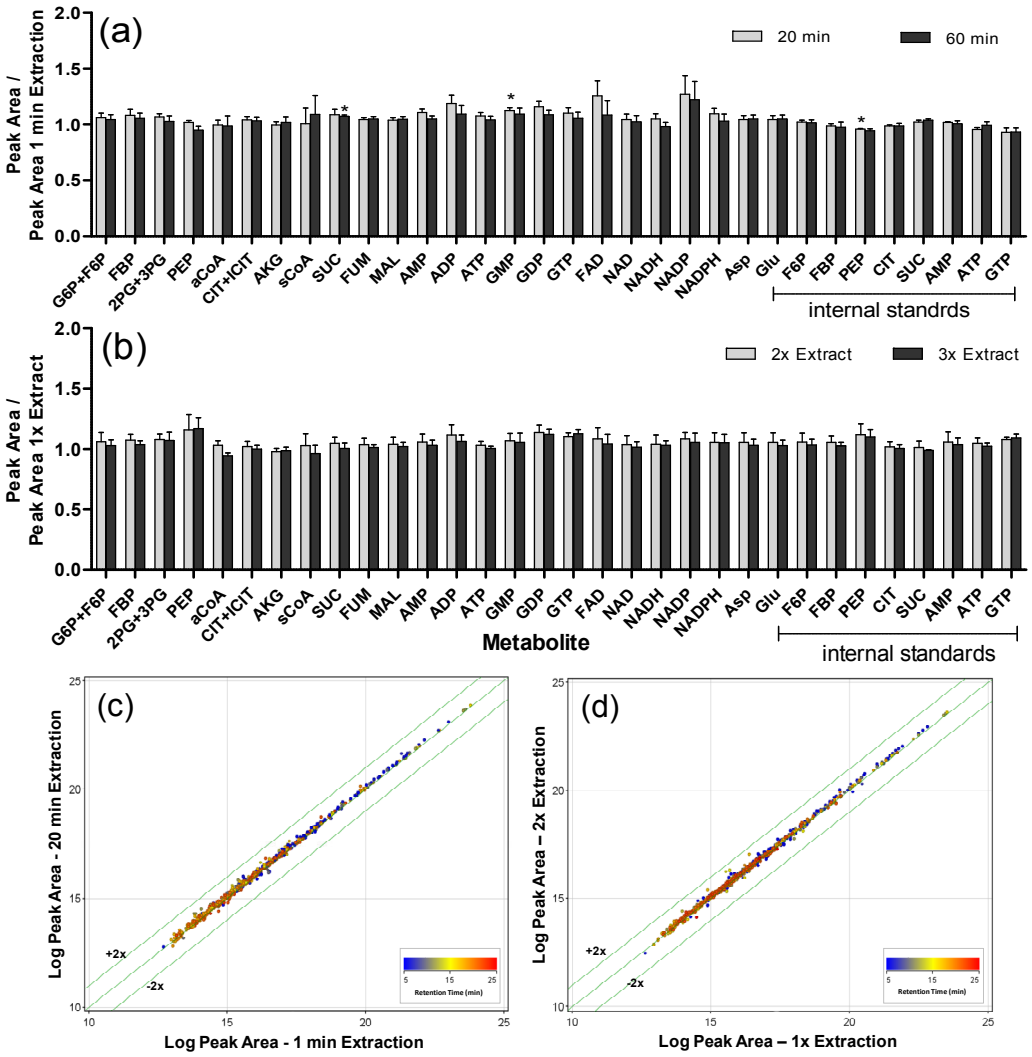

Figure 3-4. Effect of Extraction Time and Multiple Extraction Cycles on Metabolite Peak Areas from INS-1 Cells.

(a) Peak areas for metabolites in INS-1 cells extracted for 20 min and 60 min versus 1 min. Error bars represent 1 SEM, n = 3. No metabolite peak areas are statistically different compared to 1 min extraction with $p < 0.05$. (b) Peak areas for metabolites in INS-1 cells extracted 2x and 3x versus 1x extraction cycle. Error bars represent 1 standard error of the mean (SEM), n = 3. No metabolite peak areas are statistically different compared to 1x extraction cycle with $p < 0.05$. (c) Log-log plot of peak area for features detected in INS-1 cells extracted for 20 min versus 1 min. Features in this plot were detected in all replicates with RSD < 20% in each group. 22 of 981 feature peak areas were statistically different between groups with $p < 0.05$. (d) Log-log plot of peak area for features detected in INS-1 cells extracted with 2x versus 1x cycles of extraction. Plotted features were detected in all replicates with RSD < 20% in each group. 21 of 746 features plotted had peak areas that were statistically different between groups with $p < 0.05$.

Water Rinsing. After aspiration, residual media or buffer remains on the cell and dish surface which is subsequently dissolved into extraction solvent yielding potential for contamination of the intracellular metabolite pool and lowered analytical performance, e.g. due to ionization suppression. A solution to this problem is to rinse residual media/buffer from the cell surface with water prior to quenching; however, legitimate concerns have been raised that such rinsing of mammalian cells may alter intracellular metabolites[9]. We therefore evaluated the impact of rinsing cells with water to eliminate media and buffer residue prior to quenching.

Peak areas for metabolites of glycolysis, the TCA cycle, and related cofactors were compared for cells incubated in KRHB and then rinsed with either KRHB or water prior to quenching. (Non-water rinsed cells were rinsed with KRHB to act as a control by removing extracellular metabolites excreted by cells during incubation). Substantial increases in metabolite peak areas, from 1.5 to 22-fold, were observed for 26 of the measured metabolites in water rinsed samples compared to KRHB rinsed samples (Figure 3-6a). LC-MS chromatograms (Figure 3-6b) illustrate clear enhancement of metabolite signals with water rinse, especially in the 17-25 min range where TCA and glycolysis metabolites elute. A region of broad peaks observed at ~12 min, attributed to HEPES in the KRHB, is decreased by rinsing showing removal of media components. Removing this background simplifies the chromatogram and reveals more metabolites. Overall, water rinsing increased the number of high quality detectable features (i.e., features present in 3 of 3 samples with relative standard deviation (RSD) < 30%) from 237 to 452. The increased signals are attributed at least in part to removal of salts that affect ESI.

Although the increase in signal and detectable features with water rinsing is attractive, it is necessary to determine if the procedure alters the metabolome. To assess this possibility, INS-1 cells were rinsed with water for 2 or 30 s and compared to cells rinsed only with KRHB. To account for differences in MS sensitivity due to ionization suppression, all INS-1 cells were rapidly re-rinsed with KRHB for ~2 s prior to aspiration and quenching. Using this procedure, all cells had the same final matrix, but some had been pretreated with water prior to quenching. For the glycolysis and TCA compounds, no significant differences were found for cells rinsed briefly with water compared to those rinsed with KRHB (see Figure 3-6a) suggesting little alteration of these metabolic pathways or leakage during a short water rinse. In contrast, with a 30 s exposure to pure water significant differences ($p < 0.05$) in peak area are observed for

G6P+F6P, PEP, aCoA, SUC, ADP, and GDP (Figure 3-6a) demonstrating that alteration of metabolite content does occur with water exposure, but only after longer times than necessary to rinse away media.

To further expand on these observations, we compared peak areas for all features detected following a 2 s water rinse and a KRHB rinse (Figure 3-6b). Peak areas ranged from 84% to 123% of control with a mean of 104 ± 8% and no significant features were identified following p-value correction for multiple testing. Thus, little change in peak area was observed for nearly all detected features with rapid water rinse over a broad range of hydrophobicity. We conclude that the short water rinse improves signal without substantially altering the detectable metabolome.

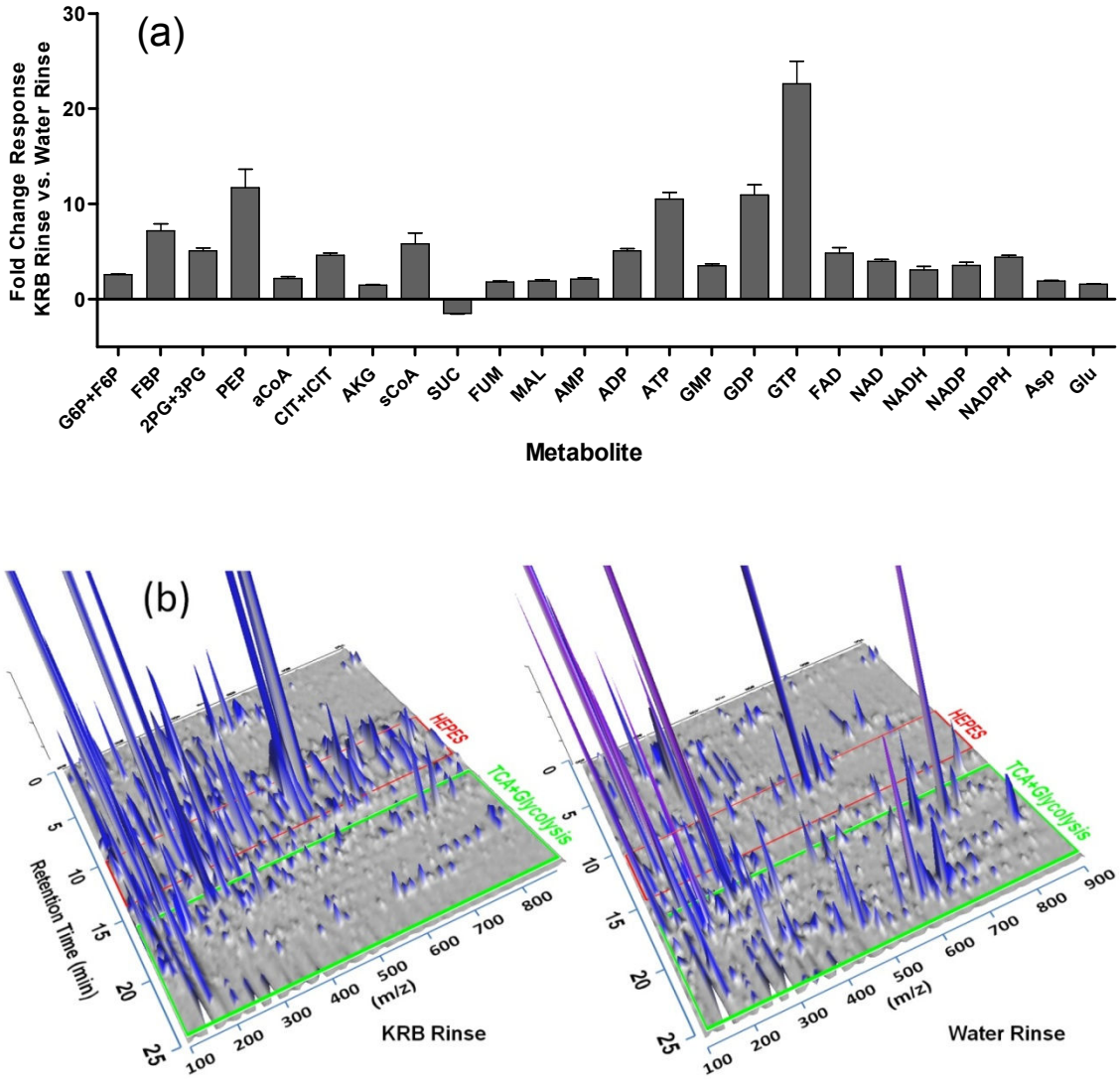

Figure 3-5. Enhancement of Metabolite Peak Area with Water Rinsing.

(a) Fold change enhancement of INS-1 metabolite peak area with water rinse versus KRB rinse. INS-1 cells rinsed with water or KRHB prior to quench and re-rinsed with KRHB to yield an identical residue matrix. (b) 3D MS-chromatograms of KRHB and water rinsed INS-1 cells. Broad peaks from 10 to 15 min are attributed to residual HEPES buffer. Substantial signal enhancement is observed for water rinse sample in 15-20 min region where TCA and glycolysis components elute. Error bars represent 1 SEM, n = 3.

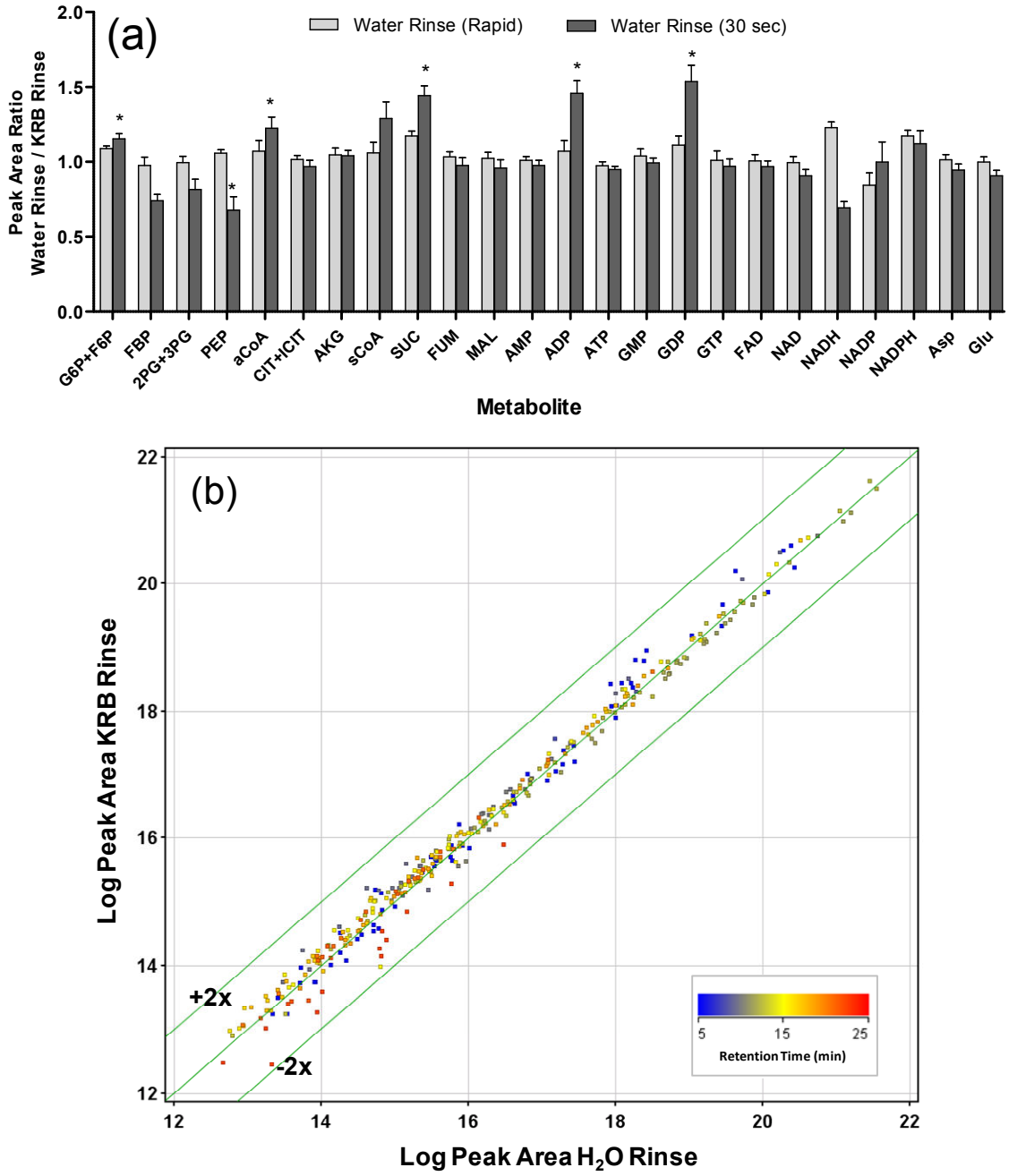

Figure 3-6. Effect of Water Rinse on Metabolite Peak Areas from INS-1 Cells on a Directed and Undirected Basis.

INS-1 cells were rinsed with KRHB, water (rapid ~2 s), or water (incubate 30 s) prior to a second rapid rinse with KRHB to yield an equivalent matrix in all samples prior to quenching. (a) Peak areas ratios for specified metabolites in extracts of cells rinsed with water versus KRHB prior to quench. Error bars represent 1 SEM, n = 3. Asterisk indicates significant difference in peak area with $p < 0.05$. (b) Log-log plot of peak areas for all features detected in extracts of INS-1 cells treated with rapid water or KRHB rinse prior to quenching. Features plotted are detected in all replicates and peak areas have RSD < 25% within each group.

Evaluation of LN_2, -75 °C, and 0 °C Quenching Methods. Most sample preparation procedures use cold organic solvents to simultaneously quench metabolism and initiate metabolite extraction. While these procedures are effective, we investigated applying LN_2 directly to plates to quench metabolism and adding extraction solvent at a later time. This approach of separating quench and extraction steps was designed to allow the analyst to focus on time sensitive biological manipulations (e.g., changing cell media at fixed times) leaving solvent measuring and subsequent extraction steps to be performed later. This approach could prove especially useful when conducting complicated extraction protocols requiring extended incubation times and multiple extraction cycles. An additional benefit of postponing extraction is the flexibility to adjust internal standard concentrations in the extraction solvent based on a preliminary sample analysis without the need to repeat the full set of biological experiments as required by some protocols.[10] Finally, we also observed improved long term (7 d) stability of samples (mean recovery = 98 ± 6% compared to 90 ± 8 %) when stored as frozen plates and extracted shortly before analysis compared to stored as extracts at -80 °C.

To evaluate the performance of the technique, we compared metabolite profiles of INS-1 cells quenched with LN_2 to those quenched and extracted simultaneously with -75 °C and 0 °C 75% 9 :1 MC (Figure 3-7). Peak areas for a majority of metabolites were similar; although, significant differences were observed in metabolite levels for 5 of 27 and 11 of 27 metabolites in -80 °C and 0 °C samples, respectively, relative to LN_2 quench. We conclude that direct LN_2 quenching provides benefits in work flow and stability (at least for the extraction procedures used here) while offering similar metabolite profiles to -75 °C and 0 °C quench methods.

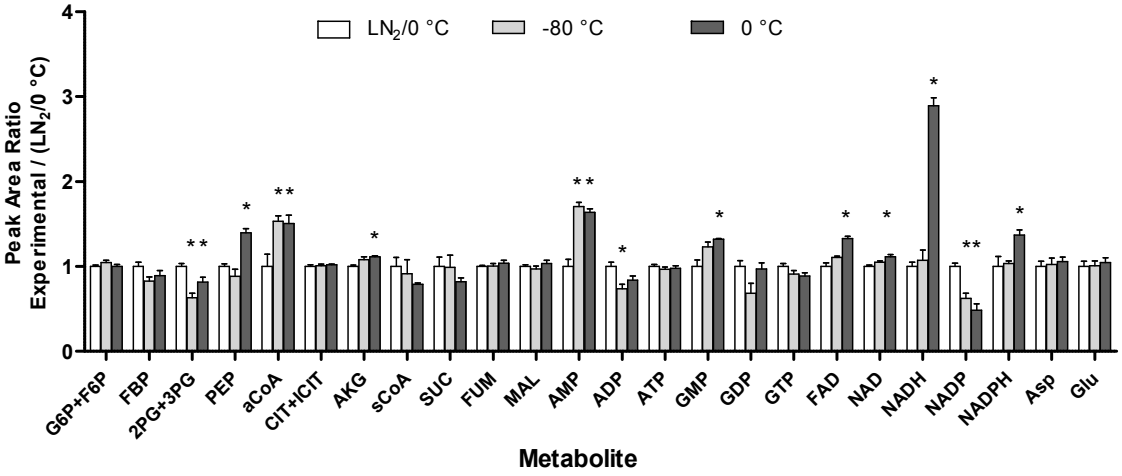

Figure 3-7. Comparison of Metabolite Peak Areas with Different Quenching Techniques.

INS-1 cells quenched with LN_2, -75 °C solvent, and 0 °C solvent, extracted, and assayed. Metabolite peak areas for each technique plotted versus peak areas from LN_2 technique. Error bars represent 1 SEM, n = 3. Asterisk indicates significant difference in peak area with $p < 0.05$.

Short Term Stability. Stability of INS-1 cells extracted with 75% 9:1 MC was evaluated by comparing peak areas for extracts stored at 4 °C for 0, 4 and 8 h (typical auto sampler storage times) before injection (Figure 3-8). Peak areas for metabolites ranged from 87 % to 114 % (mean = 98 ± 9 %) after 8 h of storage versus time 0 injection. The only exception was sCoA which is chemically labile and had a peak area of 65% versus time 0 injection. These results demonstrate that 75% 9:1 MC as extraction solvent affords excellent stability for most metabolites.

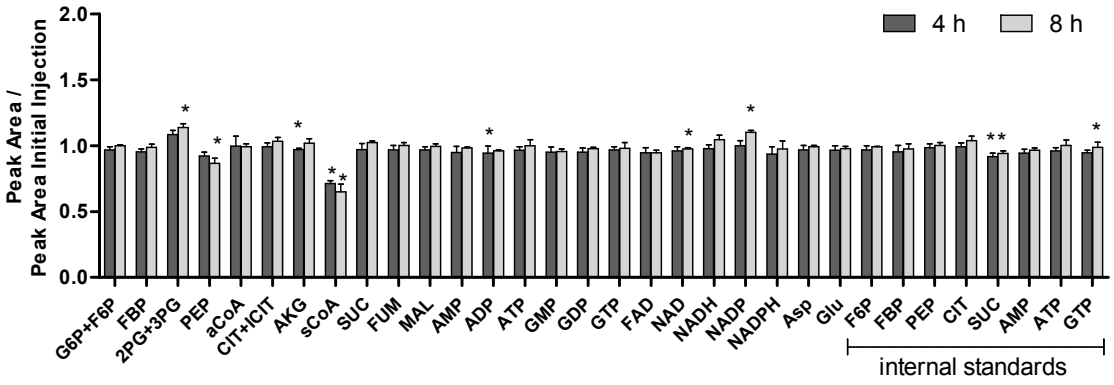

Figure 3-8. Short-term Metabolite Stability of INS-1 Extracts at 4 °C.

(a) Stability of INS-1 metabolites extracted with 75:25 9:1 MC:water after 4 and 8 h 4 °C storage. Metabolite peak area of 4 or 8 h 4 °C stored sample versus T0 sample. Error bars represent 1 SEM, n = 3. Asterisk indicates significant difference in peak area with $p < 0.05$.

Long Term Stability. Long term stability of both INS-1 extracts and non-extracted INS-1 culture plates stored at -80 °C for 7 d was assessed (Figure 3-9). The peak areas of metabolites from glycolysis, the TCA cycle, and related cofactors in culture plates stored at -80 °C were compared to those of samples extracted immediately after quenching and stored in LN_2 prior to injection (T0 control). This procedure allowed for all samples to be injected sequentially which eliminated the potential for instrument sensitivity drift to impact results.

Stability of -80 °C stored extracts was good with metabolite peak areas ranging from 80% to 102% (mean = 90 ± 8 %) versus T0 control with the exception of PEP and NADPH which had peak areas of 74% and 76% versus T0 control, respectively. Non-extracted culture plates stored at -80 °C had improved stability with metabolite peak areas ranging from 74% to 109% versus T0 control (mean = 98 ± 6%). More metabolites had statistically different peak areas relative to T0 control in extracts stored at -80 °C compared to non-extracted plates although, this difference can be attributed to the different quantification approaches used. Metabolite peak areas for stored extracts were compared to their parent T0 control replicate whereas non-extracted plates were compared as groups of true biological replicates. This data demonstrates that samples are stable for at least 1 week at -80 °C stored both as extracts and as non-extracted plates.

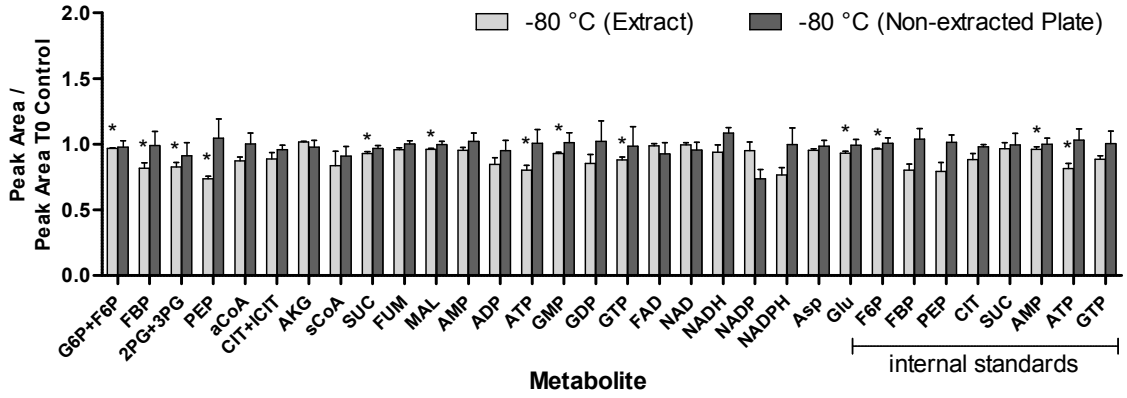

Figure 3-9. Stability of INS-1 Extracts and Non-extracted Plates Stored for 7 d at -80 °C.

Peak area ratio of metabolites in specified storage condition versus peak area in T0 control (extracted at time 0 and stored in LN_2). Error bars represent 1 SEM, n = 3. Asterisk indicates significant difference in peak area with $p < 0.05$.

Comparison of Glucose Stimulation Results with Different Quenching / Preparation Methods. To evaluate the performance of the 9:1 MC method in quantifying changes in metabolite concentration associated with glucose stimulated insulin secretion, we subjected INS-1 cells to step changes in glucose concentration and prepared samples using this method and two established methods, 80% MeOH and B-MTC (Figure 3-10). The final volume of all samples was identical allowing for a direct comparison of results between methods.

We found that the 9:1 MC method tended to give higher peak areas for the glycolytic and TCA compounds (Figure 3-10a). This result was accompanied by higher signal to noise ratios, which was significant for compounds that produced small peak areas such as aCoA, but was less important for more abundant species like MAL (see Figure 3-10b). The 9:1 MC method also allowed detection of sCoA, unlike the other methods. These results suggest overall better sensitivity obtainable by the 9:1 MC method. Because of differences in rinsing, quenching, extraction, heating, and drying steps with each preparation method, it is not possible to directly pinpoint the reasons for this effect, but based on our study we believe that the rinsing step is a key factor in the improved sensitivity as evident in substantially larger peaks for suppressive components such as HEPES in the 80% MeOH chromatograms and phosphate ion in the B-MTC sample.

The improved detection NADH, NADPH, and sCoA may also be attributable to avoiding a heating step. In addition to the improved peak areas, the 9:1 MC method had

the convenience of shorter sample preparation times. The total preparation time for six samples was ~15 min using the 9:1 MC method compared to ~5 h using 80% MeOH and B-MTC methods, with a large portion of preparation time for the 80% MeOH and B-MTC methods devoted to drying samples under N_2 stream. Although the 9:1 MC method had advantages of sensitivity, detection of heat sensitive compounds, and decreased time requirements; we did find that B-MTC method had better reproducibility with average RSD for all glycolytic and TCA components of 11%, 12%, and 7% for 9:1 MC, 80% MeOH, and B-MTC, respectively.

All three methods produced comparable relative changes in metabolites with glucose stimulation (Figure 3-10c). Further, these changes tend to agree well with expectation and previous results. Most detected components in the glycolysis and TCA pathways increased substantially following glucose addition which is consistent with increased glycolysis and anaplerosis in these cells.[23] Using the 9:1 MC method, increases in most components of glycolysis and TCA pathways were moderate (1.6 to 2.0-fold) with the exception of FBP, FUM, and MAL which increased 5.3, 5.3 and 6.9-fold, respectively. The large increases in FUM and MAL likely arise from the high levels of pyruvate carboxylase found in β-cells and the INS-1 clone used in these studies.[24] These results agree with findings from a previous study which reported increases in CIT+ICIT, MAL, AKG, aCoA, and sCoA of 1.5, 2.0, 1.8, 1.5, and 1.9-fold, respectively, upon 30 min glucose stimulation.[25] The previous study also reported little change in Asp and Glu levels which is consistent with results we obtained all three extraction methods. In a similar study, CIT and MAL were observed to increase 2 and 5 fold, respectively, after a 30 min stimulation.[23] We found that NADH increased 4.7-fold which is consistent with an anticipated increase in catabolic reduction charge due to increased glycolysis and TCA cycle flux. Mono and di-phosphonucleotides decreased from -1.2 to -1.5 fold while a slight increase of 1.2 fold was observed for ATP and GTP was little changed. This observed increase in the ATP/ADP ratio is consistent with previous observations for GSIS in islet β-cells.[26]

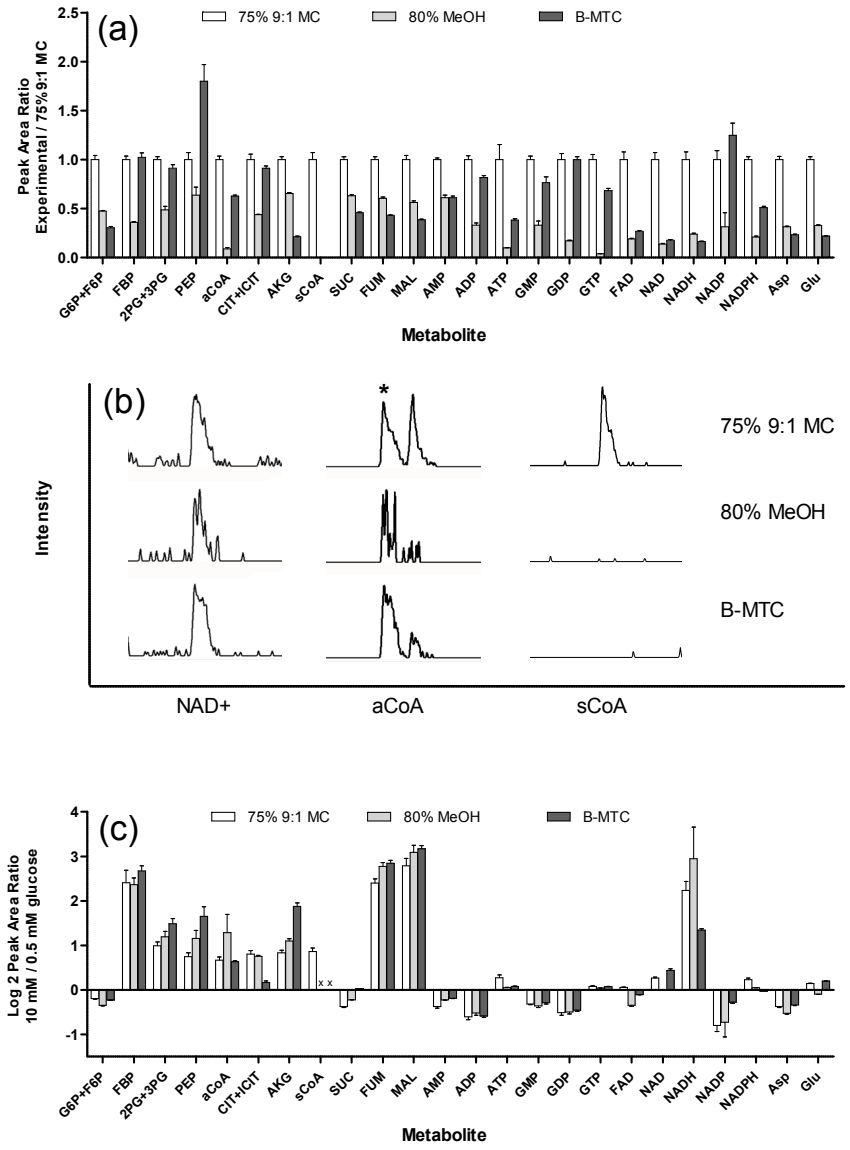

Figure 3-10. Metabolite Peak Areas, Sensitivity, and Changes in INS-1 with Glucose Stimulation Using Proposed and Established Quenching and Extraction Methods.

75% 9:1 MC is water rinse, LN_2 quench, and 1 cycle of 9:1 MC extraction. 80% MeOH is no rinse, -80 °C 8:2 MeOH:H_2O quench, 3 extraction cycles, dried with N_2, and reconstituted in 1:1 MeOH:H_2O. B-MCT is PBS rinse, 4 °C 2:1 MC quench, 2 extraction cycles of 1:1 MeOH:3.8 mM tricine and $CHCl_3$, heat 4 min at 90 °C, dry with N_2, and reconstitute in 1:1 MeOH:H_2O. INS-1 cells incubated in 0.5 mM glucose 30 min versus cells incubated in 0.5 mM glucose 30 min and stimulated to 10 mM glucose for 20 min. (a) Metabolite peak areas ratios versus 9:1 MC for 10 mM glucose samples. Error bars represent 1 SEM, n = 3. (b) Comparison of NAD^+, aCoA, and sCoA chromatograms in 0.5 mM glucose samples. Each individual chromatogram scaled to maximum peak height. Asterisk indicates aCoA peak. (c) Log 2 of the peak area ratio for metabolites in 10 mM glucose versus 0.5 mM glucose. x indicates not detected. Error bars represent 1 SEM, n = 3.

Conclusions

We have developed a sample preparation procedure for global metabolic analysis of adherent mammalian cells that uses water rinsing, LN_2 quenching, and rapid single step extraction. Individual samples can be quenched, prepared, and injected within ~5 min using only 1.5 mL of solvent for a 10 cm plate to minimize dilution. Sensitivity is enhanced by use of water rinsing, which if performed rapidly, does not alter the metabolome. The choice of 75% 9:1 MC extraction solvent yields extracts that are stable for at least 8 h at 4 °C and 7 d at -80 °C. The method produces relative changes in the metabolome that are similar to previous methods that require longer times, but with an overall increase in peak area for better sensitivity. All three methods appear to produce valid metabolite profiles for glucose-stimulation experiments.

Although we have identified conditions that reproducibly extract and stabilize components from glycolysis, the TCA cycle, and nucleotide metabolites from INS-1 cells, it would be premature to conclude that this procedure would be fully applicable to all mammalian cell lines as presented. It is anticipated that most procedural aspects should translate effectively; nevertheless, we suggest that any experiment aimed at characterizing a metabolome should be preceded by careful characterization of the sample preparation procedure.

References

1. Asfari, M., Janjic, D., Meda, P., Li, G., Halban, P.A., and Wollheim, C.B. 1992. Establishment of 2-mercaptoethanol-dependent differentiated insulin-secreting cell lines. *Endocrinology* 130:167-178.
2. Hohmeier, H.E., Mulder, H., Chen, G., Henkel-Rieger, R., Prentki, M., and Newgard, C.B. 2000. Isolation of INS-1-derived cell lines with robust ATP-sensitive K+ channel-dependent and -independent glucose-stimulated insulin secretion. *Diabetes* 49:424-430.
3. Canelas, A.B., Pierick, A., Ras, C., Seifar, R.M., van Dam, J.C., van Gulik, W.M., and Heijnen, J.J. 2009. Quantitative Evaluation of Intracellular Metabolite Extraction Techniques for Yeast Metabolomics. *Anal. Chem.* 81:7379-7389.
4. Teng, Q., Huang, W., Collette, T., Ekman, D., and Tan, C. 2009. A direct cell quenching method for cell-culture based metabolomics. *Metabolomics* 5:199-208.
5. Ritter, J.B., Genzel, Y., and Reichl, U. 2008. Simultaneous extraction of several metabolites of energy metabolism and related substances in mammalian cells: Optimization using experimental design. *Anal. Biochem.* 373:349-369.
6. Wu, J., Wu, L., and Knight, J. 1986. Stability of NADPH: effect of various factors on the kinetics of degradation [published erratum appears in Clin Chem 1987 May;33(5):724]. *Clin. Chem. (Washington, DC, U. S.)* 32:314-319.

7. Gao, L., Chiou, W., Tang, H., Cheng, X., Camp, H.S., and Burns, D.J. 2007. Simultaneous quantification of malonyl-CoA and several other short-chain acyl-CoAs in animal tissues by ion-pairing reversed-phase HPLC/MS. *J. Chromatogr., B: Anal. Technol. Biomed. Life Sci.* 853:303-313.
8. Lane, A., and Fan, T. 2007. Quantification and identification of isotopomer distributions of metabolites in crude cell extracts using 1H TOCSY. *Metabolomics* 3:79-86.
9. Munger, J., Bajad, S.U., Coller, H.A., Shenk, T., and Rabinowitz, J.D. 2006. Dynamics of the Cellular Metabolome during Human Cytomegalovirus Infection. *PLoS Pathog.* 2:1165-1175.
10. Bennett, B.D., Yuan, J., Kimball, E.H., and Rabinowitz, J.D. 2008. Absolute quantitation of intracellular metabolite concentrations by an isotope ratio-based approach. *Nat. Protocols* 3:1299-1311.
11. Hofmann, U., Maier, K., Niebel, A., Vacun, G., Reuss, M., and Mauch, K. 2008. Identification of metabolic fluxes in hepatic cells from transient 13C-labeling experiments: Part I. Experimental observations. *Biotechnology and Bioengineering* 100:344-354.
12. Fernandez, C., Fransson, U., Hallgard, E., Spegel, P., Holm, C., Krogh, M., Warell, K., James, P., and Mulder, H. 2007. Metabolomic and Proteomic Analysis of a Clonal Insulin-Producing Î²-Cell Line (INS-1 832/13). *J. Proteom. Res* 7:400-411.
13. Danielsson, A.P.H., Moritz, T., Mulder, H., and Spégel, P. 2010. Development and optimization of a metabolomic method for analysis of adherent cell cultures. *Analytical Biochemistry* 404:30-39.
14. Sellick, C.A., Hansen, R., Maqsood, A.R., Dunn, W.B., Stephens, G.M., Goodacre, R., and Dickson, A.J. 2008. Effective Quenching Processes for Physiologically Valid Metabolite Profiling of Suspension Cultured Mammalian Cells. *Anal. Chem.* 81:174-183.
15. Myint, K.T., Uehara, T., Aoshima, K., and Oda, Y. 2009. Polar Anionic Metabolome Analysis by Nano-LC/MS with a Metal Chelating Agent. *Anal. Chem.* 81:7766-7772.
16. Bajad, S.U., Lu, W., Kimball, E.H., Yuan, J., Peterson, C., and Rabinowitz, J.D. 2006. Separation and quantitation of water soluble cellular metabolites by hydrophilic interaction chromatography-tandem mass spectrometry. *J. Chromatogr., A* 1125:76-88.
17. Uehara, T., Yokoi, A., Aoshima, K., Tanaka, S., Kadowaki, T., Tanaka, M., and Oda, Y. 2009. Quantitative Phosphorus Metabolomics Using Nanoflow Liquid Chromatography-Tandem Mass Spectrometry and Culture-Derived Comprehensive Global Internal Standards. *Anal. Chem.* 81:3836-3842.
18. Bennett, B.D., Yuan, J., Kimball, E.H., and Rabinowitz, J.D. 2008. Absolute quantitation of intracellular metabolite concentrations by an isotope ratio-based approach. *Nat. Protoc.* 3:1299-1311.
19. Rabinowitz, J.D., and Kimball, E. 2007. *Analytical Chemistry* 79:6167.
20. Kimball, E., and Rabinowitz, J.D. 2006. Identifying decomposition products in extracts of cellular metabolites. *Analytical Biochemistry* 358:273-280.
21. Canelas, A.B., Pierick, A., Ras, C., Seifar, R.M., van Dam, J.C., van Gulik, W.M., and Heijnen, J.J. 2009. Quantitative Evaluation of Intracellular Metabolite Extraction Techniques for Yeast Metabolomics. *Analytical Chemistry* 81:7379-7389.
22. Ritter, J.B., Genzel, Y., and Reichl, U. 2008. Simultaneous extraction of several metabolites of energy metabolism and related substances in mammalian cells: Optimization using experimental design. *Analytical Biochemistry* 373:349-369.
23. Schuit, F., De Vos, A., Farfari, S., Moens, K., Pipeleers, D., Brun, T., and Prentki, M. 1997. Metabolic Fate of Glucose in Purified Islet Cells. *J. Biol. Chem.* 272:18572-18579.
24. Joseph, J.W., Jensen, M.V., Ilkayeva, O., Palmieri, F., Alarcon, C., Rhodes, C.J., and Newgard, C.B. 2006. The mitochondrial citrate/isocitrate carrier plays a regulatory role in glucose-stimulated insulin secretion. *J. Biol. Chem.* 281:35624-35632.
25. MacDonald, M.J. 2007. Synergistic Potent Insulin Release by Combinations of Weak Secretagogues in Pancreatic Islets and INS-1 Cells. *J. Biol. Chem.* 282:6043-6052.
26. Jensen, M.V., Joseph, J.W., Ronnebaum, S.M., Burgess, S.C., Sherry, A.D., and Newgard, C.B. 2008. Metabolic cycling in control of glucose-stimulated insulin secretion. *Am. J. Physiol. Endocrinol. Metab.* 295:E1287-1297.

CHAPTER 4
Metabolomic Analysis of INS-1 Cells Reveal Temporal Metabolic Changes Associated with Glucose-Stimulated Insulin Secretion

Introduction

Progressive reduction in β-cell mass or secretory capacity causes abnormalities of glucose metabolism, resulting in diabetes and its complications such as retinopathy, kidney failure, nerve damage, cardiovascular disease and increases in premature death. β-cells in the islets of Langerhans secrete insulin in response to elevated blood glucose and acute increases in blood glucose evokes a rapid pulse of insulin secretion lasting a few min, designated as the 1st phase, followed by a lower, extended period of secretion, (2nd phase). An early sign of β-cell dysfunction is the loss of first phase of insulin secretion.[1] Despite extensive research, the metabolic pathways that facilitate first and second phase of glucose-stimulated insulin secretion (GSIS) by β-cells are not fully understood.[2] GSIS is thought to be triggered by closure of K_{ATP} channels due to an increase in the ATP/ADP ratio concurrent with metabolism of glucose. Closure of K_{ATP} channels causes membrane depolarization, opening of voltage sensitive Ca^{2+} channels, and subsequent exocytosis of a readily available pool of insulin vesicles.[3] In addition to the K_{ATP} dependent mechanism, evidence supports the concept that other metabolic processes also facilitate GSIS in K_{ATP}-independent or amplifying pathways.[4-6] A variety of metabolic coupling factors including NADPH and long-chain acyl-CoAs generated by pyruvate/citrate, pyruvate/isocitrate, pyruvate/malate, and glycerolipid/fatty acid cycling pathways have been implicated in both triggering and amplifying GSIS.[4-6]

Measurements of metabolic changes that correlate with GSIS, both temporally and with glucose dose, are invaluable in elucidating biochemical mechanisms that underlie this process. Most work on β-cell metabolism to date has been limited to measuring a relatively small set of metabolites using enzyme and other single analyte assays. In addition, studies of changes in metabolite levels following glucose exposure have been performed in time periods that cannot dissect the important alterations that occur in the

first and second phases of insulin secretion, nor have there been detailed evaluation of changes in metabolism that result in the decline in insulin secretion in the second phase. Improvements in separations techniques and mass spectrometry have allowed measurement of a greater number of metabolites creating the opportunity for a more global view of metabolic state.[7-9] For example, a recent study of INS-1 832/1, 832/2, and 832/13 clones using GC-MS measured 44 metabolites (164 peaks were detected) following prolonged exposure (1 hour) to 3 or 17 mM glucose.[8]

In this work, we employed quenching and extraction procedures for in glucose-responsive INS-1 832/13 cells[10] which allow for quantitative and reproducible recovery of metabolites[11] followed by liquid chromatography-time of flight-mass spectrometry (LC-TOF-MS) to measure hundreds of metabolites following exposure to glucose. Measurements were made between 2 to 45 min, encompassing both first and second phases of insulin secretion. Metabolites associated with glycolysis and the TCA cycle were assessed in a targeted manner. Further, we used "undirected" analysis to monitor hundreds of metabolites following glucose treatment and compounds that changed in concentration were identified by matching accurate molecular ion mass to metabolite databases and identifications validated by comparing experimental to theoretical isotope ratios and with retention time match to commercial standards, when available. By measuring targeted and identified metabolites as they changed during both first and second phase GSIS and with glucose concentration, we were able to test prevailing hypotheses of the mechanisms of GSIS and identify new pathways of interest.

Experimental Procedures

Materials. All chemicals were purchased form Sigma-Aldrich (St. Louis, MO) unless otherwise noted. HPLC grade acetonitrile was purchased from Burdick & Jackson (Muskegon, MI). RPMI media, fetal bovine serum, 4-(2-hydroxyethyl)-1-piperazineethanesulfonic acid (HEPES), and penicillin-streptomycin were purchased from Invitrogen Corp. (Carlsbad, CA). Cells lifters and 10 cm polystyrene non-pyrogenic culture dishes were purchased from Corning (Lowell, MA).

Cell Culture. INS-1 832/13 cells cultured in RPMI supplemented with 2 mM glutamine, 1 mM sodium pyruvate, 10% FBS, 10 mM HEPES, 100 U/mL penicillin, 100

μg/mL streptomycin, 250 ng/mL amphotericin B, and 50 uM β-mercaptoethanol. Cells were plated at a density of ~14x10^3 cells/cm^2 and grown in either 6 cm or 10 cm culture dishes at 37 °C and 5% CO_2 in a humidified atmosphere to ~70% confluence over ~5 d prior to experimentation. Cells were preincubated in supplemented RPMI containing 3 mM glucose ~20 h prior to experimentation. KRHB (Krebs-Ringer-HEPES buffer) was prepared containing 10 mM glucose, 20 mM HEPES, 118 mM NaCl, 5.4 mM KCl, 2.4 mM CaCl, 1.2 mM $MgSO_4$, and 1.2 mM KH_2PO_4 and adjusted to pH 7.4 with HCl.

Glucose Stimulation Dose/Response. Following preincubation, culture media was replaced with KRHB containing 0, 2, 5, 10, or 20 mM glucose + 0.2% BSA. Cells were incubated for 30 min after which an aliquot of buffer was removed for insulin measurement. Metabolism was immediately quenched and metabolites extracted as described previously.[11]

Glucose Stimulation Time Course. Cells were transferred to KRHB containing 0.5 mM glucose and 0.2% BSA for 30 min prior to stimulation and spiked to 10 mM glucose by adding an aliquot of 1 M glucose stock. The buffer was sampled for insulin measurement 5 to 90 min after initial transfer to 0.5 mM KRHB (both pre and post stimulation). For metabolite measurements, cells were treated as indicated above (without addition of BSA) and cell plates quenched from 25 to 75 min after transfer to KRHB. Carbon flux through glucose was also assessed by stimulating cells with [U-^{13}C]- glucose for 60 min. For absolute metabolite quantification, INS-1 cells were stimulated for 30 min with 10 mM glucose and quenched. For insulin and metabolite measurements with AICAR treatment, stimulation was conducted by conditioning cells in KRHB containing 0.5 mM glucose for 30 min and replacing the buffer with KRHB containing 10 mM glucose with or without 25 μM AICAR. Incubation buffer was sampled for insulin and plates quenched from 10 to 60 min following stimulation.

Insulin measurement. Aliquots of KRHB were briefly stored on ice, centrifuged at 3000 rpm for 3 min to pellet any suspended cells, and an aliquot of supernatant was transferred to a fresh vial. Samples were stored at -20 °C and assayed using a Millipore Rat/Mouse insulin ELISA Kit. Insulin secretion rate was calculated by dividing the difference in insulin concentration of 2 consecutive time points by the time elapsed between sampling (Figure 4-1).

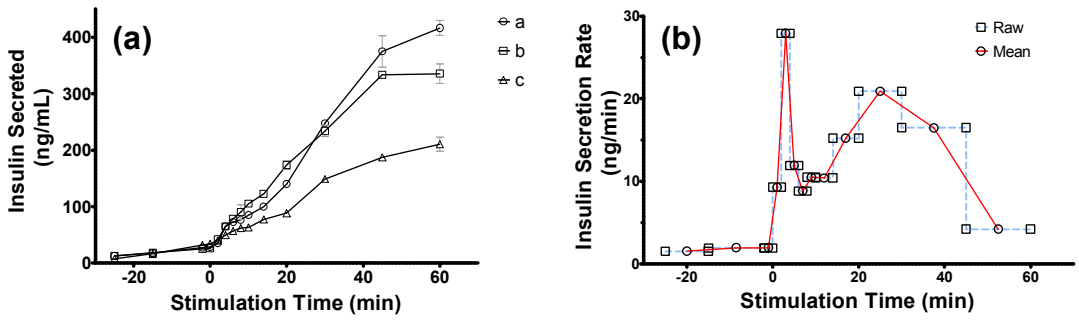

Figure 4-1. Time-Course Insulin Release from INS-1 832/13 Cells Following Glucose Stimulation.

(a) Total insulin secreted versus stimulation time (0.5 to 10 mM glucose) for 3 plates of INS-1 cells (a, b and c). Error bars represent SEM of analytical replicates, n=2. (b) Insulin secretion rate versus stimulation time. Average secretion rate calculated based on insulin released between each sampling interval and plotted (blue dash). The average rate at average sampling interval is plotted in red.

Metabolite measurement. Cell plates were rinsed, metabolism quenched, and metabolites extracted using the procedure described previously[11] and in Chapter 3. Briefly, cell plates were rapidly rinsed with water and quenched with liquid nitrogen. Metabolites were extracted with 75% 9:1 methanol:chloroform 25% water and assayed by HPLC-TOF-MS. For absolute quantification, a standard addition approach was used to quantify metabolites in cells stimulated for 30 min with 10 mM glucose. Residual protein was determined by Bradford Assay.[12] Untargeted and targeted data processing was performed as described previously.[11] Metabolites previously implicated in GSIS (e.g. glycolysis and TCA cycle) were quantified directly using standards to confirm peak assignments and ^{13}C labeled internal standards, when available, to improve precision (Table 1). Combined peak areas are reported for unresolved isomers (e.g. citrate + isocitrate and hexose phosphates). Several key metabolites such as pyruvate and oxaloacetate are not detected by the method and accurate measurement of these metabolites is difficult due to rapid degradation of oxaloacetate to pyruvate.[13] Glyceraldehyde-3-phosphate and dihydroxyacetone phosphate are also highly unstable in solution.[14] Undirected analysis was performed by identifying metabolites that changed in LC-MS peak area following a step change from 0.5 to 10 mM glucose for 25 min. Features that were detected in every chromatogram and had < 40% RSD within each group were included in the analysis. For these chromatographic peaks, each mass

spectra was evaluated to verify molecular ion assignment through investigating corresponding potential adducts and fragments. Metabolites were tentatively identified through accurate mass search of the Human Metabolome Database and further validated by comparison of theoretical and observed isotopic distributions and coelution studies with authentic standards, when available (Table 1).

Western Blot. Glucose stimulation cells were placed on ice, washed once with ice cold PBS and solubilized in 75 µL Laemelli's/extraction buffer (20 mM HEPES pH 7.5, 1% Triton X-100, 20 mM beta-glycerophosphate, 150 mM NaCl, 10 mM NaF, 1mM sodium orthovanadate, and complete protease inhibitor cocktail (Roche)). Anti-ACC was obtained from Cell Signaling and used at 1:1000. Blots were developed with ECL (Pierce, Rockford, IL) according to the manufacturer's instructions.

Statistics. Data are expressed as the mean ± standard error of the mean (SEM). Statistical significance was determined using a non-corrected two-tailed Student's t test, unpaired assuming equal variance. A p-value of < 0.05 was considered statistically significant

Results

Insulin Secretion Studies. The EC_{50} value for insulin secretion from INS-1 832/13 cells in response to glucose stimulation was 6.2 mM with near maximal insulin secretion observed at ~10 mM glucose (Figure 4-1), similar to previous reports.[10] Temporal changes in insulin secretion were observed with a relatively sharp peak at ~4 min (28 ng/mg protein min) and a lower level with a maxima at ~25 min corresponding roughly to Phase 1 and Phase 2 of insulin secretion consistent with previous reports of GSIS in islets[15] and INS-1 832/13 cells[16] (Figure 4-2).

Table 4-1. Metabolites Identified in INS-1 Extracts.

Metabolite	Abbreviation	Standard Type	ID By (U,D,F)	MF	Theoretical Mass (amu)	Measured Mass (amu)	Difference (ppm)	Concentration (nmole/mg protein)
Glycolysis								
hexose-phosphate	HP	^{13}C	D, U	$C_6H_{13}O_9P$	260.0297	260.0289	-3.0	58
fructose 1,6-bisphosphate	FBP	^{13}C	D	$C_6H_{14}O_{12}P_2$	339.9960	339.9956	-1.1	13
2-phosphoglycerate + 3-phosphoglycerate	2PG+3PG	^{13}C	D, U	$C_3H_7O_7P$	185.9929	185.9924	-2.6	11
phosphoenolpyruvate	PEP	^{13}C	D	$C_3H_5O_6P$	167.9824	167.9812	-7.0	2.3
glycerol-3-phosphate	G3P	^{12}C	U	$C_3H_9O_6P$	172.0137	172.0135	-1.0	15
lactate	LAC	^{13}C	D	$C_3H_6O_3$	90.0317	90.0315	-2.0	41
Tricarboxylic Acid Cycle								
acetyl- Coenzyme A	aCoA	^{12}C	D	$C_{23}H_{38}N_7O_{17}P_3S$	809.1258	809.1242	-1.9	1.6
citrate+isocitrate	CIT+ICIT	^{13}C	D, U	$C_6H_8O_7$	192.0270	192.0262	-4.1	110
alpha-ketogluterate	AKG	^{13}C	D, U	$C_5H_6O_5$	146.0215	146.0207	-5.3	22
succinyl-coa	sCoA	^{12}C	D	$C_{25}H_{40}N_7O_{19}P_3S$	867.1312	867.1294	-2.0	0.85
succinate	SUC	^{13}C	D, U	$C_4H_6O_4$	118.0266	118.0275	7.8	22
fumarate	FUM	^{13}C	D, U	C_4H4O_4	116.0110	116.0107	-2.4	17
malate	MAL	^{12}C	D, U	$C_4H_6O_5$	134.0215	134.0211	-2.8	67
malonyl- Coenzyme A	mCoA	^{12}C	D	$C_{24}H_{38}N_7O_{19}P_3S$	853.1156	809.1208	-6.1	0.86
aspartic acid	Asp	^{12}C	D	$C_4H_7NO_4$	133.0375	133.0372	-2.1	750
glutamic acid	Glu	^{12}C	D	$C_5H_9NO_4$	147.0532	147.0528	-2.6	2500
Pentose phosphate pathway								
ribose phosphate	R5P	^{12}C	U	$C_5H_{11}O_8P$	230.0191	230.0183	-3.4	3.4
6-phosphogluconic acid	6PG	^{12}C	U	$C_6H_{13}O_{10}P$	276.0246	276.0242	-1.4	2.7
sedoheptulose-7-phosphate	S7P	^{12}C	U	$C_7H_{15}O_{10}P$	290.0403	290.0405	0.8	12
phosphoribosyl pyrophosphate	PRPP	^{12}C	F	$C_5H_{13}O_{14}P_3$	389.9518	389.9505	-3.3	3.5
Nucletotides								
adenosine monophosphate	AMP	^{13}C	D, U	$C_{10}H_{14}N_5O_7P$	347.0631	347.0620	-3.1	11
adenosine diphosphate	ADP	^{13}C	D	$C_{10}H_{15}N_5O_{10}P_2$	427.0294	427.0282	-2.8	18
adenosine triphosphate	ATP	^{13}C	D	$C_{10}H_{16}N_5O_{13}P_3$	506.9957	506.9949	-1.5	850
guanosine monophosphate	GMP	^{12}C	D, U	$C_{10}H_{14}N_5O_8P$	363.0580	363.0577	-0.8	2.8
guanosine diphosphate	GDP	^{12}C	D, U	$C_{10}H_{15}N_5O_{11}P_2$	443.0243	443.0245	0.5	4.5
guanosine triphosphate	GTP	^{13}C	D	$C_{10}H_{16}N_5O_{14}P_3$	522.9907	522.9900	-1.3	3.9
uridine monophosphate	UMP	^{12}C	U	$C_9H_{13}N_2O_9P$	324.0359	324.0350	-2.7	na
uridine diphosphate	UDP	^{12}C	F	$C_9H_{14}N_2O_{12}P_2$	404.0022	404.0020	-0.4	na
uridine triphosphate	UTP	^{12}C	F	$C_9H_{15}N_2O_{15}P_3$	483.9685	483.9679	-1.2	na
cytidine monophosphate	CMP	^{12}C	F	$C_9H_{14}N_3O_8P$	323.0518	323.0502	-4.9	na
cytidine diphosphate	CDP	^{12}C	F	$C_9H_{15}N_3O_{11}P_2$	403.0182	403.0178	-0.9	na
cytidine triphosphate	CTP	^{12}C	F	$C_9H_{16}N_3O_{14}P_3$	482.9845	482.9833	-2.4	na
nicotinamide adenine dinucleotide	NAD	^{12}C	D	$C_{21}H_{27}N_7O_{14}P_2$	663.1091	663.1089	-0.3	37
nicotinamide adenine dinucleotide, reduced	NADH	^{12}C	D, U	$C_{21}H_{28}N_7O_{14}P_2$	665.1242	665.1240	-0.3	2.0
nicotinamide adenine dinucleotide phosphate	NADP	^{12}C	D, U	$C_{21}H_{28}N_7O_{17}P_3$	743.0755	743.0710	-6.0	0.92
nicotinamide adenine dinucleotide phosphate, reduced	NADPH	^{12}C	D	$C_{21}H_{29}N_7O_{17}P_3$	745.0911	745.0925	1.9	4.0
flavin adenine dinucleotide	FAD	^{12}C	D	$C_{27}H_{33}N_9O_{15}P_2$	785.1571	785.1565	-0.7	2.6
Amino Acids								
asparagine	Asn	^{12}C	U	$C_4H_8N_2O_3$	132.0535	132.0531	-2.9	39
glutamine	Gln	^{12}C	U	$C_5H_{10}N_2O_3$	146.0691	146.0687	-2.6	76
lysine	Lys	^{12}C	U	$C_6H_{14}N_2O_2$	146.1055	146.1050	-3.3	15
ornithine	Orn	^{12}C	U	$C_5H_{12}N_2O_2$	132.0899	132.0895	-2.9	22
serine	Ser	^{12}C	U	$C_3H_7NO_3$	105.0426	105.0421	-4.6	25
Long Chain CoAs								
14:0 Conenzyme A	14:0-CoA	na	F	$C_{39}H_{62}N_7O_{17}P_3S$	977.3135	977.3108	-2.7	na
16:0 Conenzyme A	16:0-CoA	^{12}C	U	$C_{37}H_{66}N_7O_{17}P_3S$	1005.3448	1005.3450	0.2	0.46
16:1 Conenzyme A	16:1-CoA	na	F	$C_{37}H_{64}N_7O_{17}P_3S$	1003.3384	1003.3280	-10.3	na
18:0 Conenzyme A	18:0-CoA	na	F	$C_{39}H_{70}N_7O_{17}P_3S$	1033.3761	1033.3688	-7.0	na
18:1 Conenzyme A	18:1-CoA	na	F	$C_{39}H_{68}N_7O_{17}P_3S$	1031.3605	1031.3590	-1.4	na
Sugar Nucleotide Donors								
GDP- mannose	GDP-M	^{12}C	U	$C_{16}H_{25}N_5O_{16}P_2$	605.0771	605.0780	1.5	4.2
UDP-d-galacturonate	UDP-GA	na	F	$C_{15}H_{22}N_2O_{18}P_2$	580.0343	580.0334	-1.5	na
GDP-fucose	GDP-F	na	F	$C_{16}H_{25}N_5O_{15}P_2$	589.0822	589.0827	0.9	na
UDP-GlcNAc+GalNAc	UDP-GlcNAc + GalNAc	na	F	$C_{17}H_{27}N_3O_{17}P_2$	607.0816	607.0814	-0.3	na
UDP-xylose	UDP-X	na	F	$C_{14}H_{22}N_2O_{16}P_2$	536.0444	536.0408	-6.7	na
UDP-glucose + UDP-galactose	UPD-Glc + UDP-Gal	na	F	$C_{15}H_{24}N_2O_{17}P_2$	566.0550	566.0528	-3.9	7.3
Miscellaneous								
aminoimidazole carboxamide ribonucleotide	ZMP	^{12}C	U	$C_9H_{15}N_4O_8P$	338.0627	338.0614	-3.8	4
glycineamideribotide	GAR	na	U	$C_7H_{15}N_2O_8P_1$	286.0566	286.0577	3.9	na
phosphocreatine	PCRE	^{12}C	U	$C_4H_{10}N_3O_5P$	211.0358	211.0351	-3.2	120
creatine	CRE	^{12}C	U	$C_4H_9N_3O_2$	131.0695	131.0703	6.3	8.4
phosphate	PO4	^{12}C	U	H_4O_4P	97.9769	97.9772	3.4	383
pantothenic acid	PAN	^{12}C	U	$C_9H_{17}NO_5$	219.1107	219.1120	6.0	0.035
2-o-(6-phospho-alpha-mannosyl)-d-glycerate	PMG	na	U	$C_9H_{17}O_{12}P_1$	348.0458	348.0432	-7.4	na
cytidine diphosphate- ethanolamine	CDP-EA	na	U	$C_{11}H_{20}N_4O_{11}P_2$	446.0604	446.0594	-2.2	na
beta-aspartylglycine	DG	na	U	$C_6H_{10}N_2O_5$	190.0590	190.0594	2.2	na
citicoline	CC	na	U	$C_{14}H_{26}N_4O_{11}P_2$	488.1073	488.1060	-2.6	na
farnesyl pyrophosphate	FPP	na	U	$C_{15}H_{28}O_7P_2$	382.1310	382.1296	-3.6	na
L-beta-aspartyl-L-alanine or 5-L-Glutamylglycine	DA or EG	na	U	$C_7H_{12}N_2O_5$	204.0746	204.0748	1.1	na
glycerylphosphorylethanolamine	GPEA	na	U	$C_5H_{14}NO_6P$	215.0559	215.0551	-3.6	na
Hexol phosphates	MP	na	U	$C_6H_{15}O_9P$	262.0454	262.0443	-4.1	na
HMG-CoA	HMG-CoA	^{12}C	F	$C_{27}H_{44}N_7O_{20}P_3S$	911.1574	911.1548	-2.9	na
Free Fatty Acids								
16:0	16:0	^{12}C	F	$C_{16}H_{32}O_2$	256.2402	256.2396	-2.3	na
18:0	18:0	^{12}C	F	$C_{18}H_{36}O_2$	284.2715	284.2712	-1.0	na
18:1	18:1	^{12}C	F	$C_{18}H_{34}O_2$	282.2559	282.2554	-1.7	na
18:2	18:2	na	F	$C_{18}H_{32}O_2$	280.2402	280.2398	-1.4	na
20:0	20:0	^{12}C	F	$C_{20}H_{40}O_2$	312.3028	312.3011	-5.4	na
20:1	20:1	na	F	$C_{20}H_{38}O_2$	310.2872	310.2872	0.1	na
20:2	20:2	na	F	$C_{20}H_{36}O_2$	308.2715	308.2711	-1.2	na
22:0	22:0	^{12}C	F	$C_{22}H_{44}O_2$	340.3341	340.3335	-1.7	na
22:1	22:1	na	F	$C_{22}H_{42}O_2$	338.3185	338.3193	2.4	na
22:2	22:2	na	F	$C_{22}H_{40}O_2$	336.3028	336.3031	1.0	na
22:3	22:3	na	F	$C_{22}H_{38}O_2$	334.2872	334.2855	-5.0	na
24:0	24:0	^{12}C	F	$C_{24}H_{48}O_2$	368.3654	368.3652	-0.5	na
24:1	24:1	na	F	$C_{24}H_{46}O_2$	366.3498	366.3464	-9.2	na
24:2	24:2	na	F	$C_{24}H_{44}O_2$	364.3341	364.3308	-9.0	na
24:3	24:3	na	F	$C_{24}H_{42}O_2$	362.3185	362.3182	-0.8	na

Metabolite identified by: D = directed, U = undirected, F = follow up analysis

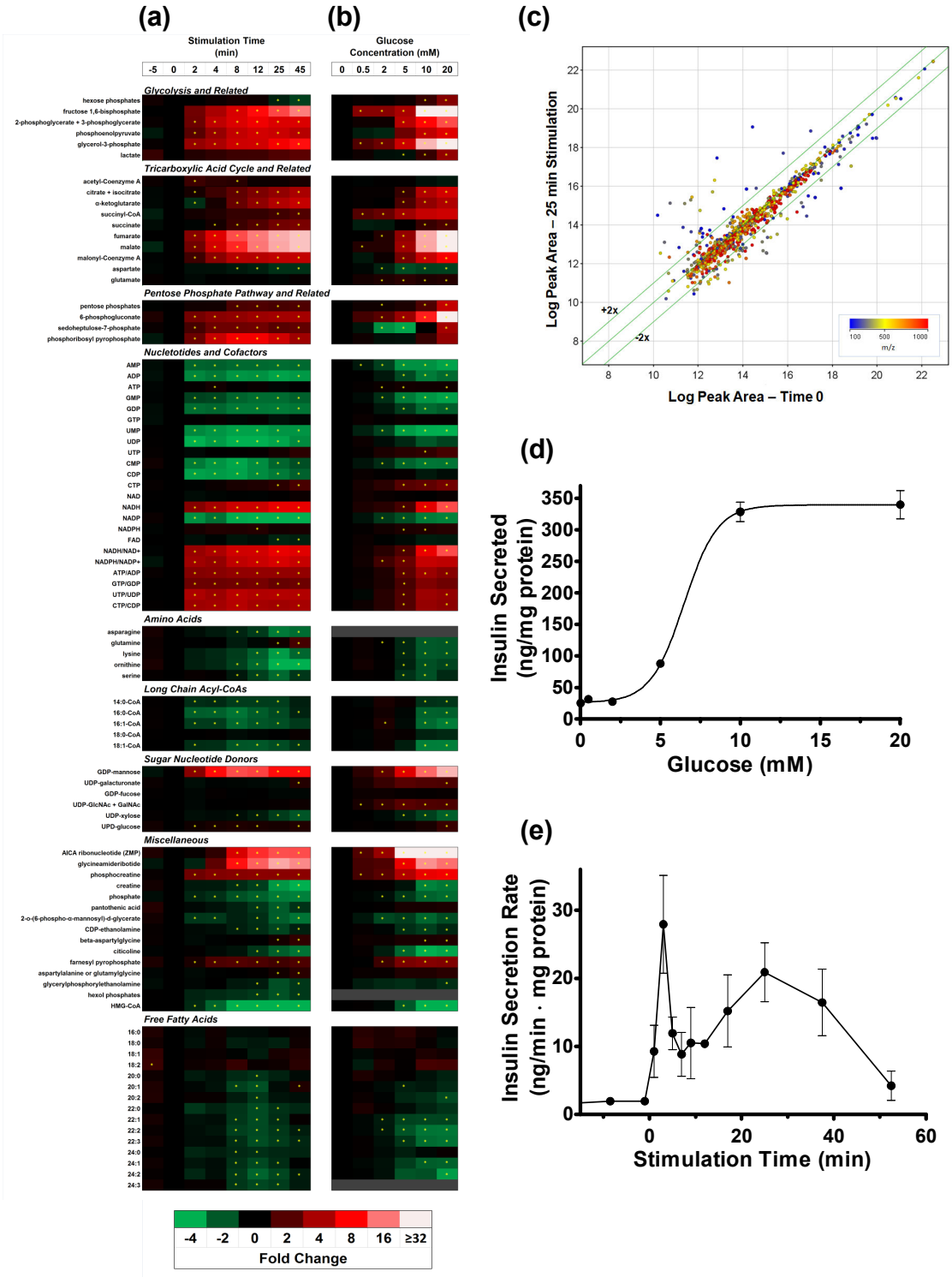

Figure 4-2. Temporal and Dose-Response Metabolite Profiles and Insulin Release with Glucose Stimulation in INS-1 832/13 cells.

(Caption continued on next page)

(a) Temporal changes in INS-1 metabolite levels expressed as fold change versus time 0 with glucose stimulation. Cells incubated in KRHB + 0.5 mM glucose for 30 min then stimulated to 10 mM glucose and sampled over 45 min. Asterisk indicates significant difference in peak area versus time 0 with $p < 0.05$. (b) Changes in INS-1 metabolite levels with glucose concentration. Changes in metabolite levels expressed as fold change versus 0 mM glucose condition. INS-1 cells incubated in KRHB + 0.2% BSA and 0 to 20 mM glucose for 30 min. Asterisk indicates significant difference in peak area versus time 0 with $p < 0.05$. (c) Log-log plot for all features detected at time 0 (0.5 mM glucose) versus 25 min of 10 mM glucose stimulation. Features colored by m/z. The 1030 features plotted were detected in all replicates with RSD < 40% for either Time 0 or 25 min groups. 130 feature peak areas change >1.5 fold and are statistically different with $p < 0.05$.Insulin secretion profiles for INS-1 cells. (d) Insulin secreted by INS-1 832/13 cells versus glucose concentration. Cells incubated in KRBH +0.2% BSA and 0 to 20 mM glucose for 30 min. Error bars are 1 SEM, n=3. (e) Insulin secretion rate versus stimulation time. INS-1 cells incubated in KRHB + 0.2% BSA + 0.5 mM glucose for 30 min and stimulated with 10 mM glucose for 50 min.

Metabolomics. Metabolites were measured using a combined targeted and untargeted metabolomics approach. A summary of the metabolites identified is given in Table 1. Undirected analysis was performed by identifying metabolites that changed in LC-MS peak area following glucose stimulation. The log of mean peak areas of 1030 features were compared for 0 and 25 min groups (Figure 4-1c). We found 190 features showed statistically significant changes ($p < 0.05$) and at least 1.5 fold differences between 0.5 and 10 mM glucose. Through accurate mass search of the Human Metabolome Database, forty metabolite identities were proposed. These identities were validated by comparison of theoretical and observed isotopic distributions and coelution studies with authentic standards, when available (Table 1). These metabolites included compounds rarely measured in the study of GSIS such as phosphocreatine, long-chain acyl-CoAs, and glycerol-3-phosphate. We also identified several metabolites that rapidly change with glucose stimulation but have not been previously reported in β-cells such as ZMP and GDP-mannose. Based on hypotheses generated through initial directed and undirected analysis, mass chromatograms were further analyzed for additional metabolites of interest. For example, after identifying GDP-mannose, we searched for other glycosyltransferase substrates in the data set and found several not detected through undirected processing. In total, 87 metabolites were assessed in detail.

All identified metabolites were quantified relative to their baseline levels in studies of glucose dose-response (0 to 20 mM) and time course following step increase in glucose (0.5 to 10 mM from 0 to 45 min) as displayed in heat-maps (Figure 4-2a). Select metabolites are re-plotted as x-y scatter plots in Figures 3-7 for discussion of specific pathways. To aid in assessing metabolite pool size, the absolute concentrations of 44

metabolites 30 min following glucose stimulation were measured by multi-point standard addition (Table 1). The incorporation of ^{13}C labeling into the glutamate pool after 60 min of stimulation with [U-^{13}C]-glucose is shown in Figure 4-6.

Glycolysis. Glycolysis comprises the first steps in glucose metabolism and accordingly plays a vital role in GSIS (Figure 1-3). Hexose phosphates changed slightly over 45 min of glucose stimulation, increasing 1.2 fold over 8 min, then decreasing by 50% over 37 min to ~58 μmole/mg protein. A 3-fold maximal increase was observed at 20 mM glucose in dose-response studies. Rapid increases in levels of fructose bisphosphate, 2-phosphoglycerate + 3-phosphoglycerate and phosphoenolpyruvate (32-, 6.7- and 5.5-fold, respectively) were observed. Lactate levels did not rise significantly following glucose exposure consistent with previous observations that little anerobic glycolysis occurs in β-cells.[17]

TCA. Metabolites in the TCA cycle participate in cyclic pathways that generate cofactors, such as NADH and NADPH, which augment GSIS[4-6] (Figure 1-4 and Figure 1-2b). Acetyl-CoA increased 1.5-fold within 2 min of stimulation and returned to prestimulation levels within 12 min of glucose addition. Coincident with first phase insulin release, only Span 2 TCA cycle metabolites, fumarate and malate, showed increases while Span 1 TCA cycle intermediates showed no increase (citrate + isocitrate, succinyl-CoA, and succinate) or a slight fall (α-ketoglutarate). The minimal early flux into Span 1 pathways is underscored by the minimal change in glutamate levels, derived from transamination of α-ketoglutarate. This is consistent with a greater initial flux through pyruvate carboxylase during initial stages of insulin release. In concert, aspartate levels fall, suggesting an increase in the malate-aspartate shuttle. Subsequently, all measured TCA cycle intermediates rise throughout the 45 min period studied in concert with phase 2 insulin release. The changes in all TCA cycle and related intermediates were also changed in a dose-dependent manner in response to glucose at 25 min (Figure 4-1b)

Pentose Phosphate Pathway (PPP). Metabolites in the pentose phosphate pathway are not often measured in investigations of GSIS but play a key part in cellular metabolism by supplying 5-carbon substrates for purine, pyrimidine, and histidine synthesis and are also important for generation of NADPH for lipid biosynthetic

pathways (Figure 1-5). NADPH is also likely to play a role as a coupling factor in GSIS. We observed that most PPP metabolites increased with increasing glucose concentration (Figure 4-2b). Rapid and substantial relative increases in the pentose phosphate pathway metabolites pentose phosphates, 6-phosphogluconate, and sedoheptulose phosphates (1.8, 3.2, and 2.4 fold increases, respectively) were observed concurrent with GSIS. Phosphoribosyl pyrophosphate, which can enter purine, pyrimidine, and histidine metabolism increased 7.4 fold. This metabolite can be converted to fructose-6-phosphate and erythrose-4-phosphate after condensation with glyceraldehyde-3-phosphate in the non-oxidative phase of the PPP. This conversion may explain, in part, the rapid sustained rise in fructose-bisphosphate seen at low concentration of glucose (Figure 4-1). While substantial increases in PPP metabolite levels are observed with glucose stimulation, the relative pool size of these metabolites is substantially smaller than for those of the TCA cycle (Table 1) supporting previous findings that the bulk of glucose carbon is oxidized by the TCA cycle and does not participate in the PPP.[18]

Nucleotides. In both glucose dose-response and time course experiments, we saw only small, generally non-significant changes in total ATP levels, but a dose- and time-dependent decrease in ADP and AMP (Figure 4-2a-b). This combination resulted in a clear glucose-dependent increase in the ATP/ADP ratio and a ~3-fold increase in the ATP/ADP ratio within 2 min of stimulation with minimal additional increase throughout 45 min (Figure 4-2a). Mono- and di-phosphonucleotides decreased by 1.7-4.3 fold within 2 min of glucose stimulation. GTP increased only slightly (< 5%) whereas UTP and CTP increased 40% and 80%, respectively. Phosphocreatine, proposed as a regulator of K_{ATP} channel activity in β-cells[19], increased 3-fold within 2 min of glucose stimulation to ~120 nmole/mg protein or ~6 x the concentration of ADP. Maximal levels of phosphocreatine were reached at 10 mM glucose in dose response study, consistent with insulin dose response profile (Figure 4-1).

Cofactors. A rapid, sustained, and dose-dependent rise in NADH was observed with glucose treatment. The absence of a change in lactate and the sustained increase in glycolytic and TCA cycle intermediates would require the shuttling of NADH into the mitochondria, likely by the malate-aspartate shuttle and glycerol-3-phosphate shuttle which are highly active in the β-cell. NADPH has been implicated as a coupling factor in

GSIS being generated by pyruvate-dependent pyruvate/malate, pyruvate/citrate, and pyruvate/isocitrate cycling pathways.[2, 20] NADPH increased slightly but insignificantly over ~12 min of glucose stimulation and $NADP^+$ significantly decreased 4.0-fold which is similar in magnitude to changes reported in islets.[21] The NADPH/$NADP^+$ ratio increased immediately after addition of glucose and increased 5.8 fold over 25 min tracking the release of insulin (Figure 4-2) and exhibited a similar glucose dose-response profile to insulin release.

Sugar Nucleotide Donors. We detected 8 of 9 common sugar nucleotide donors with GDP-mannose changing the most substantially. GDP-mannose forms from conversion of glycolytic intermediate fructose-6-phosphate to mannose-6-phosphate and mannose-1-phosphate before condensing with GDP. This metabolite has not previously been quantified in β-cells but we observe a rapid increase that peaks at 14-fold over basal (~4.2 μ mole/mg protein) within 8 min of glucose followed by a gradual decrease.

Long-chain acyl-CoAs. Long-chain acyl-CoAs and have been implicated as metabolic coupling factors in GSIS.[22] Falling levels of long-chain acyl-CoAs can increase the likelihood of K_{ATP} channel closure[23] and we found that 16:0-CoA, for example, decreased ~50% within 2 min of glucose stimulation to ~0.46 μ mole / mg protein. Similar changes are observed in 14:0, 16:1, and 18:1 CoAs upon glucose stimulation with time and in glucose dose-response profiles (Figure 4-2).

ZMP. ZMP is an endogenous metabolite in the purine synthesis pathway and a precursor to IMP. Although measurements of endogenous ZMP levels have not been reported in β-cells, we detected a 9-fold increase in ZMP to ~4.0 μ mole / mg protein that reached a maximum ~25 min after glucose stimulation. Phosphoribosyl pyrophosphate which links the pentose phosphate pathway to the nucleotide synthesis pathway and glycinamide ribonucleotide, a ZMP precursor, were also detected, with changes similar to ZMP (Figure 4-1).

AICA riboside (AICAR) is widely used to activate AMP-activated protein kinase (AMPK), an important regulator of cellular energy balance.[24] AICAR is phosphorylated in the cell to generate ZMP which substitutes for AMP in enhancing phosphorylation and activation of AMPK. Based on the timing of the increase in ZMP, we hypothesized that it may serve as a negative regulator of GSIS during second phase. To test this idea, we

treated INS-1 832/13 cells with 10 mM glucose and 25 μM AICA riboside and achieved ~4x higher intercellular ZMP levels at 40 min relative to control cells stimulated with 10 mM glucose only. This increase in ZMP significantly decreased the rate of insulin release 40 to 60 min post glucose stimulation by 20% (Figure 4-7).

To assess the potential for AMPK activation, we measured the phosphorylation of ACC1, a direct target of AMPK following glucose stimulation by Western blotting of INS-1 extracts. ACC1 phosphorylation rapidly decreased within 5 min of glucose stimulation and was completely dephosphorylated by 25 min (Figures 3 i-j and Figure 4-4i). No phosphorylation was observed at 25 min, when ZMP levels were increasing. These results suggest that while ZMP levels increase, there is minimal activation of AMPK. Thus, while AICAR treatment can increase ZMP levels and reduce insulin secretion, these effects are likely dissociated from AMPK activation.

Discussion

The use of LC-TOF-MS has allowed us to measure the temporal and dose response to increasing glucose concentration for a wide range of metabolites in INS-1 832/13 cells. These measurements allowed testing of several prevailing hypotheses on the mechanism of GSIS and identification of novel metabolites that may play a role in normal β-cell metabolism.

K_{ATP} Dependent Pathway. K_{ATP} channel closure through rise in the ATP/ADP ratio is an established trigger for GSIS and we observe a near maximal 2.9-fold increase at 2 min following glucose stimulation (Figure 4-3d). This rapid change in ATP/ADP is in agreement with previous reports of a "several fold" increase in mouse β-cells that reached a maximum 1 to 3 min following glucose stimulation[25] and an ~2-fold increase in mouse islets within 5 min of glucose stimulation.[26] ATP concentration increased <15% in this period (Figure 4-2g) which is consistent with the availability of AMP and ADP substrates that were only ~10% of the ATP pool size at 0.5 mM glucose (Table 1). Hence, a maximal increase of ~10% in ATP levels is possible from AMP and ADP substrate without de novo synthesis which is unlikely within 5 min of glucose addition. While measurements do not preclude localized increases in ATP concentrations or changes in turnover rate, they may suggest that the K_{ATP} channel may be more influenced by reductions in ADP concentrations[27], phospholipids or long chain acyl-

CoAs[28], the latter of which showed significant reductions in our studies. The rapid and sustained increase in phosphocreatine (Figure 4-2a) may buffer ATP and shows that a significant increase in the total energy available to cells has increased. Phosphocreatine may also serve as a shuttle for energy rich phosphate from the mitochondria to the plasma membrane and act on K_{ATP} channel-associated creatine kinase to phosphorylate ADP.[19]

Driving the change in ATP/ADP is a rapid acceleration of glycolysis. In addition to more proximal glycolytic metabolites (Figure 4-3a), glycerol-3-phosphate increased 3.4-fold within 2 min of glucose stimulation (Figure 4-4f). In the absence of significant increases in lactate levels, accumulated NADH is shuttled into the mitochondria via the glycerol-3-phosphate shuttle via glycerol-3-phosphate dehydrogenase may accelerate glycolysis, further increasing the ATP/ADP ratio. While glucose-6-phosphate and fructose-6-phosphate cannot be resolved using HILIC chromatography, the combined hexose phosphate pool did not accumulate, suggesting that phosphofructokinase is not a rate limiting step under these conditions. It has been proposed that long-chain acyl-CoAs participate in modulating K_{ATP}-dependent insulin secretion[23], though studies have been discordant on the actual concentration changes of long-chain acyl-CoAs associated with glucose stimulation.[22, 29] We found rapid and significant decreases in long-chain acyl-CoAs, e.g. a 50% decrease of palmitoyl-CoA, concurrent with Phase 1 GSIS (Figure 4-4g). The long chain acyl-CoA decrease may be due to rapid esterification with the rising levels of glycerol-3-phosphate (Figure 4-4f) to form mono- and di-glycoerophospholipids. Indeed, we find a rapid increase in a peak matching the mass of 16:0/16:0 (1,2-dipalmatoyl-rac-glycero-3-phosphoglycerol) upon stimulation (Figure 4-4h). Long-chain acyl-CoA concentration has an inverse dose-response relationship to glucose (Figure 4-2b), further suggesting that esterification associated with elevated glucose facilitates removal of long chain acyl-CoAs from the cytosol. These results are consistent with the hypothesis that a decrease in long-chain acyl-CoAs facilitates K_{ATP} channel closure and enhances the triggering of GSIS.

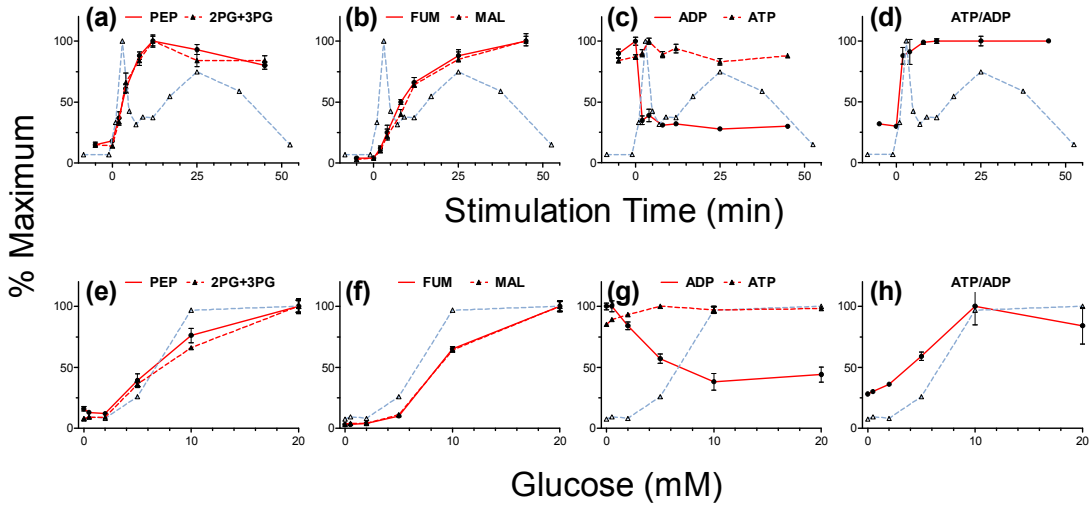

Figure 4-3. Glucose Stimulation Time Course and Glucose Dose-Response Profiles for Representative Glycolytic, TCA, and Adenine Nucleotide INS-1 Metabolites.

INS-1 cells in KRHB containing 0.5 mM glucose stimulated to 10 mM glucose over 45 min (a-d). INS-1 cells incubated in 0 to 10 mM glucose and sampled at 30 min (e-f). (a,e) phosphoenolpyruvate an 2-phosphoglycerate + 3-phosphoglycerate, (b,f) fumarate and malate, (c,g) ADP and ATP, (d,h) ATP/ADP ratio. Red lines are metabolites. Dashed lines are % maximum insulin secretion rate. Error bars represent 1 SEM, n = 3.

K_{ATP} independent pathways. Many hypotheses on the biochemical basis for the amplifying pathway of GSIS have been put forth.[4-6] The metabolomic data obtained here provide an opportunity to investigate these hypotheses. The primacy of pyruvate carboxylase compared to pyruvate dehydrogenase as a key entry point of glycolysis-derived carbons into the mitochondria[30] is supported by our observation that sharp increases in Span 2 metabolites, malate and fumarate, occur immediately after the addition of glucose to the INS-1 cells while Span 1 metabolites, and metabolites derived from Span 1 (i.e. α-ketoglutarate) rise later, during the second phase of insulin secretion (Figure 4-2b).

Malonyl-CoA Mechanism. A prominent theory is the malonyl-CoA / long-chain acyl-CoA model which states that glucose derived acetyl-CoA is carboxylated to form malonyl-CoA by acetyl-CoA-carboxylase (ACC). The resulting malonyl-CoA accumulation inhibits carnitine plamitoyl transferase 1 (CPT1) resulting in build-up of long-chain acyl-CoAs (or downstream metabolites) in the cytosol by blocking transport into the mitochondria for oxidation. According to this model, long-chain acyl-CoAs or

downstream metabolites act as signaling molecules. Our data are consistent with this idea in the following ways: 1) malonyl-CoA rapidly rises following glucose stimulation; 2) AMP levels decrease immediately after glucose addition which would be expected to reduce activity of AMPK and reduce ACC phosphorylation; 3) phospho-ACC levels decrease rapidly within 5 min of glucose addition; 4) citrate accumulates to allow allosteric activation of ACC activity;[31, 32] 5) palmitic acid and other long chain fatty acids decrease reducing their negative feedback to ACC[32]; 6) acetyl-CoA levels spiked rapidly before 1st phase insulin secretion (Figure 4-4); and 7) an increase in PG 16:0/16:0. Interestingly, we observed a rapid decrease in long-chain acyl-CoAs. We do not consider this result to be a challenge to the malonyl-CoA model because the decrease in long-chain acyl-CoAs is prior to accumulation of malonyl-CoA indicating a rapid increase in consumption that is independent of malonyl-CoA. These results are consistent with the idea that downstream metabolic products of long-chain acyl-CoAs may provide direct coupling factors for the amplifying pathway rather than the long-chain acyl-CoAs themselves.[33] Thus, in this interpretation, production of diacylglycerols and perhaps other glycerolipids consume the supply of long-chain acyl-CoAs provided by the malonyl-CoA pathway and act as more proximate coupling factors. These findings help reconcile the discrepancy between the idea that long-chain acyl-CoAs have direct inhibiting effects on insulin secretion at the K_{ATP} channel but their partitioning into the cytosol is presumed to augment secretion in the malonyl-CoA model. This view illustrates an interesting way that the triggering and amplifying pathways can interact in GSIS, i.e. increased consumption of long-chain acyl-CoAs helps close the K_{ATP} channel and produces downstream signals to amplify secretion.

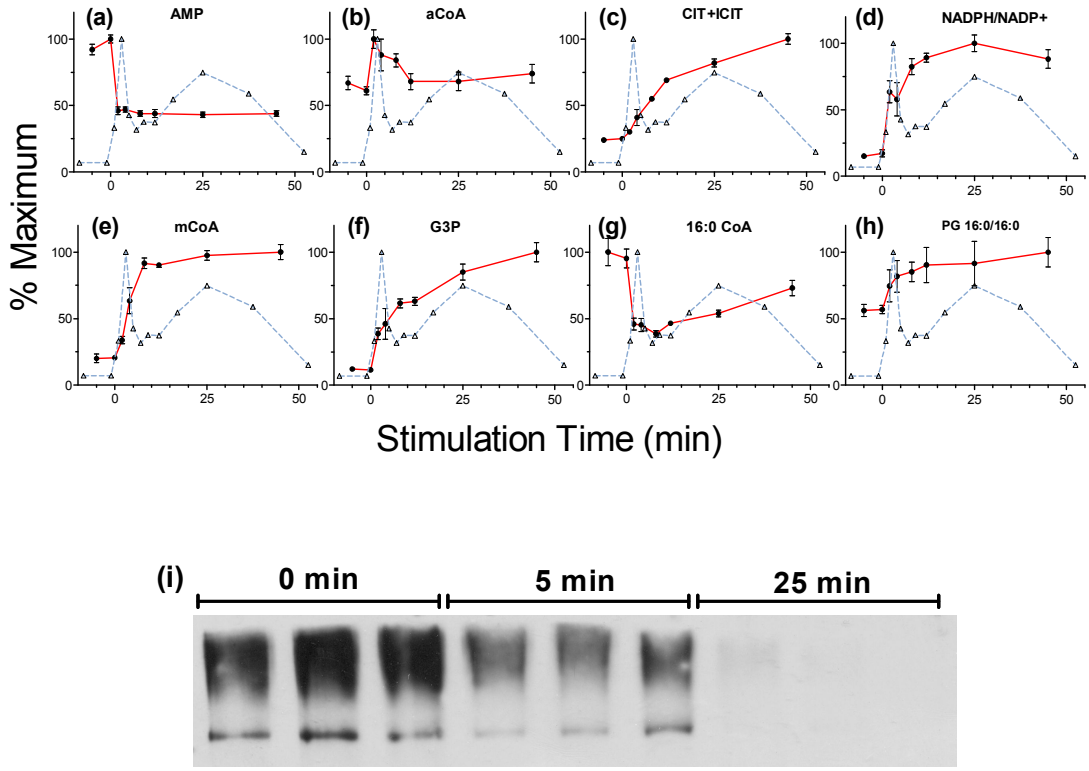

Figure 4-4. Glucose Stimulation Time Course Profiles for Metabolites and ACC Involved in the Malonyl-CoA Mechanism.

INS-1 cells in KRHB containing 0.5 mM glucose stimulated to 10 mM glucose over 45 min (a-h). (a) AMP, (b) acetyl-CoA, (c) citrate + isocitrate, (d) NDPH/$NADP^+$ ratio, (e) malonyl-CoA, (f) glycerol-3-phosphate, (g) plamitoyl-CoA, (h) 1,2-dioctadecanoyl-rac-glycero-3-phosphoglycerol. Red lines are metabolites. Dashed lines are % maximum insulin secretion rate. Error bars represent 1 SEM, n = 3. (i) Western blot of phospho-ACC 0, 5, and 25 min post stimulation with 10 mM glucose. (Western blot data by Mary Treutelaar).

Succinate Mechanism. Succinate has been proposed as a key metabolite that supplies second messengers for the K_{ATP} independent pathway based on observations that potent secretagogues have in common the ability to provide HMG-CoA reductase with substrates (NADPH and HMG-CoA) or their precursors.[34]

According this theory, mevalonate, the product of HMG-CoA reductase or one of its downstream metabolites contributes to insulin secretion. We were unable to detect mevalonate directly; however, we observed a substantial increase in succinate and decrease in HMG-CoA, similar to previous results[35] suggesting consumption of this metabolite to form mevalonate (Figure 4-5b). This change was accompanied by a slight increase in NADPH and sustained increase in NADPH/$NADP^+$ ratio which could help

drive the reaction towards mevalonate (Figure 4-5d). We also observed an increase in farnesyl pyrophosphate, a downstream product of this pathway that is involved in isoprenylation of proteins which has been implicated in GSIS[36, 37] (Figure 4-5c).

The succinate pathway has generally been discussed from the view of anaplerotic reactions which could drive the production of mevalonate.[34] The near depletion of HMG-CoA with 10 mM glucose within 10 min suggests that glucose does not provide sufficient succinate to maintain a high level of HMG-CoA. Therefore, our results are consistent with a model in which a decrease in AMP and increase in NADPH help activate and drive the reduction of HMG-CoA to mevalonic acid while anaplerosis provides HMG-CoA substrate at a limiting level. If a downstream product of this reaction is important for GSIS, the low level of HMG-CoA would potentially limit secretion at longer times in INS-1 cells, possibly contributing to the reduction in insulin secretion in the 2nd phase.

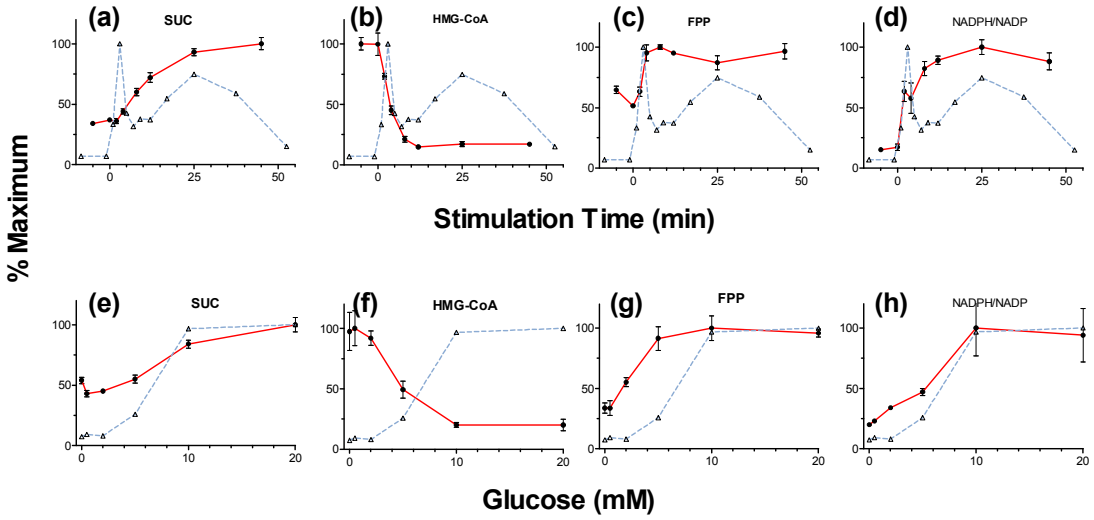

Figure 4-5. Glucose Stimulation Time Course and Glucose Dose-Response Profiles for Metabolites Involved it the Succinate Mechanism of GSIS.

INS-1 cells in KRHB containing 0.5 mM glucose stimulated to 10 mM glucose over 45 min (a-d). INS-1 cells incubated in 0 to 10 mM glucose and sampled at 30 min (e-f). (a,e) succinate, (b,f) HMG-CoA, (c,g) farsenyl pyrophosphate, (d,h) NADPH/NADP$^+$ ratio. Solid red lines are metabolites. Dashed blue lines are % maximum insulin secretion rate. Error bars represent 1 SEM, n = 3.

Glutamate hypothesis. Another theory holds that glutamate is an important coupling factor in GSIS. We find no changes in glutamate levels with glucose concentration or time following glucose application (Figure 4-6) in agreement with several other reports.[4] However, if INS-1 cells are stimulated with [U^{13}C]-glucose, then the pool of glutamate becomes substantially labeled after 60 min suggesting flux through the glutamate pool (Figure 4-6c). Thus, our data do not support the hypothesis that increases in intracellular glutamate, per se, facilitate GSIS; however, participation in non-anaplerotic cyclic pathways (e.g. aspartate-malate shuttle) could play an important role.

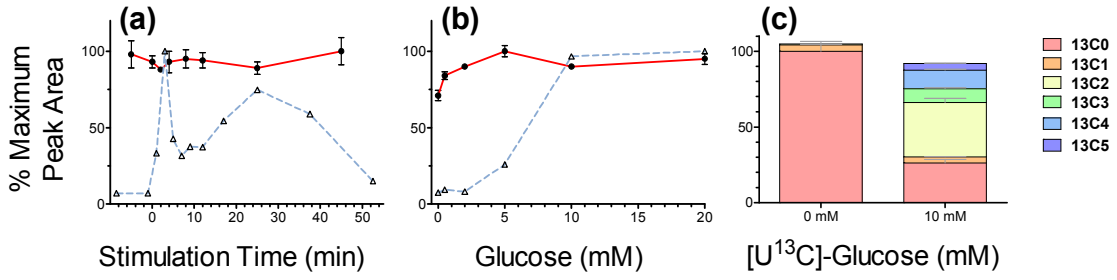

Figure 4-6. Glutamate Glucose Stimulation Time Course, Dose-Response, and Isotopomer Distribution Profiles

INS-1 cells in KRHB containing 0.5 mM glucose stimulated to 10 mM glucose over 45 min (a). INS-1 cells incubated in 0 to 10 mM glucose and sampled at 30 min (b). Solid red lines are metabolites. Dashed blue lines are % maximum insulin secretion rate. Error bars represent 1 SEM, n = 3. (c) Incorporation of ^{13}C into glutamate after 60 min of stimulation with [U-^{13}C]-glucose. Error bars represent 1 SEM, n = 3. ([U-^{13}C]-glucose data by Mahmoud Azzouny).

ZMP. A novel finding from these experiments was a 10-fold increase in ZMP within 25 min of step increase in glucose (Figure 4-2a). ZMP is an intermediate of IMP synthesis and is produced through the PPP. Accordingly, we also found accumulation of PPP intermediates glucose-6-phosphate, pentose-phosphates, and sedoheptulose. phosphates with glucose. The accumulation of immediate ZMP precursors phosphoribosyl pyrophosphate and glycinamide ribotide (Figure 4-2a) shows kinetics that are consistent with synthesis of ZMP through this pathway. ZMP has been generated *in vivo* by exposing β-cells to AICA riboside (AICAR) which is phosphorylated intracellularly to ZMP (AICA ribotide). Such studies have demonstrated decreased GSIS with acute exposure to AICA riboside;[38, 39] in some studies AICA riboside in perfused rat

pancreas and isolated islets demonstrated potentiation of insulin release.[40, 41] To determine if ZMP production could influence GSIS, we treated cells with AICAR and glucose simultaneously. AICAR elevated ZMP to ~4x endogenous levels and eventually led to a slight but significant inhibition of GSIS (Figure 4-7b).

ZMP is a known AMPK agonist; but, several observations argue against the possibility of ZMP acting through AMPK in this study. In vitro, AMP is 37-fold more active than ZMP in activating AMPK.[42] Following a step change in glucose from 0.5 to 10 mM glucose, ZMP increased from ~0.4 to ~4 nmole/mg protein while AMP decreased from ~10 to ~ 5 ng/mg protein. Therefore, ZMP at 10 mM glucose would be expected to provide negligible activation of AMPK relative to AMP at 0.5 mM glucose unless compartmentalization or other factors affected their relative potencies in vivo. Further, AMPK activation should result in decreased malonyl-CoA levels through phosphorylation and inactivation of ACC; however, AICAR had no effect on malonyl-CoA (data not shown) and re-phosphyorylation of ACC was not observed after 25 min of stimulation (Figure 4-4i). Therefore, while ZMP may restrain GSIS, at endogenous levels this effect does not seem to be through AMPK but perhaps through an alternate route such as altering lipid metabolism which AICAR has been shown to do independent of AMPK activation.[43]

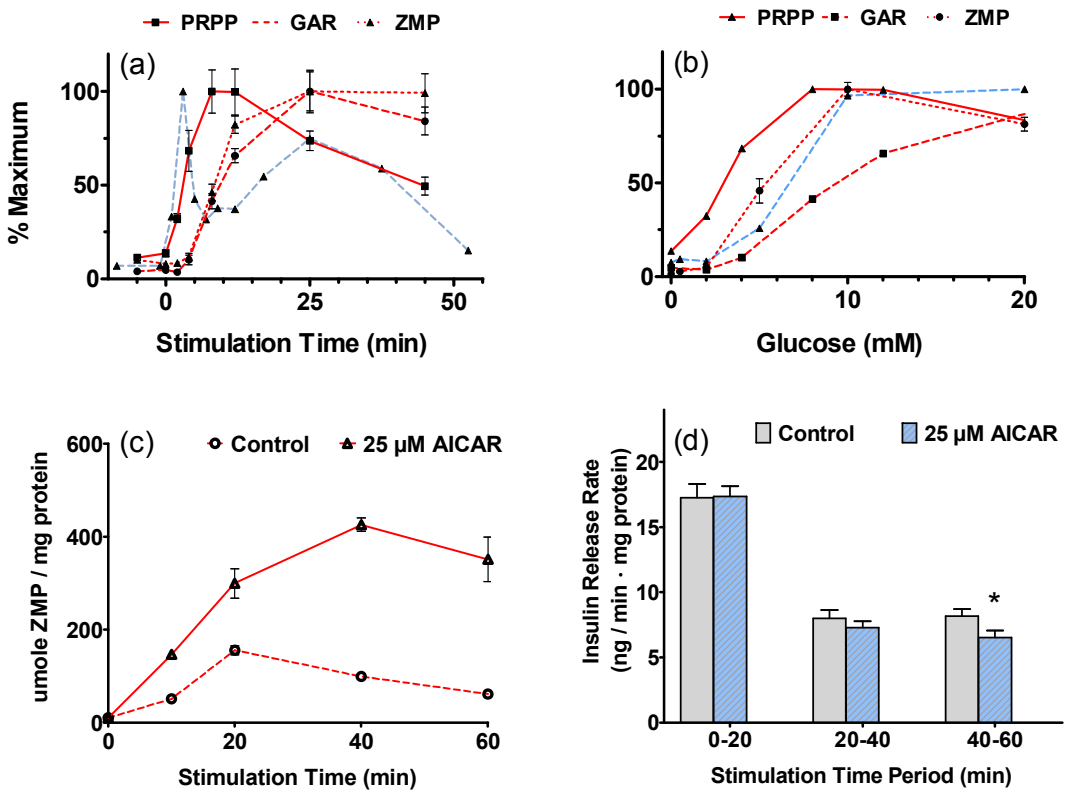

Figure 4-7. Insulin release rate in INS-1 with enhanced ZMP formation.

INS-1 cells stimulated with 10 mM glucose with or without 25 μM AICA-riboside for 60 min. (a) ZMP level in INS-1 cells over 60 min glucose. Error bars represent 1 SEM, n = 3. (b) insulin secretion rate measured by change in incubation buffer insulin concentration over indicated time period. Error bars represent 1 SEM, n = 8. Asterisk indicates significant difference in insulin release rate with $p < 0.05$

Other Metabolites. Besides the metabolites discussed above, we detected many additional metabolites that were affected by glucose. Among this group, we found several substrates for glycosyltransferases including GDP-mannose, GDP-fucose, UDP-N-acetylglucosamine + UDP-N-acetylgalactoseamine, UDP-glucose, UDP-xylose, and UDP-d-galacturonate. Of these, GDP-mannose shows by far the greatest change (12-fold increase) following glucose treatment suggesting a potential role in response to glucose by the INS-1 cells. Roles for these pathways in β-cells have not yet been extensively explored. We also observed decreases in pantothenic acid with glucose. As this metabolite is important for CoA synthesis, its decrease may reflect consumption for producing CoAs needed for β-cell function. Besides long-chain acyl-CoAs and farnesyl

pyrophosphate discussed above, we found changes in other compounds involved in lipid metabolism including decreases in free fatty acids and citicoline, an intermediate in production of phosphatidylcholine. The decrease in free fatty acids may indicate release from the cells or metabolic consumption, for example in production of lipid signaling molecules. While investigation of all these pathways is beyond the scope of one paper, these results indicate that this method may be used for studying a wide range of metabolites and pathways in regard to insulin secretion.

While observations in INS-1 may not be fully applicable to islets, metabolomic study of INS-1 832/13 affords several advantages over primary islets including high specificity β-cell metabolism (no α or γ cells are present) and more precise measurements due to ease of manipulation and procurement. One limitation in these studies is the lack of accurate measurements for pyruvate and oxaloacetate which are not detected by the method used.

Conclusions.

The time-resolved and glucose-dose response metabolomic data generated using LC-MS has provided a novel way to test and extend several hypotheses for the biochemical mechanism of GSIS. The simultaneous measurement of AMP, citrate, long-chain acyl-CoAs, and malonyl-CoA show a novel interaction of metabolites that are important in both the triggering and amplifying pathways of secretion thus helping to refine the malonyl-CoA hypothesis. We find support for the succinate hypothesis with measurements that confirm previous findings including rapid increases in NADPH and decreases in HMG-CoA. Detection of farnesyl pyrophosphate provides a novel metabolite that may play a role in GSIS from this pathway. Finally, we find that ZMP can inhibit GSIS suggesting a previously unknown role for this compound as an endogenous metabolite.

References

1. Kanat, M., Norton, L., Winnier, D., Jenkinson, C., Defronzo, R.A., and Abdul-Ghani, M.A. 2011. Impaired early- but not late-phase insulin secretion in subjects with impaired fasting glucose. *Acta Diabetol*.
2. Jensen, M.V., Joseph, J.W., Ronnebaum, S.M., Burgess, S.C., Sherry, A.D., and Newgard, C.B. 2008. Metabolic cycling in control of glucose-stimulated insulin secretion. *Am J Physiol Endocrinol Metab* 295:E1287-1297.
3. Kwan, E.P., and Gaisano, H.Y. 2007. New insights into the molecular mechanisms of priming of insulin exocytosis. *Diabetes Obes Metab* 9 Suppl 2:99-108.
4. Jitrapakdee, S., Wutthisathapornchai, A., Wallace, J.C., and MacDonald, M.J. 2010. Regulation of insulin secretion: role of mitochondrial signalling. *Diabetologia* 53:1019-1032.
5. Henquin, J.C., Nenquin, M., Ravier, M.A., and Szollosi, A. 2009. Shortcomings of current models of glucose-induced insulin secretion. *Diabetes Obes Metab* 11 Suppl 4:168-179.
6. Muoio, D.M., and Newgard, C.B. 2008. Molecular and metabolic mechanisms of insulin resistance and [beta]-cell failure in type 2 diabetes. *Nature Reviews Molecular Cell Biology* 9:193-205.
7. Fernandez, C., Fransson, U., Hallgard, E., Spégel, P., Holm, C., Krogh, M., Wårell, K., James, P., and Mulder, H. 2007. Metabolomic and Proteomic Analysis of a Clonal Insulin-Producing β-Cell Line (INS-1 832/13). *Journal of Proteome Research* 7:400-411.
8. Spegel, P., Malmgren, S., Sharoyko, V.V., Newsholme, P., Koeck, T., and Mulder, H. 2011. Metabolomic analyses reveal profound differences in glycolytic and tricarboxylic acid cycle metabolism in glucose-responsive and -unresponsive clonal beta-cell lines. *Biochemical Journal* 435:277-284.
9. MacDonald, M.J. 2007. Synergistic Potent Insulin Release by Combinations of Weak Secretagogues in Pancreatic Islets and INS-1 Cells. *Journal of Biological Chemistry* 282:6043-6052.
10. Hohmeier, H.E., Mulder, H., Chen, G., Henkel-Rieger, R., Prentki, M., and Newgard, C.B. 2000. Isolation of INS-1-derived cell lines with robust ATP-sensitive K+ channel-dependent and -independent glucose-stimulated insulin secretion. *Diabetes* 49:424-430.
11. Matthew A. Lorenz, C.F.B., Robert T. Kennedy. 2011. Rapid Sample Preparation for Metabolomic Analysis of Adherent Mammalian Cells Using INS-1 Cells as a Model System. *Analytical Chemistry* TDB:TBD.
12. Bradford, M.M. 1976. A rapid and sensitive method for the quantitation of microgram quantities of protein utilizing the principle of protein-dye binding. *Analytical Biochemistry* 72:248-254.
13. Wilcock, A.R., and Goldberg, D.M. 1972. Kinetic determination of malate dehydrogenase activity eliminating problems due to spontaneous conversion of oxaloacetate to pyruvate. *Biochemical Medicine* 6:116-126.
14. Hall, L.M. 1960. Preparation of D-glyceraldehyde-3-phosphate and dihydroxyacetone phosphate hydrazones. *Biochemical and Biophysical Research Communications* 3:239-243.
15. Straub, S.G., and Sharp, G.W. 2004. Hypothesis: one rate-limiting step controls the magnitude of both phases of glucose-stimulated insulin secretion. *Am J Physiol Cell Physiol* 287:C565-571.
16. Straub, S.G., and Sharp, G.W.G. 2002. Glucose-stimulated signaling pathways in biphasic insulin secretion. *Diabetes/Metabolism Research and Reviews* 18:451-463.
17. Sekine, N., Cirulli, V., Regazzi, R., Brown, L.J., Gine, E., Tamarit-Rodriguez, J., Girotti, M., Marie, S., MacDonald, M.J., Wollheim, C.B., et al. 1994. Low lactate dehydrogenase and high mitochondrial glycerol phosphate dehydrogenase in pancreatic beta-cells. Potential role in nutrient sensing. *Journal of Biological Chemistry* 269:4895-4902.

18. Schuit, F., De Vos, A., Farfari, S., Moens, K., Pipeleers, D., Brun, T., and Prentki, M. 1997. Metabolic fate of glucose in purified islet cells. Glucose-regulated anaplerosis in beta cells. *Journal of Biological Chemistry* 272:18572-18579.
19. Krippeit-Drews, P., Bäcker, M., Düfer, M., and Drews, G. 2003. Phosphocreatine as a determinant of K_{ATP} channel activity in pancreatic ß-cells. *Pflügers Archiv European Journal of Physiology* 445:556-562.
20. MacDonald, M.J. 1995. Feasibility of a mitochondrial pyruvate malate shuttle in pancreatic islets. Further implication of cytosolic NADPH in insulin secretion. *Journal of Biological Chemistry* 270:20051-20058.
21. Luciani, D.S., Misler, S., and Polonsky, K.S. 2006. Ca2+ controls slow NAD(P)H oscillations in glucose-stimulated mouse pancreatic islets. *The Journal of Physiology* 572:379-392.
22. Prentki, M., Vischer, S., Glennon, M.C., Regazzi, R., Deeney, J.T., and Corkey, B.E. 1992. Malonyl-CoA and long chain acyl-CoA esters as metabolic coupling factors in nutrient-induced insulin secretion. *Journal of Biological Chemistry* 267:5802-5810.
23. Bränström, R., Aspinwall, C.A., Välimäki, S., Östensson, C.G., Tibell, A., Eckhard, M., Brandhorst, H., Corkey, B.E., Berggren, P.O., and Larsson, O. 2004. Long-Chain CoA esters activate human pancreatic beta-cell K _{ATP} channels: potential role in Type 2 diabetes. *Diabetologia* 47:277-283.
24. Hardie, D.G. 2008. AMPK: a key regulator of energy balance in the single cell and the whole organism. *Int J Obes* 32:S7-S12.
25. Nilsson, T., Schultz, V., Berggren, P.O., Corkey, B.E., and Tornheim, K. 1996. Temporal patterns of changes in ATP/ADP ratio, glucose 6-phosphate and cytoplasmic free Ca2+ in glucose-stimulated pancreatic beta-cells. *Biochemical Journal* 314 (Pt 1):91-94.
26. Detimary, P., Van den Berghe, G., and Henquin, J.-C. 1996. Concentration Dependence and Time Course of the Effects of Glucose on Adenine and Guanine Nucleotides in Mouse Pancreatic Islets. *Journal of Biological Chemistry* 271:20559-20565.
27. Fridlyand, L.E., Ma, L., and Philipson, L.H. 2005. Adenine nucleotide regulation in pancreatic β-cells: modeling of ATP/ADP-Ca2+ interactions. *American Journal of Physiology - Endocrinology And Metabolism* 289:E839-E848.
28. Tarasov, A., Dusonchet, J., and Ashcroft, F. 2004. Metabolic regulation of the pancreatic beta-cell ATP-sensitive K+ channel: a pas de deux. *Diabetes* 53 Suppl 3:S113-122.
29. Liang, Y., and Matschinsky, F.M. 1991. Content of CoA-esters in perifused rat islets stimulated by glucose and other fuels. *Diabetes* 40:327-333.
30. MacDonald, M.J. 1995. Feasibility of a mitochondrial pyruvate malate shuttle in pancreatic islets. Further implication of cytosolic NADPH in insulin secretion. *J Biol Chem* 270:20051-20058.
31. Faergeman, N.J., and Knudsen, J. 1997. Role of long-chain fatty acyl-CoA esters in the regulation of metabolism and in cell signalling. *Biochem J* 323 (Pt 1):1-12.
32. Hashimoto, T., Isano, H., Iritani, N., and Numa, S. 1971. Liver acetyl-coenzyme-A carboxylase. Studies on kynurenate inhibition, isotope exchange and interaction of the uncarboxylated enzyme with citrate. *Eur J Biochem* 24:128-139.
33. Nolan, C.J., Madiraju, M.S., Delghingaro-Augusto, V., Peyot, M.L., and Prentki, M. 2006. Fatty acid signaling in the beta-cell and insulin secretion. *Diabetes* 55 Suppl 2:S16-23.
34. MacDonald, M.J., Fahien, L.A., Brown, L.J., Hasan, N.M., Buss, J.D., and Kendrick, M.A. 2005. Perspective: emerging evidence for signaling roles of mitochondrial anaplerotic products in insulin secretion. *Am J Physiol Endocrinol Metab* 288:E1-15.
35. Corkey, B.E., Glennon, M.C., Chen, K.S., Deeney, J.T., Matschinsky, F.M., and Prentki, M. 1989. A role for malonyl-CoA in glucose-stimulated insulin secretion from clonal pancreatic beta-cells. *Journal of Biological Chemistry* 264:21608-21612.
36. Kowluru, A., Veluthakal, R., Rhodes, C.J., Kamath, V., Syed, I., and Koch, B.J. 2010. Protein farnesylation-dependent Raf/extracellular signal-related kinase signaling links to cytoskeletal remodeling to facilitate glucose-induced insulin secretion in pancreatic beta-cells. *Diabetes* 59:967-977.
37. Kowluru, A. 2008. Protein prenylation in glucose-induced insulin secretion from the pancreatic islet beta cell: a perspective. *J Cell Mol Med* 12:164-173.

38. da Silva Xavier, G., Leclerc, I., Varadi, A., Tsuboi, T., Moule, S.K., and Rutter, G.A. 2003. Role for AMP-activated protein kinase in glucose-stimulated insulin secretion and preproinsulin gene expression. *Biochemical Journal* 371:761-774.
39. Zhang, S., and Kim, K.H. 1995. Glucose activation of acetyl-CoA carboxylase in association with insulin secretion in a pancreatic beta-cell line. *Journal of Endocrinology* 147:33-41.
40. Akkan, A.G., and Malaisse, W.J. 1994. Insulinotropic action of AICA riboside. I. Insulin release by isolated islets and the perfused pancreas. *Diabetes Res* 25:13-23.
41. Malaisse, W.J., Conget, I., Sener, A., and Rorsman, P. 1994. Insulinotropic action of AICA riboside. II. Secretory, metabolic and cationic aspects. *Diabetes Res* 25:25-37.
42. Corton, J.M., Gillespie, J.G., Hawley, S.A., and Hardie, D.G. 1995. 5-Aminoimidazole-4-Carboxamide Ribonucleoside. *European Journal of Biochemistry* 229:558-565.
43. Jacobs, R.L., Lingrell, S., Dyck, J.R.B., and Vance, D.E. 2007. Inhibition of Hepatic Phosphatidylcholine Synthesis by 5-Aminoimidazole-4-carboxamide-1-β-4-ribofuranoside Is Independent of AMP-activated Protein Kinase Activation. *Journal of Biological Chemistry* 282:4516-4523.

CHAPTER 5
Alterations of β-Cell Metabolism Induced by Lipotoxicity and Glucotoxicity

Introduction

Type 2 diabetes (T2D) is characterized by insulin resistance and the dysregualtion of pancreatic β-cell insulin secretion. Insulin resistance, usually in the setting of obesity, is associated with increased flux of glucose and other nutrients such as fatty acids to the β-cell. This leads to increased demand for insulin secretion. Although β-cells can adapt to this increased demand, in genetically predisposed individuals the β-cell can eventually fail in this environment. β-cell failure, both dysfunction and loss of β-cell mass, leads to reduced insulin secretion and hyperglycemia. In turn, hyperglycemia accelerates β-cell deterioration which is further exacerbated by elevated levels of free fatty acids often associated with obesity.[1-3] Despite extensive research, the biochemical mechanisms for deterioration of β-cell function are not fully understood. It is widely believed that a contributing factor is exposure to excess glucose (glucotoxicity), lipids (lipotoxicity), or both (glucolipotoxicity).

In vitro models have been developed that mimic the alterations in glucose stimulated insulin secretion (GSIS) in T2D, specifically elevation in basal levels of insulin secretion and blunted secretion at stimulatory glucose concentrations. These models are generated by treating clonal β-cell lines or isolated rodent islets in culture with elevated levels of free fatty acids (FFA, lipotoxic model), glucose (HG, glucotoxic model), or both (glucolipotoxic model) for 1 to 7 days independenly.[4] Previous studies of lipotoxicity and glucotoxicity in islets and clonal β-cells have focused primarily on determining alterations in gene[5-8] and protein[6, 8-15] expression. While highly informative, these studies may overlook modifications to β-cell metabolism that underlie the dysfunction. It is likely that global metabolite measurement in β-cells will provide insight because GSIS involves numerous metabolic pathways to facilitate Phase 1 and Phase 2 GSIS as recently reviewed[16-18] and discussed in Chapter 4.

Metabolite measurements to date in lipotoxic and glucotoxic models are rare and have generally been performed at single time points that do not allow for investigation of the temporal changes in glucose metabolism. Since the established mechanism of GSIS involves the metabolism of glucose to downstream products and coupling factors that signal insulin release[16-18], we chose to employ a temporally-resolved metabolomics approach to elucidate changes in metabolism that may impact dysregulation of GSIS in these disease models. Identification of changes in metabolites levels and/or metabolic pathways could lead to new insights in the mechanisms of lipotoxictiy and glucotoxicity in β-cells.

In this study, we quantify ~90 metabolites impacted by glucose stimulation from several different metabolic pathways in INS-1 832/13 cells exhibiting lipotoxic and glucotoxic phenotypes. Cells were pre-incubated in FFA or HG culture media and then stimulated with 10 mM glucose after a 2 h incubation in low glucose (1 mM) with no other fuels. Measurements were taken 0, 5, 25, and 45 min post stimulation with 10 mM glucose. The timeframe investigated allows for the determination of metabolic changes associated with Phase 1 and Phase 2 GSIS. We also treated cells with 10 mM [U-^{13}C]-glucose to assess glycolytic flux. These measurements allowed assessment of variety of metabolic pathways including glycolysis, the TCA cycle, and pentose phosphate shunt. Proposed GSIS coupling factors including NADPH and long-chain acyl-CoAs generated by pyruvate/citrate, pyruvate/isocitrate, pyruvate/malate, and glycerolipid/fatty acid cycling pathways implicated in both amplifying and triggering signals for GSIS were measured as well.[16-18]

In the glucotoxic model, profound alterations in the PPP metabolites were observed (increasing more that 200-fold relative to control) demonstrating a substantial alteration in glucose usage. We also observed high levels of gluconate, a metabolite not previously quantified in β-cells that could impact Ca^{2+} signaling. We report broad and persistent increases in key energy ratios in both lipotoxic and glucotoxic models supporting a metabolic basis for dysregualtion of GSIS and hyperinsulinemia at basal glucose levels.

Experimental

Materials and Reagents. All chemicals were purchased form Sigma-Aldrich (St. Louis, MO) unless otherwise noted. HPLC grade acetonitrile was purchased from Burdick & Jackson (Muskegon, MI). RPMI media, fetal bovine serum, 4-(2-hydroxyethyl)-1-piperazineethanesulfonic acid (HEPES), and penicillin-streptomycin were purchased from Invitrogen Corp. (Carlsbad, CA). Cells lifters and 10 cm polystyrene non-pyrogenic culture dishes were purchased from Corning (Lowell, MA). KRHB (Krebs-Ringer-HEPES buffer) was prepared containing 10 mM glucose, 20 mM HEPES, 118 mM NaCl, 5.4 mM KCl, 2.4 mM CaCl, 1.2 mM MgSO4, and 1.2 mM KH_2PO_4 and adjusted to pH 7.4 with HCl. 10 mM FFA solution (3.33 mM palmitate, 6.66 mM oleate) in KRHB was prepared by adding palmitate and oleate sodium salts finely ground with mortar and pestle and 10% FFA free BSA to a centrifuge tube, diluting with KRHB and stirring at ~37 °C for 24 h. The pH was adjusted to 7.4 with 1 M NaOH. FFA media (1 mM FFAs) was made by diluting the 10X stock with supplemented RPMI and sterile filtering with a Whatman 0.22 µm filter. A control was made using the same procedure, without addition of FFAs.

Cell Culture. INS-1 832/13 cells were cultured in RPMI supplemented with 2 mM glutamine, 1 mM sodium pyruvate, 10% FBS, 10 mM HEPES, 100 U/mL penicillin, 100 µg/mL streptomycin, 250 ng/mL amphotericin B, and 50 uM β-mercaptoethanol. Cells were plated at a density of ~$14x10^3$ cells/cm^2 and grown in 6 cm culture dishes or 6-well plates at 37 °C and 5% CO_2 in a humidified atmosphere to confluence over ~5 d. For lipotoxicity studies, cells were incubated an additional 5 days in supplemented RPMI + 1% fatty acid free BSA (control) or 1% fatty acid free BSA + 1 mM fatty acids (2:1 oleate:palmitate). For glucotoxicity studies, cells were either incubated an additional 3 days in fully supplemented RPMI alone (control) or supplemented RPMI containing 25 mM glucose. Accelerated growth with FFA and HG treatment relative to controls was observed in preliminary experiments involving non-confluent cells. In addition, expression of lipotoxic and glucotoxic phenotypes was inconsistent without prior confluence, presumably due to utilization of excess nutrient for cell growth. Hence, treatments were initiated after confluence was reached.

Insulin and Protein Measurement. Following exposure to lipotoxic or glucotoxic incubation conditions, cells were transferred to KRHB containing 0.2% BSA and 1 mM glucose. After 2 h, the buffer was replaced with KRHB containing 0.2% BSA and either 3 mM or 10 mM glucose for 30 min. Following stimulation, aliquots of KRHB were removed from each well, briefly stored on ice and centrifuged at 3000 x g for 3 min to pellet any suspended cells. An aliquot of supernatant was transferred to a fresh vial, stored at -20 °C, and assayed for insulin. Total insulin was extracted by aspirating the buffer, adding 2 mL of 0.2 mM HCl in 75:25 ethanol:water to each well, and incubating on ice for 2 h.[19] The cells were scraped, transferred to a microcentrifuge tube and centrifuged. Supernatants were diluted with KRHB + 0.2% BSA and insulin measured using a Millipore Rat/Mouse insulin ELISA Kit. Total protein was measured by adding 2 mL of 7 M urea / 2 M thiourea / 1% CHAPS buffer to each well and scraping to dissolve proteins. Protein content was determined by Bradford Assay.[20]

Glucose Stimulation Time Course Metabolite Measurements. Metabolites were measured following exposure to lipotoxic or glucotoxic incubation conditions. Cells were transferred to KRHB containing 1 mM glucose for 2 h then stimulated with KRHB containing 10 mM glucose for 0, 5, 25, and 45 min. One set of samples was rinsed briefly (~10 s) with KRHB (-120 min time point) to measure metabolite levels in FFA or HG culture media. Carbon flux through glucose was also assessed by stimulating cells with [U-^{13}C]-glucose for 25 min. For each time point, a set of cell plates was rinsed, metabolism quenched, and metabolites extracted using the procedure described previously.[21] Briefly, cell plates were rapidly rinsed with water and quenched with liquid nitrogen. Metabolites were extracted with 75% 9:1 methanol:chloroform 25% water and assayed by HPLC-TOF-MS using a hybrid hydrophobic interaction liquid chromatography/anion exchange method similar to that descirbed previously.[22] Targeted data processing was performed as described previously.[21] Metabolites implicated in GSIS (e.g. glycolysis and TCA cycle) in previous reports were quantified directly using standards to confirm peak assignments and ^{13}C labeled internal standards, when available, to improve precision (Table 4-1).

Statistics. Data are expressed as the mean ± standard error of the mean (SEM). Statistical significance was determined using a non-corrected two-tailed Student's t test, unpaired assuming equal variance. A p-value of < 0.05 was considered significant.

Results and Discussion

Insulin Secretion. Insulin secreted into media from INS-1 832/13 cells was measured following treatment with 1 mM free fatty acids (FFA) for 5 days, or 25 mM glucose (HG) for 3 days, conditions similar to those previously described as inducing glucotoxic or lipotoxic phenotypes in β-cells[4, 9, 23-25](Figure 5-1 a-b). Prolonged incubation in FFAs increased insulin secretion at 3 mM glucose by 280% relative to control while secretion at 10 mM glucose was blunted to 60% of control. The increase in insulin secretion from 3-10 mM glucose in the FFA treated cells was only 13% compared to a 530% increase for control cells. These results were similar to previous studies of INS-1 cells[6, 23] and rat islets.[26] Similar results were observed for HG conditions in and 3 mM glucose increased insulin release by 160% (not significant) relative to control and 10 mM glucose stimulated release was blunted to a 20% increase over baseline while control cells increased 440% from 3-10 mM glucose (Figure 1a). Similar results were observed in previous studies of INS-1[9] and MIN6[15] cells. Additional studies found no change in basal insulin release in INS-1E cells after 3 d of 20 mM glucose treatment[9] and a decrease in basal insulin release of ~40% in INS-1 after 4 d in 30 mM glucose.[7] Total insulin content (Figure 5-2a) with FFA and HG treatment was reduced by 37% and 60% relative to controls, consistent with previous reports of β-cells expressing lipotoxic[26] and glucotoxic[15] phenotypes. Total protein content (Figure 5-2b) was similar between each experimental and control sample indicating equivalent biomass; 42% higher levels of protein were observed for FFA samples relative to HG samples, possibly due the additional 2 d of cell growth.

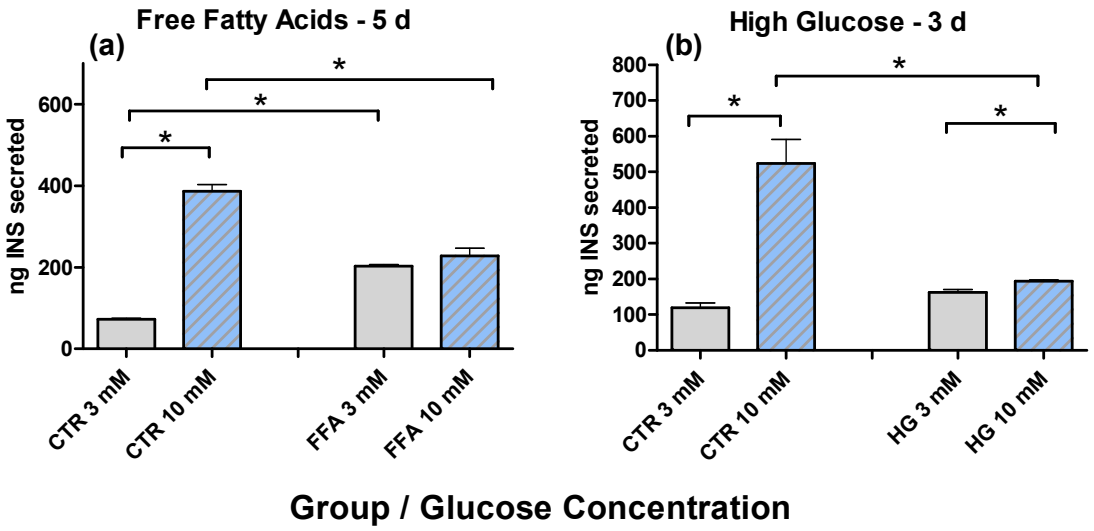

Figure 5-1. Insulin Release from INS-1 Cells with 3 and 10 mM Glucose Post Treatment with Free Fatty Acids and High Glucose.

(a) FFA group cultured in RPMI supplemented with 1 mM 1:2 palmitate:oleate bound to 1% fatty acid free BSA for 5 d, incubated in KRHB containing 1 mM glucose for 2 h, and stimulated with either 3 or 10 mM glucose in KRHB containing 0.2% BSA for 30 min. CTR group treated identically, without addition of free fatty acids to culture media. Error bars represent 1 SEM, n = 6. (b) HG group cultured in RPMI supplemented with 25 mM glucose for 3 d, incubated in KRHB containing 1 mM glucose for 2 h, and stimulated with either 3 or 10 mM glucose in KRHB containing 0.2% BSA for 30 min. CTR group treated identically with 11 mM glucose in culture media. Error bars represent 1 SEM, n = 3. Asterisk represents $p < 0.05$.

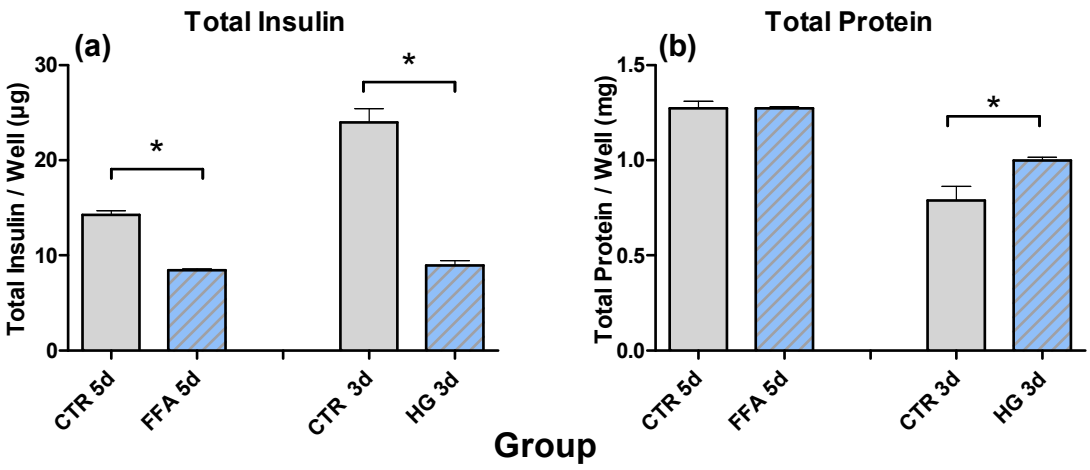

Figure 5-2. Total Insulin and Total Protein in INS-1 Cells Treated with Free Fatty Acids (1 mM) or High Glucose (25 mM).

(a) Total insulin in INS-1 cells. FFA group cultured in RPMI supplemented with 1 mM 1:2 palmitate:oleate bound to 1% fatty acid free BSA for 5 d. CTR group treated identically, without addition of free fatty acids to culture media. HG group cultured in RPMI supplemented with 25 mM glucose for 3 d. CTR group treated identically with 11 mM glucose in culture media. Error bars represent 1 SEM, n = 6 and 3 for FFA and HG experiments, respectively. (b) Total protein in INS-1 cells. Cells treated identically as described for total insulin (above). Error bars represent 1 SEM, n = 6 and 3 for FFA and HG experiments, respectively. Asterisk represents $p < 0.05$.

Metabolomics. Metabolites from the lipotoxic and glucotoxic models were quantified relative to their respective controls at the time 0 (Figure 5-3) and over the 5, 25, and 45 min post stimulation time points studied (Figure 5-4). These data are replotted as scatter plots in Figure 5-9 through Figure 5-11 to highlight specific metabolite changes. In control conditions, the metabolite concentrations were essentially identical to each other indicating excellent reproducibility of the biological and analytical methods and minimal impact of BSA (control for FFA) on metabolite concentrations. Following FFA and HG treatments, we observed significant alterations in metabolite levels relative to controls in all metabolite classes. The changes in lipotoxic and glucotoxic models point to alterations in β-cell metabolism concurrent with alterations in insulin secretion.

In general, changes were more pronounced in HG conditions relative to FFA treatment with significant increases in nearly all glycolysis, TCA, PPP, sugar nucleotide donors, and free fatty acid metabolites relative to control. HG treated cells also displayed blunted increases in metabolite concentrations on stimulation as fewer analytes changed significantly with 10 mM glucose stimulation relative to time 0 compared with controls or FFA treated cells (Figure 5-3).

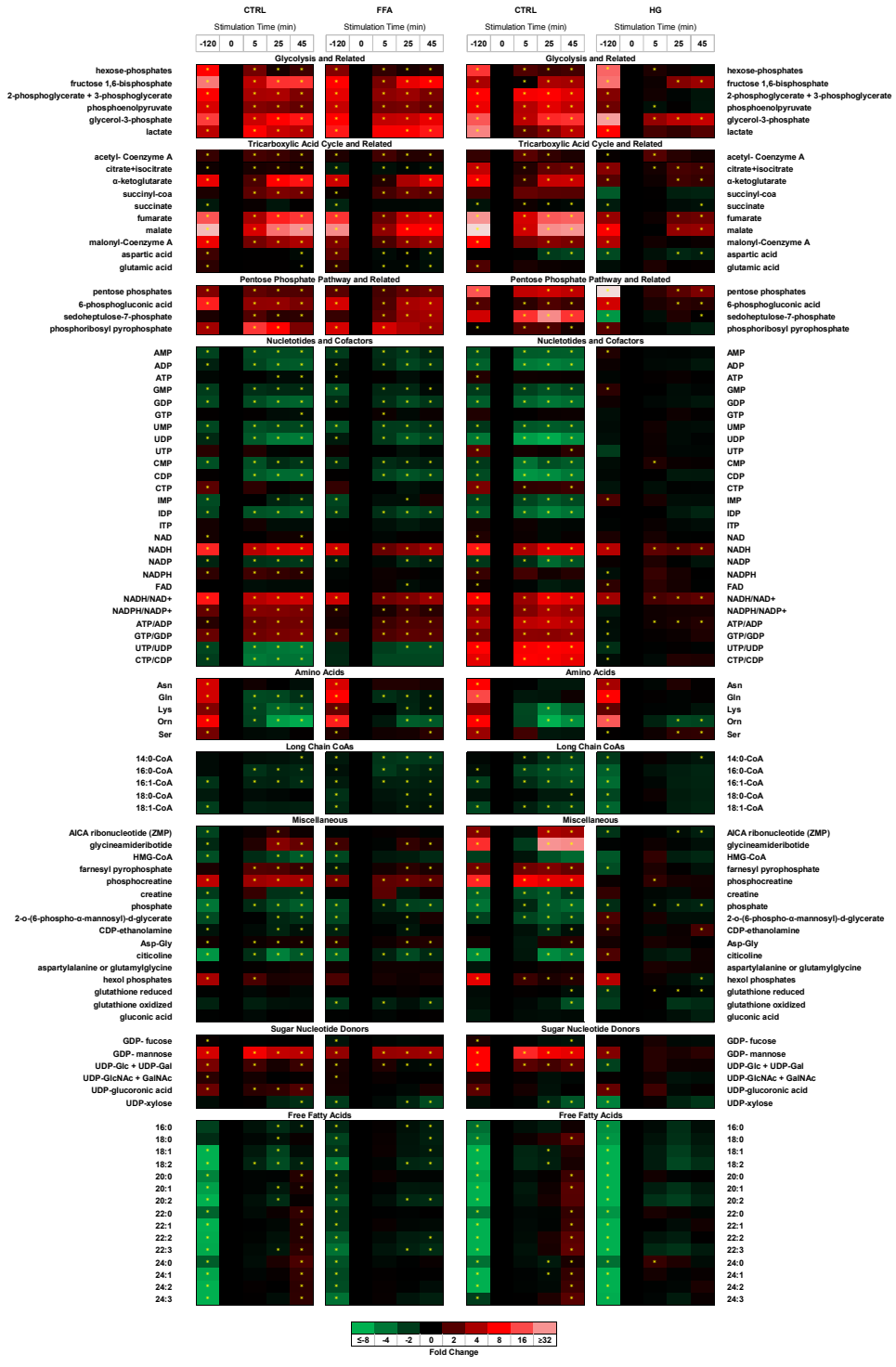

Figure 5-3. Time-Course Changes in Metabolite Concentration with Glucose Stimulation for Free Fatty Acid and High Glucose Treated INS-1 832/13 Cells.

Cells incubated in 11 mM glucose + 1 mM fatty acids (1:2 palmitate:oleate) + 1% BSA for 5 d or 25 mM glucose for 3 d. Cells transferred to KRHB + 1 mM glucose for 2 h and stimulated with 10 mM glucose for 45 min. Metabolite levels relative to time 0 for each group. Asterisk represents $p < 0.05$ relative to time-0, n = 3.

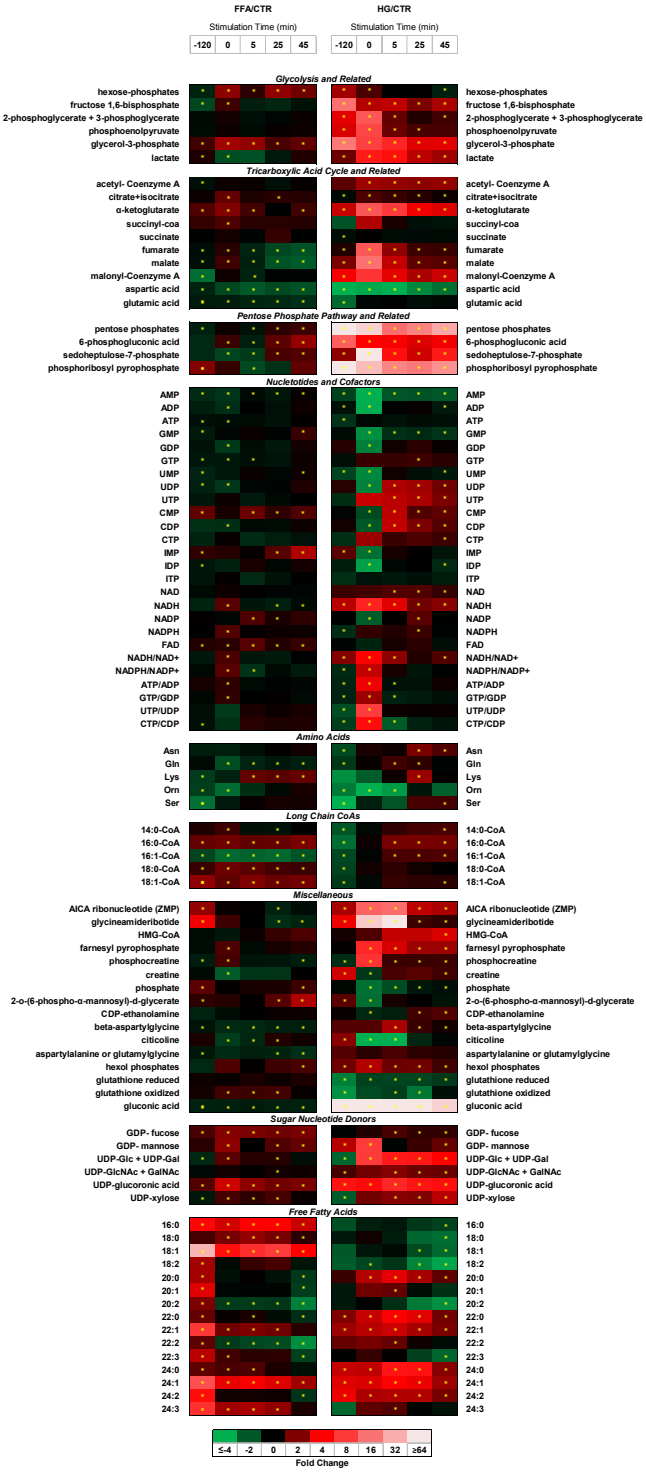

Figure 5-4. Alteration in Metabolite Levels Relative to Controls in Culture and with Glucose Stimulation for Free Fatty Acid and High Glucose Treated INS-1 832/13 Cells.

Cells incubated in 11 mM glucose + 1 mM fatty acids (1:2 palmitate:oleate) + 1% BSA for 5 d or 25 mM glucose for 3 d. Cells transferred to KRHB + 1 mM glucose for 2 h, and stimulated with 10 mM glucose for 45 min. Differences in metabolite levels relative to control for each time point and condition. Asterisk represents $p < 0.05$ relative to control, $n = 3$.

Glycolysis. As the pathway comprising the first steps of glucose metabolism (Figure 1-3), glycolysis plays a crucial role in GSIS and alterations in these metabolites with FFA or HG conditions could have substantial implications for insulin release.

Fatty acid. Hexose-phosphates decreased in FFA culture (-120 min) despite the presence of 11 mM glucose in the RPMI media, but increased at time 0 and post stimulation (130 to 220%) relative to control (Figure 5-4). This observation suggests decreased utilization of glucose in the lipotoxic model under culture conditions where free fatty acids are an abundant energy source and increased glycolytic flux with glucose stimulation post starvation. These findings conflict with a previous study that demonstrated reduced glucose-6-phosphate levels in islets which the authors attributed to increased phosphofructokinase activity after 24 h culture with 0.25 mM oleate.[27] This difference could be due to variation in β-cell type, FFA composition, and duration of exposure. Increases in the majority of glycolytic intermediates with 10 mM glucose stimulation as seen in control cells was not affected by FFA treatment (Figure 5-3).

High Glucose. All measured glycolytic metabolites increased with HG treatment relative to control with the exception of hexose-phosphates which were significantly elevated at -120 min and time 0, showed no significant change 5 and 25 min post 10 mM glucose stimulation, and a significant 20% decrease at 45 min. Although absolute hexose-phosphate levels were not significantly different 25 min post stimulation, experiments with [U-^{13}C]glucose demonstrate enhanced glycolytic flux in HG cells as a larger portion of the hexose phosphate pool is turned over at 25 minutes (Figure 5-5). This is supported by the finding of increased levels of downstream metabolites such as fructose 1,6-bisphosphate and acetyl-CoA (Figure 5-3).

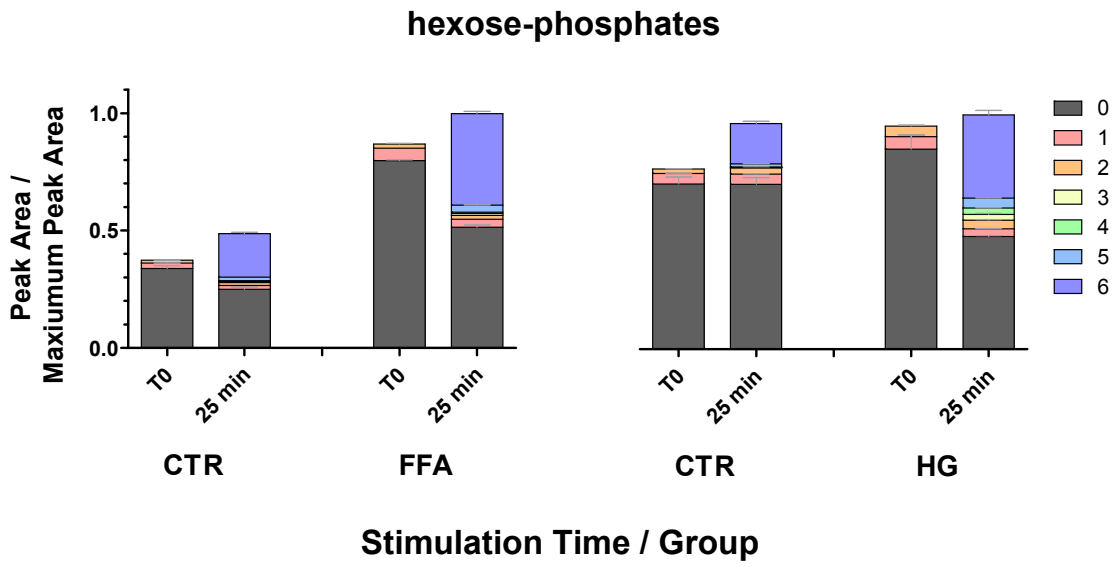

Figure 5-5. Incorporation of ^{13}C into Hexose-Phosphates with [U-^{13}C]-glucose Stimulation in Free Fatty Acid and High Glucose Treated INS-1 832/13 Cells.

Cells incubated in 11 mM glucose + 1 mM fatty acids (1:2 palmitate:oleate) + 1% BSA for 5 d or 25 mM glucose for 3 d. Cells transferred to KRHB + 1 mM glucose for 2 h, and stimulated with 10 mM [U-^{13}C]-glucose for 25 min. Metabolite peak areas normalized to maximum value measured in each control + experimental group. Error bars represent 1 SEM, n = 3.

TCA cycle. The TCA cycle plays a critical role in cellular respiration by generating reduced cofactors for ATP production in the electron transport chain both through oxidation of carbon from glucose and beta-oxidation of fatty acids (Figure 1-4). Furthermore, key proposed coupling factors to GSIS such as NADPH and malonyl-CoA are generated by cyclic pathways comprised of anaplerotic TCA cycle metabolites (Figure 1-2b). Hence, changes in TCA metabolite concentrations are expected to have a substantial impact on GSIS.

Fatty acids. In the lipotoxic model, span-1 TCA metabolites (citrate + isocitrate, α-ketoglutarate, and succinyl-CoA) were elevated at all time-points relative to controls whereas span-2 metabolites (fumarate and malate) were lower (Figure 5-4). This observation suggests decreased flux through pyruvate carboxylase which converts pyruvate to malate through oxaloacetate consistent with reports of ablated pyruvate cycling in a lipotoxic model of INS-1[23] (see Figure 1-2b and Figure 1-4). [U-^{13}C]-glucose stimulation data suggests increased exchange of TCA metabolites with glutamate in FFA treated cells as a larger percentage of the glutamate pool is turned-over (65 versus 50%

decrease in [U-^{12}C]-glutamate) after 25 minutes (Figure 5-6 c). Thus, the increased generation of glutamate from α-ketoglutarate in the TCA cycle suggests a catapleurotic flux of substrates which could contribute to the relative reduction in fumarate and malate. Aspartate is derived primarily from transamination of glutamate to oxaloacetate forming aspartate and α-ketoglutarate in the mitochondria as part of the malate-aspartate shuttle under increased glucose flux conditions. Aspartate is carried to the cytosol to regenerate oxaloacetate and malate, essentially carrying NADH into the mitochondria. Reduction in this shuttle in FFA treated cells is suggested by the smaller increase in 'unlabled' malate found in cells following FFA treatment compared to control cells (Figure 6a). Thus, the reduction in oxaloacetate and malate could limit the shuttle activity and reduce insulin secretion by limiting the transfer of NADH flux into the mitochondria which is important in maintaining insulin secretion[28, 29].

High glucose. In the glucotoxic model, citrate + isocitrate, α-ketoglutarate, fumarate, and malate were elevated at all time points. The largest differences were observed at time-0 with levels 150, 1100, 1100, and 1600% relative to controls, respectively. These findings are consistent with reports of a sustained elevation in citrate and malate concentrations in HG treated INS-1 cells[8] and suggest a continued high rate of energy metabolism to deplete nutrient stores (e.g. triglycerides and glycogen) produced during prolonged incubation in high glucose. The observation that incorporation of [U-^{13}C]-glucose carbon is equivalent or greater for malate and citrate following high glucose exposure (Figure 5-6 a and b) support the concept of increased metabolic rate in the glucotoxic model as opposed to an alternate interpretation of permanently elevated levels due to pathway blockage and/or severe metabolic dysfunction. Non-^{13}C labeled malate increased or remained constant presumably due to the supply from substantial pools of non-^{13}C labeled glutamate and aspartate and high malate-aspartate shuttle activity.

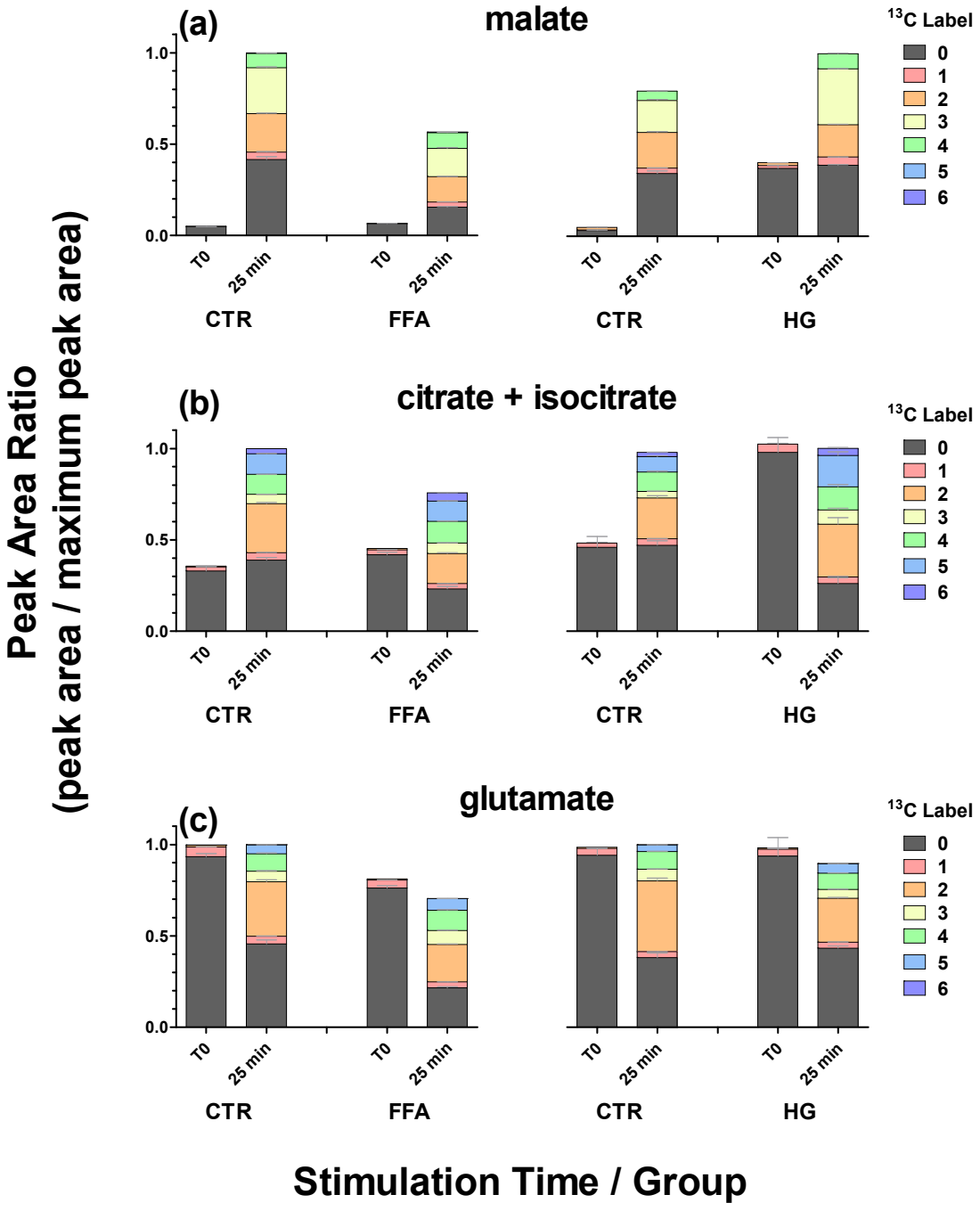

Figure 5-6. Incorporation of ^{13}C into Citrate, Malate, and Glutamate with [U-^{13}C]-glucose Stimulation in Free Fatty Acid and High Glucose Treated INS-1 832/13 Cells.

Cells incubated in 11 mM glucose +1 mM fatty acids (1:2 palmitate:oleate) + 1% BSA for 5 d or 25 mM glucose for 3 d. Cells transferred to KRHB + 1 mM glucose for 2 h, and stimulated with 10 mM [U-^{13}C]-glucose for 25 min. Metabolite peak areas normalized to maximum value measured in each control + experimental group. Error bars represent 1 SEM, n = 3.

Pentose Phosphate Pathway. The pentose phosphate pathway (Figure 1-5) has been implicated in the alteration of metabolism with HG treatment. A decrease in 6-phosphogluconate dehydrogenase (the first and rate limiting enzyme linking glycolysis to the PPP), with HG treatment was reported in a study of MIN6 and over-expression of G6PD improved insulin secretion.[13] The PPP has the potential to serve as a compensatory pathway to metabolize excess glucose into nucleotides, nucleic acids, and aromatic amino acids. The PPP also generates the proposed coupling factor NADPH which is required to regenerate the antioxidant glutathione.

Fatty Acids. Pentose phosphate levels were lower or not significantly different from controls in FFA treated cells at -120, 0, and 5 min time-points and increased significantly at 25 and 45 min to 126 and 140% relative to controls (Figure 5-4). Similar results were observed for 6-phosphogluconate, and sedheptulose-7-phosphate although a significant elevation at 140% of control was observed at time 0 for 6-phosphogluconate. Glycineamide ribonucleotide and ZMP, downstream PPP metabolites in the nucleotide synthetic pathway, were both elevated in FFA treated cells at -120 min at 370 and 222% relative to controls, respectively, and decreased slightly (70-91% relative to controls) at 25 and 45 min following stimulation. The 6-phosphogluconate pool in FFA-treated and control cells was labeled similarly with [U-^{13}C]-glucose treatment (Figure 7) suggesting that flux through the PPP was relatively unaffected by prolonged exposure to FFA.

High Glucose. The most profound alteration in INS-1 metabolism with HG treatment occurred in PPP intermediates in agreement with a previous study of INS-1.[30] Increases in PPP metabolites in HG treated cells ranged from 2 to 220-fold relative to controls at time 0 (Figure 5-4). Glycineamide ribonucleotide and ZMP were elevated modestly at the -120 min time point (360 and 250% relative to controls) and increased considerably on stimulation to 105 and 15-fold of control, respectively. The increase in ZMP is especially interesting given elevated levels of ZMP are associated with a decrease in insulin secretion[31, 32] as discussed in Chapter 4.

Stimulation with [U-^{13}C]-glucose resulted in increased labeling of the 6-phosphogluconate pool without changes in the unlabeled pool suggesting both an enhanced activity of glucose-6-phosphate dehydrogenase and a relatively slow turnover of the non-labeled 6-phosphogluconate pool (Figure 5-7). These observations are in contrast to a study of MIN6 cells, another β-cell cell line[33], in which a decrease in glucose-6-phosphate dehydrogenase activity was reported and associated with a potential decrease in regeneration of reduced glutathione.[16] We clearly demonstrate

substantial enhancement of the PPP, though we also observed decreased levels of both reduced and oxidized glutathione relative to control (Figure 5-8). A decrease in glutathione could contribute substantially to reactive oxygen species (ROS) cytotoxicity since β-cells already express abnormally low levels of antioxidant enzymes.[13] While this finding indicates a reduced antioxidant capacity in the glucotoxic model, it does not support a decrease in PPP flux and subsequent decrease in NADPH cycling as the cause.

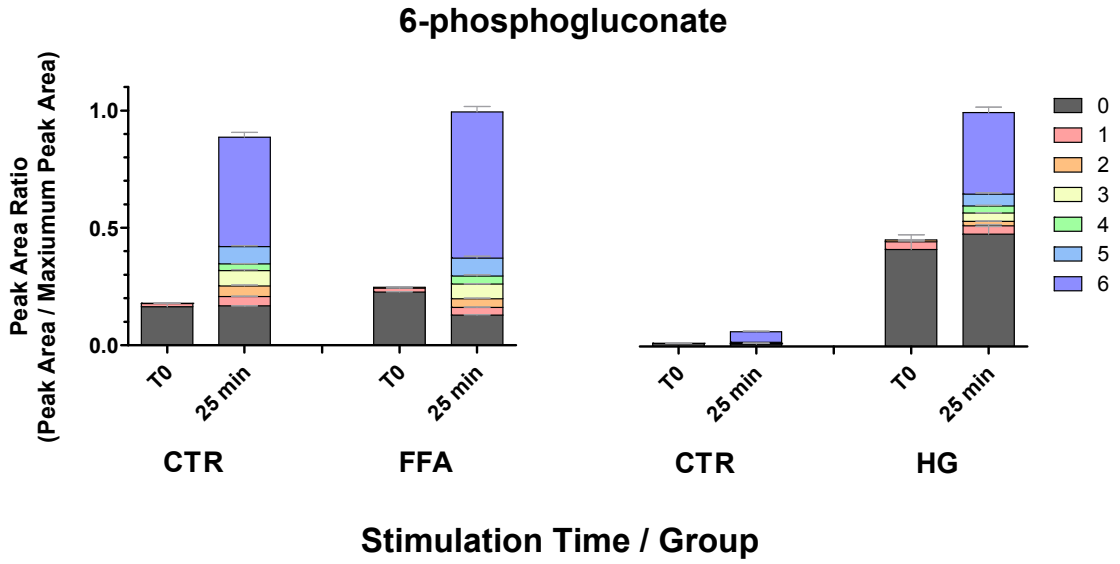

Figure 5-7. Incorporation of ^{13}C into 6-phosphogluconate and with [U-^{13}C]-glucose Stimulation in Free Fatty Acid and High Glucose Treated INS-1 832/13 Cells.

Cells incubated in 11 mM glucose + 1 mM fatty acids (1:2 palmitate:oleate) + 1% BSA for 5 d or 25 mM glucose for 3 d. Cells transferred to KRHB + 1 mM glucose for 2 h, and stimulated with 10 mM [U-^{13}C]-glucose for 25 min. Metabolite peak areas normalized to maximum value measured in each control + experimental group. Error bars represent 1 SEM, n = 3.

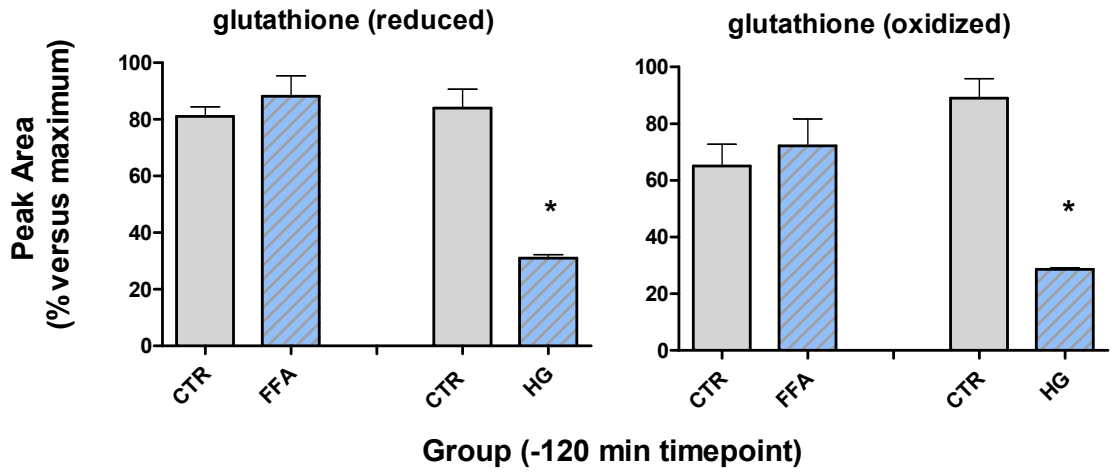

Figure 5-8. Reduced and Oxidized Glutathione Levels in Free Fatty Acid and High Glucose Treated INS-1 832/13 Cells.

Cells incubated in 11 mM glucose + 1 mM fatty acids (1:2 palmitate:oleate) + 1% BSA for 5 d or 25 mM glucose for 3 d. Cells rinsed with KRHB + 10 mM glucose and quenched. Metabolite peak areas normalized to maximum value measured in each control + experimental group. Error bars represent 1 SEM, n = 3. Asterisk indicates $p < 0.05$ relative to control.

Nucleotides and Cofactors. Adenine nucleotides and NAD^+ and $NADP^+$ nucleotides are important for mediating acute and chronic events in insulin secretion as discussed in Chapter 4. Healthy β-cells have a high ATP/ADP ratio and redox potential ($NADH/NAD^+$ and $NADPH/NADP^+$) in growth media that decreases during preincubation in low glucose and rapidly increase on glucose stimulation (Figure 5-4 and Figure 5-3).

Fatty acids. Mono-, di-, and triphosphorylated adenosine nucleotides levels were lower relative to control following FFA exposure at -120 and 0 min time points and increased to a similar level following glucose exposure (Figure 5-9 a-b). The ATP/ADP ratio was significantly increased at 128% of control (Figure 5-9d,h and Figure 5-10c,f) but was similar to control cells following 10 mM glucose stimulation. Guanosine nucleotides were similarly lower than control while CMP, IMP, and FAD levels were elevated at 115-256% relative to control (Figure 5-4). The $NADPH/NADP^+$ ratio varied dynamically and was significantly elevated at 161% of control at time 0, significantly lower at 70% of control 5 min post glucose stimulation, and not significantly different at 25 and 45 min time points (Figure 5-10 c). These observations suggest a modest

increase in energy metabolism to generate ATP at basal levels that may contribute to elevated insulin release at basal glucose concentrations.

High Glucose. In the glucotoxic model, mono- and di-adenosine and guanine nucleotides had decreased concentrations at time 0 from 19 to 37% relative to control (Figure 5-9e-f). ATP/ADP and NADPH/$NADP^+$ ratios were elevated at 364 and 289% relative to control (Figure 5-9 h and Figure 5-10 f). ATP levels were slightly lower (Figure 5-9c,g) in agreement with observations for a glucotoxic model in MIN6.[15] Similar to the lipotoxic model, the findings suggest a substantial elevation in energy metabolism at basal glucose levels that may contribute to elevated basal insulin release at basal glucose concentrations.

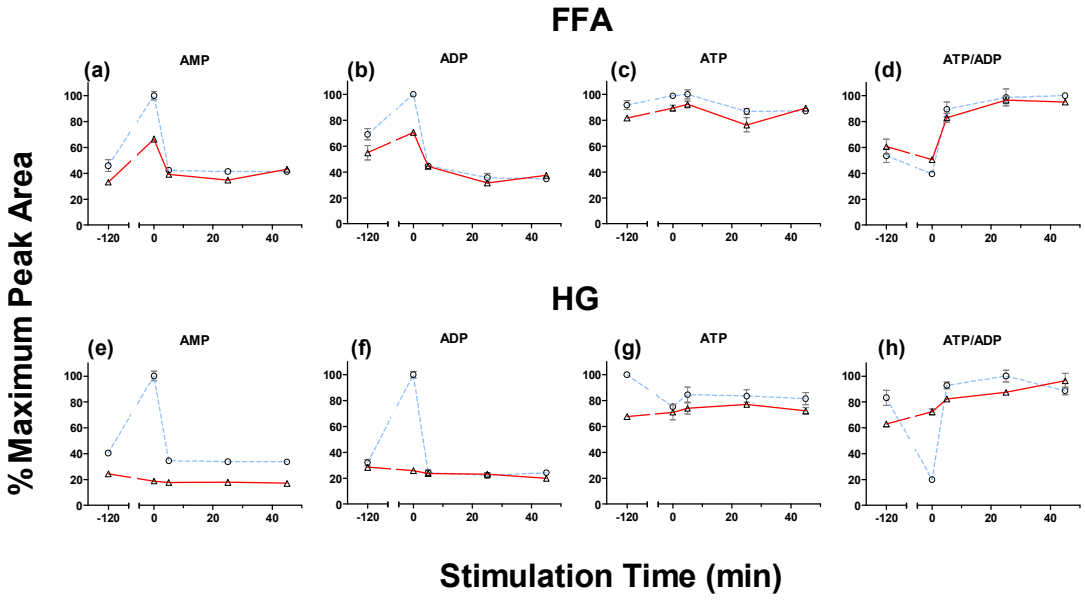

Figure 5-9. Time-Course Adenosine Nucleotide Concentrations with Glucose Stimulation in Free Fatty Acid and High Glucose Treated INS-1 832/13 Cells.

Cells incubated in 11 mM glucose + 1 mM fatty acids (1:2 palmitate:oleate) + 1% BSA for 5 d or 25 mM glucose for 3 d. Cells transferred to KRHB + 1 mM glucose for 2 h and stimulated with 10 mM glucose for 45 min. Metabolite peak areas normalized to maximum value measured in each control + experimental group. Red solid line = experimental, blue dash = control. Error bars represent 1 SEM, n = 3.

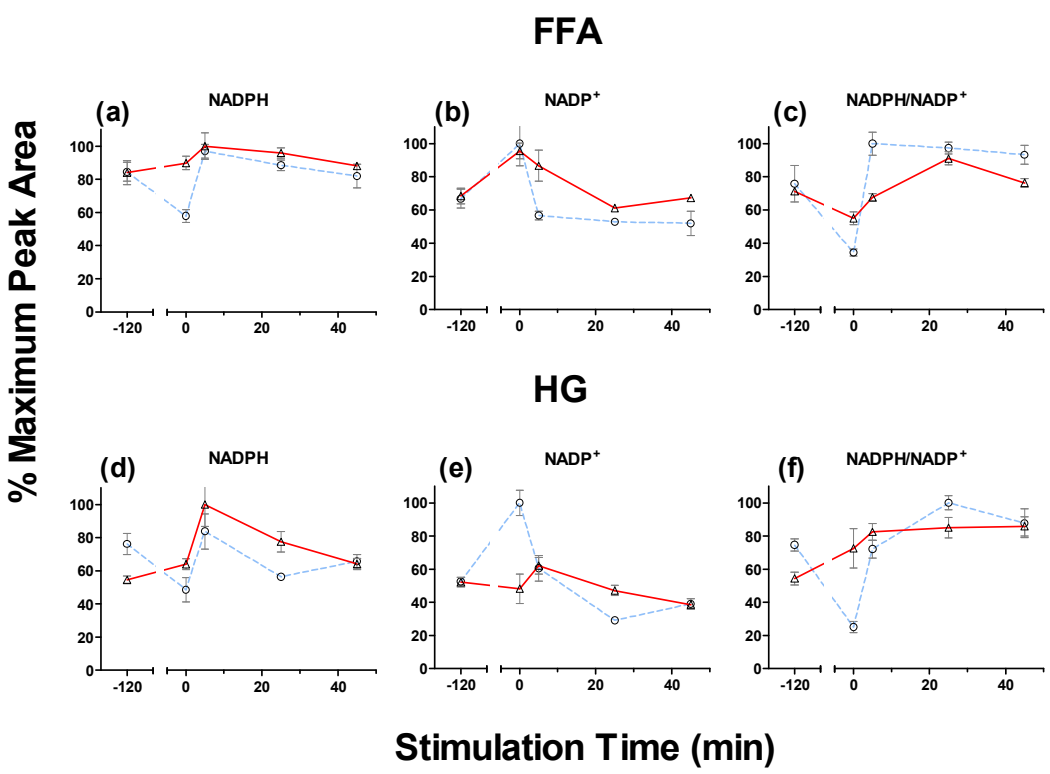

Figure 5-10. Time-Course $NADP^+$ and NADPH Profiles with Glucose Stimulation in Free Fatty Acid and High Glucose Treated INS-1 832/13 Cells.

Cells incubated in 11 mM glucose + 1 mM fatty acids (1:2 palmitate:oleate) + 1% BSA for 5 d or 25 mM glucose for 3 d. Cells transferred to KRHB + 1 mM glucose for 2 h and stimulated with 10 mM glucose for 45 min. Metabolite peak areas normalized to maximum value measured in each control + experimental group. Red solid line = experimental, blue dash = control. Error bars represent 1 SEM, n = 3.

Long-Chain Acyl-CoAs. Long-chain acyl-CoAs have been implicated as metabolic coupling factors in GSIS[34] and can open K_{ATP} channels[35]. In control cells, long-chain acyl-CoAs decrease rapidly on glucose stimulation (Figure 5-3) potentially aiding in K_{ATP} channel closure.

Fatty Acids. In the lipotoxic model, 16:0, 18:0, and 18:1-CoAs were significantly elevated at all time-points ranging from 137 to 219% of control (Figure 5-4). 16:1-CoA levels were significantly lower and ranged from 44 to 58%, presumably due to excess of 16:0 and 18:1 FFAs supplied by the media. These elevations in long-chain acyl-CoAs post stimulation provide a possible mechanism for decreased GSIS as elevated levels could hinder K_{ATP} channel closure associated with Phase 1 GSIS.

High Glucose. In the glucotoxic model, all measured long-chain acyl-CoAs were significantly lower at -120 min (42 to 65%) of control, not significantly different at time-0, and elevated following stimulation. 16:0 and 16:1-CoAs were significantly elevated post stimulation ranging from 150 to 190% relative to controls.

Lipid Precursors. In control cells, glycerol-3-phosphate increases rapidly in concert with the decrease in long-chain acyl-CoAs. These affects may result in synthesis of lipid molecules with signaling implications such as diacyl-phosphoglycerols as discussed in Chapter 4.

Fatty Acids. In the lipotoxic model, malonyl-CoA levels decreased to 42% of controls (-120 min) presumably due to decreased fatty acid synthesis inhibited and inhibition of acetyl-CoA carboxylase by excess 16:0 and 18:1 supplied by the FFA media (Figure 5-11a). Glycerol-3-phosphate is similar to control at time 0 and elevated pre- and post-stimulation (143 to 240% of control) presumably due to up-regulation for increased lipid synthesis (Figure 5-11c).

High Glucose. Metabolites involved in lipogenesis were enhanced remarkably in the glucotoxic model. Malonyl-CoA levels were 381% of control at -120 min and remained elevated at time 0 and throughout simulation at 253-748% of control (Figure 5-11e) presumably due to increased rates of fatty acid synthesis. Glycerol-3-phosphate levels were strongly elevated at -120 min (17-fold higher than control) and remained elevated at time 0 and throughout stimulation at 340-863% of control (Figure 5-11g). Most long-chain fatty acids were elevated as well with significant increases in 20:0, 22:0, 22:1, 24:0, 24:1, and 24:2 of 137 to 504% of control (Figure 5-4).

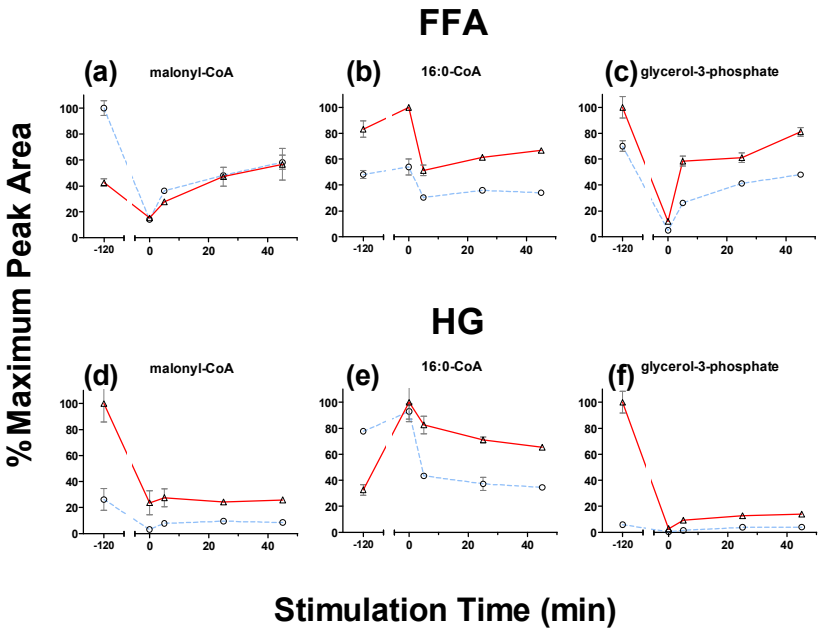

Figure 5-11. Time-Course Metabolite Profiles for Lipid Precursors with Glucose Stimulation in Free Fatty Acid and High Glucose Treated INS-1 832/13 Cells.

Cells incubated in 11 mM glucose + 1 mM fatty acids (1:2 palmitate:oleate) + 1% BSA for 5 d or 25 mM glucose for 3 d. Cells transferred to KRHB + 1 mM glucose for 2 h and stimulated with 10 mM glucose for 45 min. Metabolite peak areas normalized to maximum value measured in each control + experimental group. Red solid line = experimental, blue dash = control. Error bars represent 1 SEM, n = 3.

Sugar Nucleotide Donors. Sugar nucleotide donors are not often measured in β-cells although several metabolites in this class were observed to increase in control cells with glucose stimulation (Figure 5-3), particularly GDP-mannose discussed in Chapter 4. These metabolites are particularly interesting in relation to GSIS in conditions of excess nutrient flux due to their role in glucose polymerization, protein glycosylation, and signaling. Sugar nucleotide donors mostly increased relative to control in lipotoxic and glucotoxic models (Figure 5-4) with sustained elevations in UDP-glucuronate for both models ranging from 157 to 635% of control. UDP-glucuronate is an intermediate in ascorbic acid synthesis and is involved in cellular detoxification. Increases in this metabolite could serve as an adaptive response to oxidative stress caused by lipotoxic and glucotoxic culture conditions.

Gluconate. Gluconate is a non-enzymatically derived metabolite in mammals although it was observed at high levels in HG treated cells in agreement with a previous observation of INS-1[30]. Gluconate can be generated from glucose *in vitro* with hydrogen peroxide which suggests a possible mechanism of gluconate formation with HG treatment as several studies have reported increased reactive oxygen species in HG treated β-cells[4, 13]. Gluconate levels in HG treated cells are 50 to 80-fold higher than control (Figure 5-4). This finding is of particular interest in relation to GSIS since gluconate is a Ca^{2+} chelator and could potentially interfere with Ca^{2+} signaling required for insulin release. Indeed, alterations in Ca^{2+} signaling have been reported in a glucotoxic model of INS-1 cells which exhibited elevated intercellular Ca^{2+} and increased amplitude and shortened duration of depolarization-evoked rises Ca^{2+}.[9] The study linked these changes to a defect in the final steps of exocytosis supported by down regulation of several proteins required for calcium induced exocytosis of secretory granules. It would be of great interest to determine if the presence of high gluconate concentrations in β-cells could also be linked to alteration in Ca^{2+} signaling, perhaps by permeabilizing cells with surfactant to allow introduction of exogenous gluconate.

Conclusions

INS-1 832/13 cells were treated with free fatty acids and high glucose in culture to generate models of lipotoxicity and glucotoxicity that exhibited increased insulin secretion at basal glucose levels and blunted insulin secretion at high glucose levels. Time resolved metabolomic measurements of these cells were made in culture, at basal glucose levels, and following glucose stimulation at time points concurrent with Phase 1 and Phase 2 GSIS. Dramatic alterations in metabolism were observed in both lipotoxic and glucotoxic models. An elevation in basal rates of energy metabolism was common to both models and resulted in increased ATP/ADP ratio, an important parameter in K_{ATP} channel closure and insulin release. Long-chain acyl-CoAs that also impact K_{ATP} channel closure were substantially altered both pre and post stimulation relative to controls. A large increase in glycolytic flux through the PPP was measured in addition to decreased levels of reduced and oxidized glutathione. Gluconate, a rarely measured β-cell metabolite was measured at concentrations and has potential implications for Ca^{2+} signaling.

References

1. Aschner, P. 2010. Metabolic syndrome as a risk factor for diabetes. *Expert Rev Cardiovasc Ther* 8:407-412.
2. Poitout, V., Amyot, J., Semache, M., Zarrouki, B., Hagman, D., and Fontes, G. 2010. Glucolipotoxicity of the pancreatic beta cell. *Biochim Biophys Acta* 1801:289-298.
3. Karaca, M., Magnan, C., and Kargar, C. 2009. Functional pancreatic beta-cell mass: involvement in type 2 diabetes and therapeutic intervention. *Diabetes Metab* 35:77-84.
4. Poitout, V., and Robertson, R.P. 2008. Glucolipotoxicity: Fuel Excess and β-Cell Dysfunction. *Endocrine Reviews* 29:351-366.
5. Pinnick, K., Neville, M., Clark, A., and Fielding, B. 2010. Reversibility of metabolic and morphological changes associated with chronic exposure of pancreatic islet β-cells to fatty acids. *Journal of Cellular Biochemistry* 109:683-692.
6. Brun, T., Assimacopoulos-Jeannet, F., Corkey, B.E., and Prentki, M. 1997. Long-chain fatty acids inhibit acetyl-CoA carboxylase gene expression in the pancreatic beta-cell line INS-1. *Diabetes* 46:393-400.
7. Park, K.-G., Lee, K.-M., Seo, H.-Y., Suh, J.-H., Kim, H.-S., Wang, L., Won, K.-C., Lee, H.-W., Park, J.-Y., Lee, K.-U., et al. 2007. Glucotoxicity in the INS-1 Rat Insulinoma Cell Line Is Mediated by the Orphan Nuclear Receptor Small Heterodimer Partner. *Diabetes* 56:431-437.
8. Roche, E., Farfari, S., Witters, L.A., Assimacopoulos-Jeannet, F., Thumelin, S., Brun, T., Corkey, B.E., Saha, A.K., and Prentki, M. 1998. Long-term exposure of beta-INS cells to high glucose concentrations increases anaplerosis, lipogenesis, and lipogenic gene expression. *Diabetes* 47:1086-1094.
9. Dubois, M., Vacher, P., Roger, B.t., Huyghe, D., Vandewalle, B., Kerr-Conte, J., Pattou, F., Moustaïd-Moussa, N., and Lang, J. 2007. Glucotoxicity Inhibits Late Steps of Insulin Exocytosis. *Endocrinology* 148:1605-1614.
10. Liu, Y.Q., Tornheim, K., and Leahy, J.L. 1998. Shared biochemical properties of glucotoxicity and lipotoxicity in islets decrease citrate synthase activity and increase phosphofructokinase activity. *Diabetes* 47:1889-1893.
11. El-Assaad, W., Joly, E., Barbeau, A., Sladek, R., Buteau, J., Maestre, I., Pepin, E., Zhao, S., Iglesias, J., Roche, E., et al. 2010. Glucolipotoxicity Alters Lipid Partitioning and Causes Mitochondrial Dysfunction, Cholesterol, and Ceramide Deposition and Reactive Oxygen Species Production in INS832/13 ß-Cells. *Endocrinology* 151:3061-3073.
12. Chu, K.Y., Lin, Y., Hendel, A., Kulpa, J.E., Brownsey, R.W., and Johnson, J.D. 2010. ATP-Citrate Lyase Reduction Mediates Palmitate-induced Apoptosis in Pancreatic Beta Cells. *Journal of Biological Chemistry* 285:32606-32615.
13. Zhang, Z., Liew, C.W., Handy, D.E., Zhang, Y., Leopold, J.A., Hu, J., Guo, L., Kulkarni, R.N., Loscalzo, J., and Stanton, R.C. 2010. High glucose inhibits glucose-6-phosphate dehydrogenase, leading to increased oxidative stress and β-cell apoptosis. *The FASEB Journal* 24:1497-1505.
14. Liu, Y.Q., Moibi, J.A., and Leahy, J.L. 2004. Chronic High Glucose Lowers Pyruvate Dehydrogenase Activity in Islets through Enhanced Production of Long Chain Acyl-CoA. *Journal of Biological Chemistry* 279:7470-7475.
15. Kim, W.-H., Lee, J.W., Suh, Y.H., Hong, S.H., Choi, J.S., Lim, J.H., Song, J.H., Gao, B., and Jung, M.H. 2005. Exposure to Chronic High Glucose Induces β-Cell Apoptosis Through Decreased Interaction of Glucokinase With Mitochondria. *Diabetes* 54:2602-2611.
16. Jitrapakdee, S., Wutthisathapornchai, A., Wallace, J.C., and MacDonald, M.J. 2010. Regulation of insulin secretion: role of mitochondrial signalling. *Diabetologia* 53:1019-1032.
17. Henquin, J.C., Nenquin, M., Ravier, M.A., and Szollosi, A. 2009. Shortcomings of current models of glucose-induced insulin secretion. *Diabetes Obes Metab* 11 Suppl 4:168-179.
18. Muoio, D.M., and Newgard, C.B. 2008. Molecular and metabolic mechanisms of insulin resistance and [beta]-cell failure in type 2 diabetes. *Nature Reviews Molecular Cell Biology* 9:193-205.

19. Guay, C., Madiraju, S.R., Aumais, A., Joly, E., and Prentki, M. 2007. A role for ATP-citrate lyase, malic enzyme, and pyruvate/citrate cycling in glucose-induced insulin secretion. *Journal of Biological Chemistry* 282:35657-35665.
20. Bradford, M.M. 1976. A rapid and sensitive method for the quantitation of microgram quantities of protein utilizing the principle of protein-dye binding. *Analytical Biochemistry* 72:248-254.
21. Matthew A. Lorenz, C.F.B., Robert T. Kennedy. 2011. Rapid Sample Preparation for Metabolomic Analysis of Adherent Mammalian Cells Using INS-1 Cells as a Model System. *Analytical Chemistry* TDB:TBD.
22. Lorenz, M.A., Burant, C.F., and Kennedy, R.T. 2011. Reducing Time and Increasing Sensitivity in Sample Preparation for Adherent Mammalian Cell Metabolomics. *Analytical Chemistry*:null-null.
23. Boucher, A., Lu, D., Burgess, S.C., Telemaque-Potts, S., Jensen, M.V., Mulder, H., Wang, M.-Y., Unger, R.H., Sherry, A.D., and Newgard, C.B. 2004. Biochemical Mechanism of Lipid-induced Impairment of Glucose-stimulated Insulin Secretion and Reversal with a Malate Analogue. *Journal of Biological Chemistry* 279:27263-27271.
24. Patanè, G., Anello, M., Piro, S., Vigneri, R., Purrello, F., and Rabuazzo, A.M. 2002. Role of ATP Production and Uncoupling Protein-2 in the Insulin Secretory Defect Induced by Chronic Exposure to High Glucose or Free Fatty Acids and Effects of Peroxisome Proliferator-Activated Receptor-γ Inhibition. *Diabetes* 51:2749-2756.
25. Milburn, J.L., Hirose, H., Lee, Y.H., Nagasawa, Y., Ogawa, A., Ohneda, M., BeltrandelRio, H., Newgard, C.B., Johnson, J.H., and Unger, R.H. 1995. Pancreatic - Cells in Obesity. *Journal of Biological Chemistry* 270:1295-1299.
26. Zhou, Y.P., and Grill, V.E. 1994. Long-term exposure of rat pancreatic islets to fatty acids inhibits glucose-induced insulin secretion and biosynthesis through a glucose fatty acid cycle. *The Journal of Clinical Investigation* 93:870-876.
27. Liu, Y.Q., Tornheim, K., and Leahy, J.L. 1998. Fatty acid-induced beta cell hypersensitivity to glucose. Increased phosphofructokinase activity and lowered glucose-6-phosphate content. *The Journal of Clinical Investigation* 101:1870-1875.
28. Casimir, M., Rubi, B., Frigerio, F., Chaffard, G., and Maechler, P. 2009. Silencing of the mitochondrial NADH shuttle component aspartate-glutamate carrier AGC1/Aralar1 in INS-1E cells and rat islets. *Biochem J* 424:459-466.
29. Bender, K., Newsholme, P., Brennan, L., and Maechler, P. 2006. The importance of redox shuttles to pancreatic beta-cell energy metabolism and function. *Biochem Soc Trans* 34:811-814.
30. Göhring, I. 2008. Characterisation of pancreatic INS-1 insulinoma cells under chronic high glucose conditions as glucose toxicity model. In *Department of Medicine*. Berlin: University Medicine Berlin.
31. da Silva Xavier, G., Leclerc, I., Varadi, A., Tsuboi, T., Moule, S.K., and Rutter, G.A. 2003. Role for AMP-activated protein kinase in glucose-stimulated insulin secretion and preproinsulin gene expression. *Biochemical Journal* 371:761-774.
32. Zhang, S., and Kim, K.H. 1995. Glucose activation of acetyl-CoA carboxylase in association with insulin secretion in a pancreatic beta-cell line. *Journal of Endocrinology* 147:33-41.
33. Miyazaki, J., Araki, K., Yamato, E., Ikegami, H., Asano, T., Shibasaki, Y., Oka, Y., and Yamamura, K. 1990. Establishment of a pancreatic beta cell line that retains glucose-inducible insulin secretion: special reference to expression of glucose transporter isoforms. *Endocrinology* 127:126-132.
34. Prentki, M., Vischer, S., Glennon, M.C., Regazzi, R., Deeney, J.T., and Corkey, B.E. 1992. Malonyl-CoA and long chain acyl-CoA esters as metabolic coupling factors in nutrient-induced insulin secretion. *Journal of Biological Chemistry* 267:5802-5810.
35. Bränström, R., Aspinwall, C.A., Välimäki, S., Östensson, C.G., Tibell, A., Eckhard, M., Brandhorst, H., Corkey, B.E., Berggren, P.O., and Larsson, O. 2004. Long-Chain CoA esters activate human pancreatic beta-cell K _{ATP} channels: potential role in Type 2 diabetes. *Diabetologia* 47:277-283.

CHAPTER 6
Summary and Future Directions

Summary

We developed an LC-MS separation method and rapid preparation/quenching method for the metabolomic analysis of insulin secreting β-cells and applied these techniques to investigate the insufficiently understood metabolic mechanisms of GSIS. This investigation provided unique insights into the dynamic changes of established and novel β-cell metabolites in models of both healthy and disease states on timescales relevant to Phase 1 and Phase 2 GSIS.

The HILIC/AEX LC-MS separation method developed in this work is well suited to the analysis of difficult to chromatograph metabolites. We screened a variety of stationary phases (reverse phase and HILIC) and evaluated chromatographic performance (e.g. retention, resolution, and peak symmetry) of representative glycolytic, TCA, amino acid, and cofactor metabolites. A HILIC/AEX method provided superior performance and was chosen for further development. We evaluated the impact of ionic strength and column temperature on chromatographic performance and chose conditions designed to provide enhanced sensitivity and column lifetime. The final method uses a Luna propyl amine stationary phase with 5 mM ammonium acetate mobile phase at pH 9.9 (linear gradient with acetonitrile) and has provided robust performance in its application to β-cell metabolomics.

We developed a rapid sample preparation method for the metabolomic analysis of adherent mammalian cells. Through evaluation of metabolite recovery with extraction solvent, extraction time, and number of extraction cycles, we defined a procedure that uses a quick water rinse, LN_2 quenching, and a rapid single step extraction with 75% 9:1 MC extraction solvent that yields stable extracts. We demonstrated that a rapid water rinse removes contaminants and substantially improves sensitivity without altering the metabolome. We also showed that LN_2 quenching provides convenience with equivalent results to conventional cold organic solvent quenching. We demonstrated that our

method detects relative changes in the metabolome with GSIS that are similar to previous methods but with an overall increase in sensitivity and speed.

We applied these chromatographic and extraction methods to study GSIS in INS-1 832/13 cells on a directed and undirected basis. Through this effort we quantified an unprecedented number of metabolites in β-cells (~90) on a directed basis that changed significantly concurrent with GSIS. These metabolites included those deemed relevant to GSIS by previous reports as well as several metabolites novel in the study of GSIS or not often measured including glycerol-3-phosphate, ZMP, and GDP-mannose which were identified through undirected metabolomic analysis. Metabolite measurements were performed in both time-resolved and glucose-dose response experiments and generated metabolomic data that allowed us to test and extend several hypotheses for the biochemical mechanism of GSIS in parallel. For example, the simultaneous measurement of AMP, citrate, long-chain acyl-CoAs, and malonyl-CoA demonstrate a novel interaction of metabolites that are important in both the triggering and amplifying pathways of secretion thus helping to refine the malonyl-CoA hypothesis. We found support for the succinate hypothesis with measurements that confirm previous findings including rapid increases in NADPH/$NADP^+$ ratio and decreases in HMG-CoA. We detected increases in farnesyl pyrophosphate that may play a role in GSIS from this pathway. Identification of a decrease in AMP prior to decreases in HMG-CoA shows that regulation by AMPK may play a role in this pathway as well in the malonyl-CoA pathway. Finally, we find that ZMP can inhibit GSIS suggesting a previously unknown role for this compound as an endogenous metabolite.

We further investigated GSIS in INS-1 832/13 cells treated with free fatty acids and high glucose in culture to generate models of lipotoxicity and glucotoxicity. These models exhibited increased insulin secretion at basal glucose levels and blunted insulin secretion at high glucose levels, behavior similar to that expressed in patients with type 2 diabetes. Time resolved metabolomic measurements of these β-cells were made in culture, at basal glucose levels, and following glucose stimulation at time points concurrent with Phase 1 and Phase 2 GSIS. Dramatic alterations in metabolism were observed in both lipotoxic and glucotoxic models. Elevation in basal rates of energy metabolism relative to controls was common to both models and resulted in an increase in ATP/ADP ratio, an important parameter in K_{ATP} channel closure and insulin secretion. Long-chain acyl-CoAs that also impact K_{ATP} channel closure were substantially elevated both pre and post stimulation relative to controls in both glucotoxic and lipotoxic models.

A large increase in glycolytic flux through the PPP was measured in cells cultured in HG conditions in addition to decreased levels of reduced and oxidized glutathione, antioxidant species important for limiting ROS cytotoxicity. Sugar nucleotide donors also increased substantially. Gluconate, a rarely measured β-cell metabolite was found at high concentrations in the glucotoxic model and may have implications for Ca^{2+} signaling involved in insulin secretion.

Future Directions

Non-glucose nutrient secretagogues. Nutrients other than glucose induce insulin secretion and studying their impact on metabolic networks could prove valuable in advancing our understanding of GSIS. These cell-permeable nutrient secretagogues include pyruvate, methyl-succinate (converts to succinate in cytosol), glyceraldehyde, α-ketoisocaproate, and glutamine + leucine (combined only)[1]. Each of these secretagogues enter metabolic pathways at different points and evaluating their impact on levels of proposed metabolic coupling factors resulting insulin secretion may aid in affirming or dismissing current models of GSIS. For example, stimulation with pyruvate should bypass the PPP and limit cycling of glycerol-3-phosphate (from glycolytic dihydroxyacetone phosphate). Comparison of metabolite levels and insulin release relative to glucose could reveal the relative importance of these pathways in GSIS.[2] In addition, it would be of great interest to measure metabolites with glucose stimulation in combination with extracellular fatty acids since studies have reported augmented GSIS in their presence, even though they do not initiate GSIS independent of glucose.[3]

Islets. The majority of multi-metabolite measurements in β-cells to date have been conducted in clonal β-cells such as the INS-1 832/13 line used in our studies. Since these immortal tumor cell lines may favor metabolic pathways devoted to cell growth rather than cellular respiration, the relevance of experimental observations to primary β-cells may be of concern.[4] Therefore, performing global metabolomics measurements in islets initially or to validate results from the study of clonal lines could be of great benefit in diabetes research. Several challenges have limited the use of isolated islets in metabolomic studies including difficulty in islet isolation in quantities sufficient for routine LC-MS based analysis and challenges in sample manipulation (e.g. rapid rinsing and quenching). Metabolomic investigations of isolated islets could benefit

substantially from LC-MS techniques developed for and ultra-high sensitivity with small samples such as nano-LC-MS discussed below.

Nano-LC-MS. Capillary chromatography is ideally suited to the analysis of small samples. Capillary columns have internal diameters as low as 25 μm compared to the 2.1 mm bore columns used in conventional LC-MS. The ~80 fold decrease in column diameter corresponds to an ~7,000 fold decrease in optimal flow rate (to ~300 nL/min) compatible with nano-ESI sources. Nano-ESI can enhance sensitivity relative to conventional ESI through improved ionization efficiency in conjunction with the use of small electrospray emitters.[5] Nano-ESI is also less susceptible to ionization suppression further enhancing sensitivity.[6] Accordingly, detection limits with nano-ESI in the low attomole range have been reported.[7] Challenges with band broadening during sample loading on capillary columns are more difficult to overcome for metabolite analysis compared to peptides where nano-LC is commonly employed. Metabolites often have low retention and organic solvents present in the sample solution broaden bands at the column head.[8] Although moderate success has been reported for HILIC[9] and ion pair[10] methods that provide enhanced retention and therefore improved column focusing for polar analytes. Furthermore, coupling nano-LC with more sensitive mass analyzers such as QQQ could provide substantial improvements for directed studies over the LC-TOF instrumentation used in our experiments.

Global internal standardization. The use of stable-labeled internal standards can provide improved precision and accuracy in metabolite quantification. INS-1 832/13 or similar cells could be grown in media containing [U-^{13}C]-glucose as the primary energy source. Theoretically, extracts from these cells should contain similar metabolite concentrations to those grown in non-labeled media, only with incorporation of large percentages of ^{13}C in all endogenously synthesized metabolites. These labeled species can then be quantified using non-labeled standards to determine their absolute concentration. The extracts can then be added to experimental extracts and endogenous non-labeled metabolites quantified by isotope dilution. Alternatively, these ^{13}C labeled extracts could simply be used as internal references to improve precision by correcting for ionization suppression and instrument drift. Metabolomic investigations into GSIS could benefit from this approach by improving precision to discern smaller but significant changes in metabolite levels with secretagogue stimulation. The ability to

routinely quantify the absolute concentration of metabolites would also be beneficial by providing information on changes in metabolite pool size for a large number of metabolites allowing for an assessment of mass balance in the cell. This approach has been applied to large-scale metabolite quantification in *E coli and* human fibroblasts.[9, 11] Complications in quantification with these approaches may arise due to incomplete isotopic labeling which can generate a wide distribution of metabolite isotopes thereby decreasing the sensitivity and specificity of mass spectrometry detection. Hence, the use of higher resolution mass analyzers such as TOF, FT-ICR, and Orbitrap may be necessary.

Fluxomics. The cell-wide quantification of intracellular metabolite turnover rates known as fluxomics[12] is the next "omics" field to be applied to systems biology and has the potential to greatly expand our study of metabolic networks.[13, 14] The power of metabolomic flux measurements was demonstrated to a limited extent in Chapters 4 and 5 by showing, for example, that the glutamate pool in INS-1 832/13 cells remains constant 25 min after glucose stimulation, but is turned-over ~50% suggesting extensive cycling with TCA intermediates. Hence, the potential for glutamate involvement in GSIS through cyclic shuttles could be overlooked without concurrent flux experimentation. The pathways of β-cell metabolism related to insulin secretion can be further investigated by the use of specifically labeled secretagogues to provide additional information on carbon and or nitrogen flux. For example, glucose flux through PPP relative to glycolysis could be measured by determining the differential isotopic enrichment of pyruvate between stimulation with [1-$^{13}C_1$]-glucose and [6-$^{13}C_1$]-glucose. Carbon 1 of glucose is removed by decarboxylation in the PPP during formation of ribose-5-phosphate whereas it is converted to carbon 3 of pyruvate through glycolysis (Figure 6-1). Measuring the difference between isotopic enrichment with [1-$^{13}C_1$]-glucose versus [6-$^{13}C_1$]-glucose would yield a relative difference in flux between the two pathways. A second measurement important in the study of β-cell metabolism that can be made using this approach is the measurement of glucose flux through cataplerotic pyruvate dehydrogenase and anaplerotic pyruvate carboxylase by stimulation with [3,4-$^{13}C_2$]-glucose and non-labeled glucose. Carbon 3 and 4 of glucose are removed by decarboxylation during conversion of pyruvate to acetyl-CoA by pyruvate dehydrogenase but converted to carbon 3 of oxaloacetate by pyruvate carboxylase (Figure 6-1). Hence the % of carbon entering the TCA through pyruvate

dehydrogenase versus pyruvate carboxylase can be determined by measuring the isotopic enrichment of TCA metabolites with [3,4-$^{13}C_2$]-glucose compared to non-labeled glucose. Measurement of differential flux through these enzymes has been reported using ^{1}H-NMR studies of glutamate[15] but at relatively long (2 h) time points and do not allow assessment of dynamic changes in rates of flux over shorter timeframes relevant to maxima in phase 1 and phase 2 GSIS.

Advanced mechanistic modeling techniques can be applied to measure *in vivo* reaction rates using time course data and modeling software such as FiatFlux[16], 13C-FLUX[17] and OpenFLUX[18]. It would be of particular interest to measures changes in flux during phase 1 and phase 2 GSIS to help further elucidate biochemical triggering mechanisms.

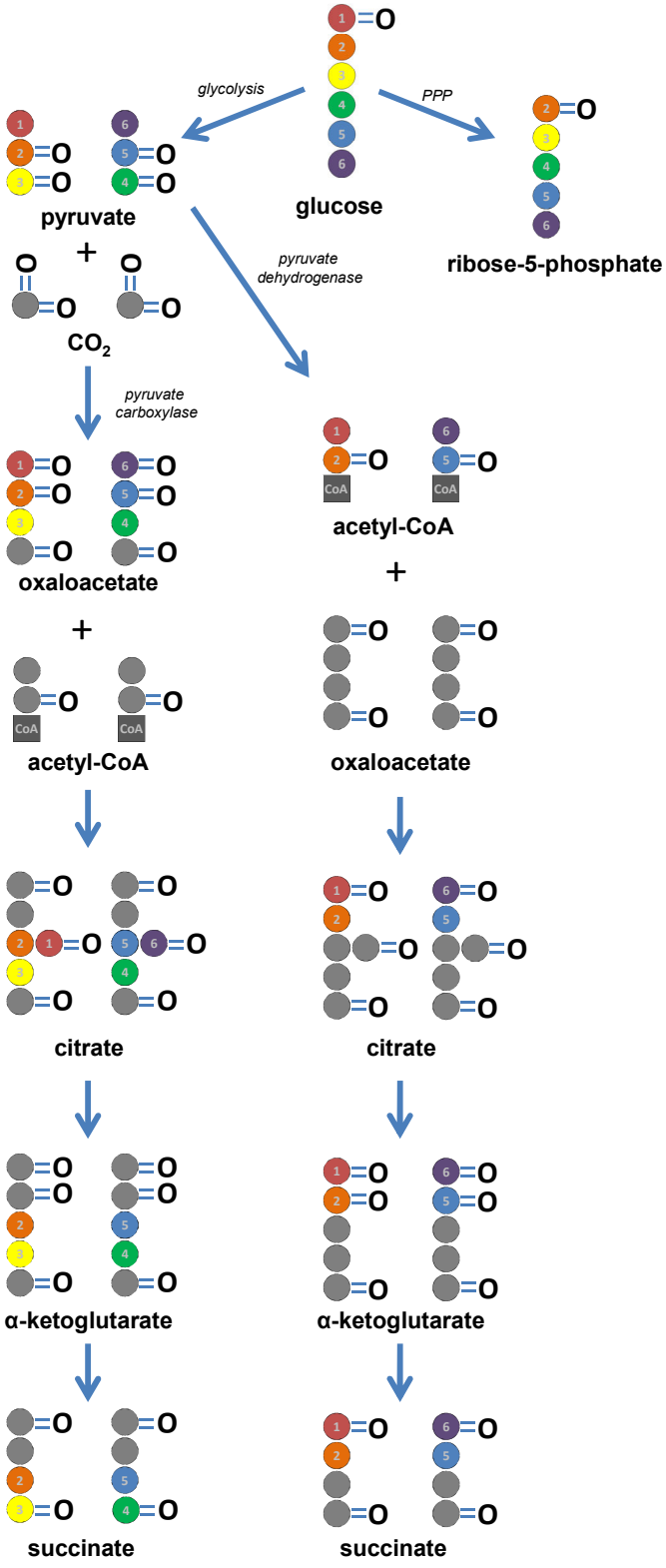

Figure 6-1. Flux of ^{13}C Labeled Carbon from Glucose through Glycolysis and the TCA Cycle.

References

1. Mulder, H., and Ling, C. 2009. Mitochondrial dysfunction in pancreatic [beta]-cells in Type 2 Diabetes. *Molecular and Cellular Endocrinology* 297:34-40.
2. MacDonald, M.J., Fahien, L.A., Brown, L.J., Hasan, N.M., Buss, J.D., and Kendrick, M.A. 2005. Perspective: emerging evidence for signaling roles of mitochondrial anaplerotic products in insulin secretion. *Am J Physiol Endocrinol Metab* 288:E1-15.
3. Prentki, M., and Nolan, C.J. 2006. Islet β cell failure in type 2 diabetes. *The Journal of Clinical Investigation* 116:1802-1812.
4. Fernandez, C., Fransson, U., Hallgard, E., Spégel, P., Holm, C., Krogh, M., Wårell, K., James, P., and Mulder, H. 2007. Metabolomic and Proteomic Analysis of a Clonal Insulin-Producing β-Cell Line (INS-1 832/13). *Journal of Proteome Research* 7:400-411.
5. Karas, M., Bahr, U., and Dülcks, T. 2000. Nano-electrospray ionization mass spectrometry: addressing analytical problems beyond routine. *Fresenius' Journal of Analytical Chemistry* 366:669-676.
6. Gangl, E.T., Annan, M.M., Spooner, N., and Vouros, P. 2001. Reduction of signal suppression effects in ESI-MS using a nanosplitting device. *Analytical Chemistry* 73:5635-5644.
7. Haskins, W.E., Wang, Z., Watson, C.J., Rostand, R.R., Witowski, S.R., Powell, D.H., and Kennedy, R.T. 2001. Capillary LC−MS2 at the Attomole Level for Monitoring and Discovering Endogenous Peptides in Microdialysis Samples Collected in Vivo. *Analytical Chemistry* 73:5005-5014.
8. Yuan, W., and Edwards, J.L. 2010. Capillary separations in metabolomics. *Bioanalysis* 2:953-963.
9. Uehara, T., Yokoi, A., Aoshima, K., Tanaka, S., Kadowaki, T., Tanaka, M., and Oda, Y. 2009. Quantitative Phosphorus Metabolomics Using Nanoflow Liquid Chromatography-Tandem Mass Spectrometry and Culture-Derived Comprehensive Global Internal Standards. *Analytical Chemistry* 81:3836-3842.
10. Kiefer, P., Delmotte, N.l., and Vorholt, J.A. 2010. Nanoscale Ion-Pair Reversed-Phase HPLC−MS for Sensitive Metabolome Analysis. *Analytical Chemistry* 83:850-855.
11. Bennett, B.D., Yuan, J., Kimball, E.H., and Rabinowitz, J.D. 2008. Absolute quantitation of intracellular metabolite concentrations by an isotope ratio-based approach. *Nat. Protocols* 3:1299-1311.
12. Feng, X., Page, L., Rubens, J., Chircus, L., Colletti, P., Pakrasi, H.B., and Tang, Y.J. 2010. Bridging the Gap between Fluxomics and Industrial Biotechnology. *Journal of Biomedicine and Biotechnology* 2010.
13. Tang, Y.J., Martin, H.G., Myers, S., Rodriguez, S., Baidoo, E.E.K., and Keasling, J.D. 2009. Advances in analysis of microbial metabolic fluxes via 13C isotopic labeling. *Mass Spectrometry Reviews* 28:362-375.
14. Paul Lee, W.N., Wahjudi, P.N., Xu, J., and Go, V.L. 2010. Tracer-based metabolomics: Concepts and practices. *Clinical Biochemistry* 43:1269-1277.
15. Jensen, M.V., Joseph, J.W., Ronnebaum, S.M., Burgess, S.C., Sherry, A.D., and Newgard, C.B. 2008. Metabolic cycling in control of glucose-stimulated insulin secretion. *Am J Physiol Endocrinol Metab* 295:E1287-1297.
16. Zamboni, N., Fischer, E., and Sauer, U. 2005. FiatFlux--a software for metabolic flux analysis from 13C-glucose experiments. *BMC Bioinformatics* 6:209.
17. Wiechert, W., Möllney, M., Petersen, S., and de Graaf, A.A. 2001. A Universal Framework for 13C Metabolic Flux Analysis. *Metabolic Engineering* 3:265-283.
18. Quek, L.E., Wittmann, C., Nielsen, L.K., and Kromer, J.O. 2009. OpenFLUX: efficient modelling software for 13C-based metabolic flux analysis. *Microb Cell Fact* 8:25.